Improved Rules for the Stability Check of Unequal-Leg Angle Members

Auteur : Charlier, Loïc
Promoteur(s) : Demonceau, Jean-François
Faculté : Faculté des Sciences appliquées
Diplôme : Master en ingénieur civil des constructions, à finalité spécialisée en "civil engineering"
Année académique : 2025-2026
URI/URL : http://hdl.handle.net/2268.2/26054

UNIVERSITE DE LIEGE
FACULTE DES SCIENCES APPLIQUEES

Improved Rules for the Stability Check of Unequal-Leg Angle Members

Charlier Loïc

Thesis presented to obtain the degree of :
Master of Science in Civil Engineering

Thesis supervisor :
Demonceau Jean-François

Guidance :
Bezas Marios-Zois
Saufnay Loris

Members of the jury :
Bezas Marios-Zois
Demonceau Jean-François
Geuzaine Margaux
Saufnay Loris

Academic year: **2025 - 2026**

Acknowledgments

I would first like to express my sincere gratitude to my supervisor, Professor Jean-François Demonceau, for giving me the opportunity to carry out this master's thesis and for his guidance, availability and valuable advice throughout this work.

I would also like to warmly thank Lorys Saufnay and Marios-Zois Bezas for their involvement in the regular meetings, their continuous interest in the progress of this thesis and the many insightful discussions that contributed to its development. Their support, technical expertise and constructive comments were greatly appreciated throughout this project.

I would like to thank the members of the jury, Professor Jean-François Demonceau, Marios-Zois Bezas and Margaux Geuzaine, for the time dedicated to reading and evaluating this work.

I am deeply grateful to my mother for her constant support and encouragement throughout my studies and far beyond the scope of this thesis. Her presence, patience and confidence in me have been an invaluable source of motivation.

I would also like to thank my brother and my sister for all the moments that allowed me to step away from the demands of this work and clear my mind. Their interest in the progress of this thesis and their continuous support have been greatly appreciated throughout its completion.

I am equally grateful to my father for his constant interest in the development of this thesis and for the time he dedicated to discussing its progress. His remarks and opinions, particularly on some of the more technical aspects of the work, provided valuable insight and were always greatly appreciated.

Finally, I would like to thank my friends and fellow leaders at the Patro. The time spent with them offered a welcome balance alongside this thesis and allowed me to focus on other things whenever needed, even if it sometimes meant having to decline their seemingly endless invitations to go out. Their encouragement, support and genuine interest in the progress of this work were greatly appreciated throughout this journey.

To all of them, I extend my sincere thanks.

Résumé

Cette thèse de master étudie le comportement au flambement des cornières à ailes inégales soumises à une compression centrée. En raison de l'interaction entre les modes de flambement par flexion et par flexion-torsion, la réponse mécanique de ces éléments présente une complexité particulière qui n'est pas toujours correctement représentée par les règles de dimensionnement actuelles de l'EN 1993-1-1. Par ailleurs, le développement des aciers à haute limite d'élasticité soulève des interrogations quant à l'adéquation de règles de calcul principalement calibrées pour les nuances d'acier de référence.

Dans un premier temps, un modèle par éléments finis intégrant les non-linéarités géométriques, les non-linéarités matérielles et les imperfections initiales est développé et validé à partir de résultats expérimentaux disponibles dans la littérature. Ce modèle est ensuite utilisé pour réaliser une vaste étude paramétrique couvrant différentes géométries de sections, élancements et nuances d'acier comprises entre S235 et S690. Les résultats numériques obtenus servent à évaluer les performances des règles actuelles de l'EN 1993-1-1 ainsi que celles de formulations améliorées proposées dans la littérature.

Les analyses mettent en évidence que les dispositions actuelles de l'EN 1993-1-1 ne représentent pas pleinement l'influence des interactions modales. Un conservatisme important est observé pour les colonnes gouvernées par le flambement par flexion-torsion, tandis que des prédictions non sécuritaires apparaissent dans la zone de transition entre les différents modes d'instabilité. La sévérité de ces écarts dépend fortement du rapport géométrique (h/b), identifié comme un paramètre clé dans le développement des interactions modales.

L'influence de la nuance d'acier sur la résistance normalisée au flambement est ensuite étudiée. Sur la base des résultats numériques, une nouvelle formulation du facteur d'imperfection dépendant de la limite d'élasticité est proposée et combinée à des corrections tenant compte des interactions modales. La formulation obtenue améliore significativement la précision et la cohérence des prédictions tout en réduisant l'incertitude associée au modèle.

Enfin, une analyse de fiabilité est réalisée conformément à la procédure de l'EN 1990 sur une base de données comprenant 1188 simulations GMNIA pour chaque configuration d'imperfection. Les résultats montrent que la formulation proposée conserve un niveau de fiabilité comparable à celui des dispositions actuelles de l'EN 1993-1-1 tout en permettant des prédictions plus précises et moins conservatrices.

Dans l'ensemble, ce travail met en évidence les complexités mécaniques liées aux interactions modales dans les cornières à ailes inégales, identifie certaines limites des règles actuelles de l'EN 1993-1-1 et propose un cadre physiquement cohérent pour le développement futur de règles de dimensionnement mieux adaptées aux cornières à ailes inégales en acier à haute limite d'élasticité.

Summary

The buckling behaviour of unequal-leg angle members subjected to axial compression is investigated in this master's thesis. Owing to the interaction between flexural and torsional–flexural buckling modes, the mechanical response of these members is particularly complex and may not be fully represented by the current EN 1993-1-1 design provisions. Furthermore, the increasing use of high-strength steels raises questions regarding the applicability of design rules that were primarily calibrated for conventional steel grades.

A geometrically and materially nonlinear finite element model with imperfections (GMNIA) is first developed and validated against available experimental results. An extensive parametric study is then conducted on hot-rolled unequal-leg angle members covering a wide range of cross-sectional geometries, member slenderness values and steel grades from S235 to S690. The generated numerical results are employed to evaluate the resistance predictions of EN 1993-1-1 as well as existing improved design approaches proposed in the literature.

The analyses reveal that the current EN 1993-1-1 provisions do not fully capture the influence of modal interactions. Significant conservatism is observed for members governed by torsional–flexural buckling, while unsafe predictions develop in the transition region between instability modes. The severity of these discrepancies is shown to depend strongly on the cross-sectional aspect ratio h/b, which is identified as a key parameter governing the development of modal interactions.

The beneficial effect of increasing steel grade on the normalised buckling resistance is subsequently investigated. Based on the numerical results, a modified steel-grade-dependent imperfection factor formulation is proposed and combined with existing modal interaction corrections. The resulting design approach significantly improves the accuracy and consistency of the resistance predictions while reducing the associated model uncertainty.

Finally, a reliability assessment is performed in accordance with the procedure of EN 1990 using a database comprising 1188 GMNIA simulations for each imperfection configuration. The results indicate that the proposed formulation maintains a reliability level comparable to that of the current EN 1993-1-1 provisions while providing more accurate and less conservative resistance predictions.

Overall, this work highlights the mechanical complexities associated with modal interactions in unequal-leg angle members, identifies limitations of the current EN 1993-1-1 provisions and proposes a physically motivated framework for future improvements of buckling design rules for high-strength steel unequal-leg angle members.

Use of Artificial Intelligence Tools

Artificial intelligence tools were used during the preparation of this thesis exclusively for language-related purposes, including proofreading, grammar correction, spelling verification and assistance with the translation of certain passages between French and English.

All scientific analyses, numerical simulations, calculations, interpretations, conclusions and design recommendations presented in this work were developed and validated by the author. The use of artificial intelligence tools did not contribute to the generation of the scientific content or research findings reported in this thesis.

Contents

List of Figures

List of Tables

Chapter 1

Introduction

1.1 Context and motivation

Steel structures play a major role in modern civil engineering due to their high strength-to-weight ratio, ease of fabrication and adaptability to a wide range of structural applications. They are widely used in buildings, bridges, industrial facilities, transmission towers and offshore structures, where efficient structural solutions are often required to satisfy both economic and performance criteria.

In recent decades, increasing attention has been devoted to the development of more sustainable and resource-efficient construction practices. In this context, high-strength steels have attracted growing interest since they offer the possibility of reducing member sizes and structural self-weight while maintaining the required load-carrying capacity. Such reductions may lead to significant material savings, improved transportation and erection efficiency, as well as a decrease in the environmental impact associated with steel production.

The benefits of high-strength steels can, however, only be fully exploited if reliable and accurate design provisions are available. Unlike conventional structural steels, the behaviour of high-strength steel members is often governed by stability phenomena rather than by material yielding. Consequently, the accurate prediction of buckling resistance becomes a key aspect of structural design.

Within the European design framework, the buckling resistance of steel compression members is commonly evaluated using the provisions of EN 1993-1-1. These design rules are based on the Perry–Robertson approach and account for the influence of geometric imperfections, residual stresses and material nonlinearities through the use of buckling curves and associated imperfection factors. Although these provisions have proven to be efficient for a wide range of structural members, their applicability to more complex structural forms and to high-strength steel grades remains an active area of research.

Among the structural members commonly used in engineering practice, unequal-leg angle sections exhibit particularly complex buckling behaviour. Their monosymmetric geometry may lead to significant interactions between flexural and torsional–flexural instability modes, making the prediction of their buckling resistance more challenging than for doubly symmetric sections. Furthermore, several recent studies have suggested that the conservatism associated with the current buckling curves tends to increase as the steel grade increases, raising questions regarding the suitability of the existing design rules for high-strength steel unequal-leg angle members.

The present work is motivated by these observations and focuses on two key aspects influencing the buckling behaviour of unequal-leg angle members: the influence of modal interactions and the influence of steel grade. Through numerical investigations and reliability assessments, the objective is to evaluate the limitations of the current design provisions and to develop improved design recommendations capable of providing a more accurate representation of the buckling resistance of high-strength steel unequal-leg angle members.

1.1.1 Specificities of unequal angle sections

Unequal-leg angle sections are widely used in engineering structures such as lattice towers, transmission towers, truss systems and bracing members. Their popularity stems from their simple geometry, ease of fabrication and efficient connection detailing. In addition, their relatively low weight and favourable strength-to-weight ratio make them attractive structural solutions for compression and tension members.

Unlike doubly symmetric sections, unequal-leg angle members exhibit a monosymmetric geometry. As a result, the centroid, shear centre and principal axes do not coincide, leading to a more complex structural response. In particular, axial compression may induce coupled flexural and torsional deformations, which significantly influence the stability behaviour of the member.

The buckling behaviour of unequal-leg angle members is therefore more complex than that of conventional I-sections or hollow sections. While pure flexural buckling may govern the response for some geometries, torsional–flexural buckling can become critical for others. Furthermore, the transition between these instability modes is often characterised by significant modal interactions, making the prediction of the buckling resistance particularly challenging.

Previous research has shown that the severity of these interactions is strongly influenced by the cross-sectional geometry, especially the aspect ratio h/b. Members with relatively low h/b ratios generally exhibit stronger interactions between instability modes, whereas members with larger h/b ratios tend to behave in a manner closer to the assumptions underlying conventional buckling formulations.

The cross-sectional aspect ratio h/b is therefore generally regarded as a key parameter governing the development of modal interactions and the resulting buckling behaviour of unequal-leg angle members.

These specific characteristics make unequal-leg angle members an interesting but challenging structural form for design purposes. Consequently, the adequacy of existing design provisions for such members deserves further investigation.

1.1.2 Structural advantages of high-strength steels

The continuous demand for lighter, more efficient and more sustainable structures has stimulated the increasing use of high-strength steels in civil engineering applications. According to EN 1993-1-1:2022, structural steels with a yield strength greater than or equal to 460 MPa are generally classified as high-strength steels (HSS). Steel grades such as S460, S500, S550 and S690 are now commonly employed in bridges, transmission towers, industrial structures and offshore facilities, where high load-carrying capacities are required.

The primary advantage of high-strength steels lies in their increased yield strength compared with conventional structural steels. Their superior strength-to-weight ratio enables substantial reductions in member size and structural self-weight while maintaining the required load-carrying capacity. Such reductions may provide significant economic benefits through decreased fabrication, transportation and erection costs. Furthermore, reducing the quantity of steel required for a structure contributes to lowering the associated environmental impact through a reduction in the demand for raw materials and associated carbon emissions.

The use of high-strength steels may also improve the structural efficiency of compression members by enabling larger load-carrying capacities without increasing the overall dimensions of the structure. This aspect is particularly attractive for truss structures, transmission towers and other weight-sensitive applications where compression members represent a substantial proportion of the total steel consumption.

Despite these advantages, the efficient use of high-strength steels requires design provisions capable of accurately representing their structural behaviour. While the fundamental material behaviour remains similar to that of conventional steels, several studies have shown that the conservatism associated with current buckling design rules tends to increase with increasing yield strength. As a consequence, part of the potential benefits offered by high-strength steels may be lost when existing design provisions are directly applied without considering the influence of steel grade.

These observations highlight the need for a better understanding of the buckling behaviour of high-strength steel members and motivate the present investigation on unequal-leg angle sections.

1.2 Research objectives and scope of the thesis

The observations presented in the previous sections highlight the need for a better understanding of the buckling behaviour of unequal-leg angle members, particularly when high-strength steels are considered. Although the current EN 1993-1-1 provisions provide a practical design framework, questions remain regarding their ability to accurately represent the influence of modal interactions and steel grade on the buckling resistance of such members.

The main objective of the present thesis is therefore to investigate the flexural buckling behaviour of hot-rolled unequal-leg angle members over a wide range of steel grades, ranging from S235 to S690, and to assess the adequacy of the current Eurocode design provisions.

To achieve this objective, a geometrically and materially non-linear finite element modelling strategy is developed and validated against available experimental results. The validated numerical models are then used to perform an extensive parametric study covering different cross-sectional geometries, member slenderness values and steel grades.

Particular attention is devoted to the influence of the initial imperfection shape, the cross-sectional aspect ratio h/b, the interaction between flexural and torsional–flexural buckling modes, and the influence of steel grade on the member resistance. The applicability of recently proposed design improvements is subsequently assessed and further developments are investigated to better account for the behaviour of high-strength steel unequal-leg angle members.

Finally, the reliability of the proposed design recommendations is evaluated according to the procedures of EN 1990 in order to assess their suitability for practical design applications.

1.3 Thesis outline

The remainder of this thesis is organised as follows.

Chapter 2 – State of the Art presents the theoretical background relevant to the present study. The current EN 1993-1-1 design provisions for the buckling of compression members are first reviewed, followed by a discussion of the buckling behaviour of unequal-leg angle members and the improved design approaches proposed in the literature.

Chapter 3 – Numerical Model Description and Assumptions describes the numerical modelling strategy adopted in this work. The finite element formulation, material modelling assumptions, residual stresses, boundary conditions and geometric imperfections are presented together with the scope of the numerical investigations.

Chapter 4 – Numerical Model Validation examines the influence of the modelling assumptions on the numerical predictions and validates the adopted finite element model against available experimental results. The suitability of the retained modelling strategy for the subsequent parametric study is then assessed

Chapter 5 – Parametric Study presents an extensive numerical investigation of hot-rolled unequal-leg angle members. The influence of cross-sectional geometry, member slenderness and imperfection shape on the buckling behaviour is analysed. The numerical results are compared with the current EN 1993-1-1 provisions and with existing improved design proposals.

Chapter 6 – Proposal of an Improved Imperfection Factor investigates the influence of steel grade on the imperfection sensitivity and buckling behaviour of unequal-leg angle members. A modified steel-grade-dependent imperfection factor formulation is developed and combined with existing modal interaction corrections. The performance and reliability of the resulting design approach are subsequently evaluated.

Chapter 7 – Conclusions and Perspectives summarises the main findings of the study, presents the proposed design recommendations and identifies potential directions for future research.

Chapter 2

State of the Art

2.1 Design Rules According to EN 1993-1-1

The design of compression members in European standards is governed by the provisions of EN 1993-1-1.

In European standards, the design formula for members under pure compression is based on the Ayrton–Perry formulation:

$$N_{b,Rd} = \frac{\chi \cdot \beta \cdot A \cdot f_y}{\gamma_{M1}} \geq N_{Ed} \tag{2.1}$$

In this expression, the product of the cross-sectional area and the yield strength represents the compression resistance of the gross section, i.e. without accounting for global instability or local buckling effects. This resistance therefore increases proportionally with both the cross-sectional area and the yield strength.

However, beyond the cross-sectional area, the geometry of the section also plays a significant role. If part of the section is too slender, local buckling may occur. This effect is taken into account by reducing the effective cross-sectional area. The ratio between the effective area and the gross area is represented by the parameter β, defined as:

$$A_{\text{eff}} = \beta \cdot A \tag{2.2}$$

To assess whether a section is too slender, Eurocode introduces the concept of cross-section classification. Four classes are defined: Class 1 (plastic), Class 2 (compact), Class 3 (semi-compact), and Class 4 (slender). The class of a cross-section is governed by its most critical plate element.

As shown in Figure 2.1, the classification of angle sections is based on the ratio between the leg length and the thickness. It also depends on the parameter $\epsilon = \sqrt{235/f_y}$, which implies that higher steel grades lead to more restrictive classification limits.

Regarding compression resistance, no distinction is made between Classes 1 to 3. Only Class 4 sections require a reduction of the gross area. Therefore:

$$\begin{aligned} &A_{\text{eff}} = A \quad \Rightarrow \quad \beta = 1 && \text{for Classes 1–3} \\ &A_{\text{eff}} = \beta \cdot A, \quad \beta < 1 && \text{for Class 4} \end{aligned}$$

For Class 4 sections, the effective area, and thus the value of β, depends on the width-to-thickness ratio of the legs. As this ratio increases, the element becomes more slender, leading to a greater reduction of the effective area. Consequently, the compression resistance of Class 4 sections is governed more by local buckling than by the yield strength. This indicates that local buckling effects become more significant for slender sections.

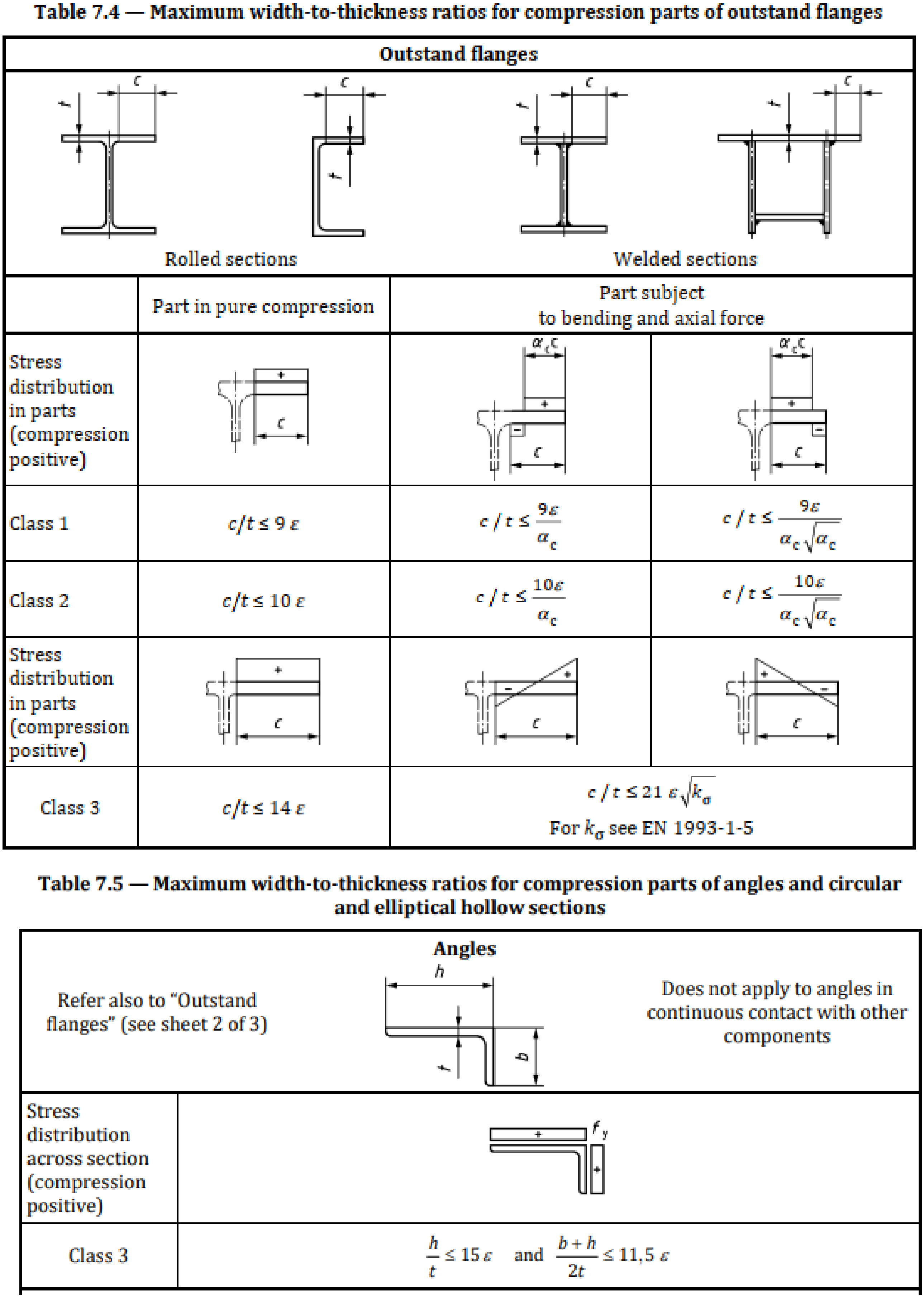

Table 7.4 — Maximum width-to-thickness ratios for compression parts of outstand flanges

Outstand flanges			
Rolled sections		Welded sections	
	Part in pure compression	Part subject to bending and axial force	
Stress distribution in parts (compression positive)			
Class 1	$c/t \leq 9\,\varepsilon$	$c\,/\,t \leq \frac{9\varepsilon}{\alpha_c}$	$c\,/\,t \leq \frac{9\varepsilon}{\alpha_c\sqrt{\alpha_c}}$
Class 2	$c/t \leq 10\,\varepsilon$	$c\,/\,t \leq \frac{10\varepsilon}{\alpha_c}$	$c\,/\,t \leq \frac{10\varepsilon}{\alpha_c\sqrt{\alpha_c}}$
Stress distribution in parts (compression positive)			
Class 3	$c/t \leq 14\,\varepsilon$	$c\,/\,t \leq 21\,\varepsilon\sqrt{k_\sigma}$ For k_σ see EN 1993-1-5	

Table 7.5 — Maximum width-to-thickness ratios for compression parts of angles and circular and elliptical hollow sections

Angles		
Refer also to "Outstand flanges" (see sheet 2 of 3)		Does not apply to angles in continuous contact with other components
Stress distribution across section (compression positive)		
Class 3	$\frac{h}{t} \leq 15\,\varepsilon$ and $\frac{b+h}{2t} \leq 11{,}5\,\varepsilon$	

Figure 2.1: Cross-section classification limits for angle sections according to EN 1993-1-1:2022 [1]

As mentioned previously, a second effect must be considered, namely global instability. This effect is accounted for through the reduction factor χ, which represents the influence of global buckling. The following expression is given in the design standards:

$$\chi = \frac{1}{\phi + \sqrt{\phi^2 - \bar{\lambda}^2}} \tag{2.3}$$

with:

$$\phi = 0.5 \cdot \left(1 + \eta + \bar{\lambda}^2\right) \quad \text{where} \quad \eta = \alpha \cdot (\bar{\lambda} - 0.2) \tag{2.4}$$

In this formulation, $\bar{\lambda}$ denotes the relative slenderness. This parameter characterises the susceptibility of the member to instability phenomena. It provides an indication of the extent to which the resistance is governed by buckling as opposed to yielding

The relative slenderness is defined as:

$$\bar{\lambda} = \sqrt{\frac{\text{Characteristic resistance}}{\text{Resistance to elastic buckling}}} = \sqrt{\frac{N_{pl,Rk}}{N_{cr}}} \tag{2.5}$$

For low values of $\bar{\lambda}$, the resistance is governed by yielding, whereas for high values of $\bar{\lambda}$, it is governed by elastic buckling. A lower limit of $\bar{\lambda} = 0.2$ is introduced, below which instability effects are assumed to have no influence on the resistance.

$N_{pl,Rk}$ corresponds to the characteristic cross-sectional resistance and is defined, as mentioned previously, as $\beta \cdot A \cdot f_y$.

N_{cr} represents the elastic critical buckling load. In most cases, and for commonly used structural sections (such as IPE or HE profiles), this corresponds to the Euler critical load, i.e.:

$$N_{cr} = \frac{\pi^2 \cdot E \cdot I}{L_{cr}^2} \tag{2.6}$$

which is associated with a flexural buckling mode.

However, for unequal-leg angle sections, the critical load is generally associated with a combined flexural–torsional buckling mode, denoted as $N_{cr,TF}$. This aspect will be discussed in more detail in Subsection 2.1.1.

In Eq. (2.4), the parameter η is introduced to account for the detrimental effects of geometric imperfections and residual stresses through the imperfection factor α. The imperfection factor α therefore implicitly accounts for both geometric imperfections and residual stresses in the design formulation.

In order to develop a practical design approach based on buckling curves of the form $\chi = f(\bar{\lambda})$, five buckling curves are defined in the design standards. These curves have been calibrated on the basis of numerous experimental results and theoretical studies, covering a wide range of cross-sections.

A semi-sinusoidal out-of-plane imperfection with an amplitude of $L/1000$, together with residual stress distributions specific to each type of cross-section, is represented through the parameter α. The values that this parameter can take are given in Table 2.1.

Buckling curve	a_0	a	b	c	d
Imperfection factor α	0.13	0.21	0.34	0.49	0.76

Table 2.1: Buckling curves according to EN 1993-1-1:2022 [1]

For unequal-leg angle sections, the selection of the buckling curve depends on both the manufacturing process and the steel grade. In the present study, only hot-rolled sections are considered.

According to the design provisions 2.2, buckling curve b is adopted for steel grades lower than S460, corresponding to an imperfection factor $\alpha = 0.34$, while buckling curve a is adopted for steel grade equal or greater than S460, corresponding to $\alpha = 0.21$.

Cross-section		Limits	Buckling about axis	Buckling curve S235 S275 S355 S420	Buckling curve S460 up to S700 inclusive
U-, T- and solid sections	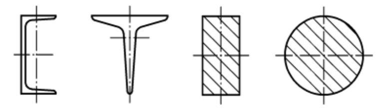		any	c	c
L-sections		Rolled sections	any	b	a
	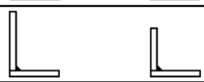	Welded sections $t \leq 40$ mm	any	c	c

Figure 2.2: Selection of buckling curve for flexural buckling according to EN 1993-1-1:2022 [1]

2.1.1 Critical Loads

As mentioned in the introduction, despite their simple geometry, unequal-leg angle sections exhibit complex mechanical behaviour. This complexity arises from two main factors. First, the point of load application rarely coincides with the centroid of the cross-section, which inevitably induces bending. Second, the shear centre does not coincide with the centroid, meaning that bending is inherently coupled with torsion.

As a result, the buckling behaviour may involve both local and global deformation modes, including torsion, minor-axis flexure, and major-axis flexure, as illustrated in Figure 2.3. Minor-axis flexure is characterised by a lateral displacement of the corner in the direction of the major axis, while major-axis flexure corresponds to a displacement in the direction of the minor axis. Torsional deformation is characterised by a rotation of the entire cross-section about the shear centre, which is located near the intersection of the two legs.

Due to the non-coincidence of the shear centre and the centroid, bending and torsion are inherently coupled, leading to a combined torsional–flexural buckling mode.

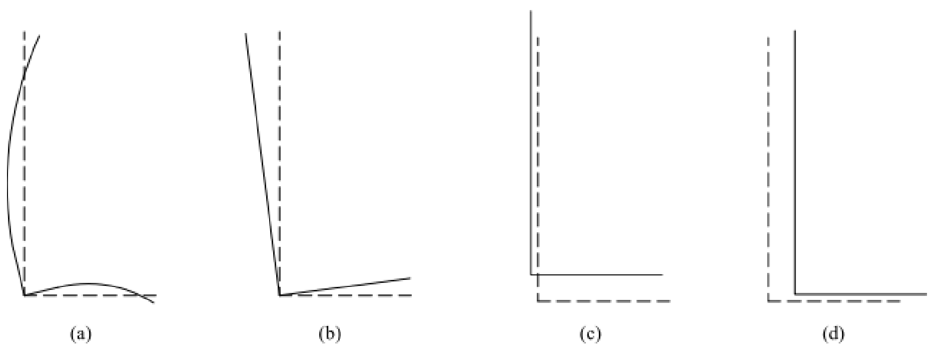

Figure 2.3: Isolated elastic (a) local, (b) torsional, (c) major-axis flexural and (d) minor-axis flexural buckling modes for unequal-leg angle section members subjected to axial compression [2]

This coupling between deformation modes plays a key role in determining the critical buckling load of unequal-leg angle members.

The critical loads associated with flexural buckling about the major and minor axes are given by the classical Euler expressions:

$$N_{cr,u} = \frac{\pi^2 E I_u}{L_{cr,u}^2} \qquad\qquad N_{cr,v} = \frac{\pi^2 E I_v}{L_{cr,v}^2} \tag{2.7}$$

where E is the Young's modulus of steel, I_u and I_v are the second moments of area about the major and minor principal axes, respectively, and $L_{cr,u}$ and $L_{cr,v}$ are the corresponding buckling lengths. For pinned–pinned boundary conditions, these are equal to the member length.

The critical load for torsional buckling of open sections is given by [3]:

$$N_{cr,T} = \frac{1}{i_0^2}\left(GJ + \frac{\pi^2 E I_w}{L_{cr,T}^2}\right) \tag{2.8}$$

where:

$i_0^2 = i_p^2 + u_0^2 + v_0^2$	: polar radius of gyration about the shear centre
$i_p^2 = \dfrac{I_u + I_v}{A}$	
$u_0,\ v_0$	: distances between the shear centre and the centroid along the u and v axes
G	: shear modulus of steel
$J = \dfrac{(h+b)t^3}{3}$	: Saint-Venant torsional constant
$I_w = \dfrac{(h^3+b^3)t^3}{36}$	: warping constant
$L_{cr,T} = \beta_w \cdot L$	: torsional buckling length
β_w	: buckling length factor for torsional buckling (see Figure 2.4)

The expressions used for the torsional constant J and the warping constant I_w are derived from thin-walled theory, which assumes that the wall thickness is small compared to the other cross-sectional dimensions [7, 8]. Under this assumption, simplified analytical expressions can be obtained for open sections [9]. However, for thicker sections, these formulations become less accurate and more advanced analytical or numerical methods, such as finite element analysis, are required [8].

The equation governing the elastic critical load accounting for the interaction between flexural and torsional buckling modes is provided in [3] and reads:

$$\begin{aligned}&(N_{cr,u} - N_{cr})(N_{cr,v} - N_{cr})(N_{cr,T} - N_{cr})i_0^2 \\ &\quad - \alpha_{zw} v_0^2 N_{cr}^2 (N_{cr,u} - N_{cr}) - \alpha_{yw} u_0^2 N_{cr}^2 (N_{cr,v} - N_{cr}) = 0\end{aligned} \tag{2.9}$$

where α_{yw} and α_{zw} are coefficients that depend on the combination of bending and torsional boundary conditions (see Figure 2.4).

	FBCs = Flexural Boundary Condition 1-10 (Buckling length factor β_y and β_z)	TBCs = Torsional Boundary Conditions I-X, (Buckling length factor β_w)									
		Non-sway TBCs				Sway TBCs					
		I (0,5)	II (0,7)	III (0,7)	IV (1,0)	V (1,0)	VI (1,0)	VII (2,0)	VIII (2,0)	IX (2,0)	X (2,0)
Non-sway FBCs	1. (0,5)	1	0,9	0,9	0,9	0,7	0,7	0,8	0,8	0,8	0,8
	2. (0,7)	0,9	1	0,8	0,9	0,6	0,6	0,7	0,8	0,8	0,7
	3. (0,7)	0,9	0,8	1	0,9	0,6	0,6	0,8	0,7	0,7	0,8
	4. (1,0)	0,9	0,9	0,9	1	0,4	0,4	0,7	0,7	0,7	0,7
Sway FBCs	5. (1,0)	0,1	0,1	0,1	0,1	1	1	0,9	0,9	0,9	0,9
	6. (1,0)	0,1	0,1	0,1	0,1	1	1	0,9	0,9	0,9	0,9
	7. (2,0)	0,2	0,2	0,2	0,2	0,9	0,9	1	0,6	0,6	1
	8. (2,0)	0,2	0,2	0,2	0,2	0,9	0,9	0,6	1	1	0,6
	9. (2,0)	0,2	0,2	0,2	0,2	0,9	0,9	0,6	1	1	0,6
	10. (2,0)	0,2	0,2	0,2	0,2	0,9	0,9	1	0,6	0,6	1

NOTE Conservatively α_{yw} = 1,0 or α_{zw} = 1,0 may be used for any combination of bending 1 - 10 and torsion I – X boundary condition

Figure 2.4: Values of α_{yw} and α_{zw} for different combinations of bending and torsional boundary conditions according to [3]

Symbol in Table 4.1	Deformation of member end	Torsion boundary condition
	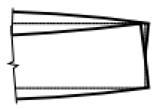	Rotation restrained, warping free
	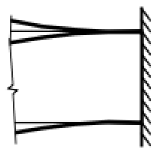	Rotation restrained, warping restrained
	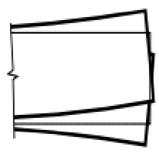	Rotation free, warping free
	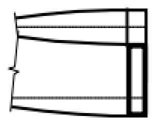	Rotation free, warping restrained

Figure 2.5: Torsional boundary conditions corresponding to Figure 2.4, according to [3]

The smallest root of Eq. (2.9) defines the governing elastic critical load.

For unequal-leg angle sections, the critical mode generally involves a combination of torsion, minor-axis flexure, and major-axis flexure, and is therefore referred to as torsional–flexural buckling, denoted as $N_{cr,TF}$.

It is generally observed that the torsional–flexural (TF) buckling mode governs over a wide range of member slenderness. In other words, $N_{cr,TF}$ is the minimum among $N_{cr,TF}$, $N_{cr,T}$, $N_{cr,u}$, and $N_{cr,v}$.

For short members, torsional effects dominate and $N_{cr,TF}$ approaches $N_{cr,T}$. For slender members, minor-axis flexural buckling becomes predominant and $N_{cr,TF}$ approaches $N_{cr,v}$. For members of intermediate slenderness, a gradual transition occurs between torsion-dominated and flexure-dominated behaviour.

The solution of this equation may be inconvenient for practical design purposes. Therefore, a simplified expression can be obtained by dividing Eq. (2.9) by $(N_{cr,u} - N_{cr})$, assuming that N_{cr} remains sufficiently smaller than $N_{cr,u}$. This leads to:

$$(N_{cr,v} - N_{cr})(N_{cr,T} - N_{cr})i_0^2 - \alpha_{zw} v_0^2 N_{cr}^2 - \alpha_{yw} u_0^2 N_{cr}^2 \frac{(N_{cr,v} - N_{cr})}{(N_{cr,u} - N_{cr})} = 0 \tag{2.10}$$

Since $N_{cr,u}$ is generally significantly larger than $N_{cr,v}$ and $N_{cr,T}$ for typical geometries of unequal-leg angle sections, the contribution of the third term becomes negligible [2]. This results in the following simplified expression:

$$(N_{cr,v} - N_{cr})(N_{cr,T} - N_{cr})i_0^2 - \alpha_{zw} v_0^2 N_{cr}^2 = 0 \tag{2.11}$$

An approximate value of the torsional–flexural elastic critical load can therefore be obtained as the smallest root of the following quadratic equation:

$$N_{cr,TF} = \frac{N_{cr,T} + N_{cr,v} - \sqrt{(N_{cr,T} + N_{cr,v})^2 - 4\left(1 - \alpha_{zw}\frac{v_0^2}{i_0^2}\right) N_{cr,v} N_{cr,T}}}{2\left(1 - \alpha_{zw}\frac{v_0^2}{i_0^2}\right)} \tag{2.12}$$

Dai et al. [2] assessed this approximation against the exact solution and reported that it slightly overestimates the elastic critical load, while maintaining an acceptable level of accuracy. The discrepancy is typically below 5% for practical h/b ratios, although the method remains marginally unconservative.

In the present study, the exact solution is adopted to avoid this slight unconservative bias. However, the simplified formulation remains suitable for practical design purposes due to its acceptable accuracy.

2.2 Literature review

2.2.1 Experimental and Numerical Studies on Unequal-Leg Angle Sections

The first research studies and experimental investigations on unequal-leg angle sections date back to the 1980s. These studies considered various structural members (columns, beams, and beam-columns), different materials (such as aluminium and steel), and a range of boundary conditions (simply supported or fixed).

Among the early contributions, Liao [10], Wu [11], and Zhang et al. [12, 13] conducted experimental investigations on extruded aluminium unequal-leg angles subjected to concentric compression.

Laracuente et al. [14, 15] and Sippel and Blum [16] conducted a total of 18 tests on fixed-ended hot-rolled austenitic stainless steel unequal-leg angle sections under compression.

Guo et al. [17] conducted experiments on fixed-ended cold-formed steel equal- and unequal-leg angle section members under axial compression.

Kitipornchai and Lee [5] carried out tests on both equal-leg and unequal-leg steel angle columns. They showed that all specimens failed in the inelastic range, with buckling modes involving a combination of minor-axis flexure and torsion.

Liu et al. [6] also conducted experimental investigations on unequal-leg steel angle sections subjected to both concentric and eccentric loading, in order to study their beam-column behaviour. A total of 26 specimens were tested. The results highlight the significant influence of load eccentricity on both the ultimate load-carrying capacity and the post-buckling behaviour. In addition to ultimate loads, load–displacement curves for different specimens were also reported.

Dinis et al. [18] also performed experimental studies on steel angle columns with lengths ranging from short to intermediate. Based on these results, a more detailed investigation of buckling, post-buckling behaviour, and ultimate resistance was conducted. It was highlighted that, except for very short and very slender members, buckling generally involves a combination of torsion, major- and minor-axis flexure, and local deformations. Torsion tends to dominate for shorter members, while minor-axis flexure governs for more slender members, with a gradual transition between these behaviours. Major-axis flexure and local deformations were found to have a relatively minor influence.

It was also shown that the cross-sectional asymmetry plays a significant role in this transition. A higher degree of asymmetry (i.e. a larger h/b ratio) leads to a smoother transition between buckling modes, whereas lower asymmetry results in a more abrupt change.

Based on these experimental findings, several researchers have demonstrated that current design rules exhibit excessive conservatism for certain slenderness ranges [19]. Modifications have therefore been proposed to reduce this conservatism. In some cases, the torsional buckling curve has been shown to be more appropriate than the flexural buckling curve currently used in design standards [20]. Plots of resistance as a function of reduced slenderness have highlighted that different reduction factors may be obtained for the same slenderness value.

It has also been observed that existing design rules may lead to inaccurate, and in some cases unsafe, [21]. This has been attributed to the lack of consideration of interactions between buckling modes.

Dai et al. [2] proposed modifications to the existing design rules in order to improve the accuracy and consistency of the predictions, while reducing both the excessive conservatism and the potentially unsafe results identified in previous studies.

To achieve this, a numerical database comprising approximately 1200 finite element simulations was generated. A wide range of cross-sections was considered in order to cover a broad range of geometric ratios, in particular the h/b ratio, which had previously been identified by Dinis et al. [18] as a key parameter influencing the buckling behaviour.

All numerical simulations were performed considering steel grade S355. The numerical models were validated against experimental results available in the literature.

Their findings confirmed the observations reported in previous studies. An excessive level of conservatism was observed for low slenderness values, corresponding to torsion-dominated buckling, while potentially unsafe predictions were identified for intermediate slenderness values, associated with the transition between buckling modes and the interaction between torsion and flexural behaviour.

These observations clearly indicate that current design approaches do not adequately capture the transition between torsion-dominated and flexure-dominated buckling regimes, leading to inconsistent predictions depending on the slenderness range. This limitation is primarily attributed to the use of simplified buckling curves, which are not specifically calibrated for asymmetric sections exhibiting strong mode interaction. This highlights the need for improved design formulations capable of accurately capturing the interaction between torsional and flexural buckling modes.

2.2.2 High-Strength Steel Members and Modified Buckling Curves

Several researchers have also investigated the economic and structural benefits of high-strength steels (HSS) as emerging construction materials. Early studies on high-strength steels mainly focused on the structural behaviour of welded sections fabricated from high-strength steel plates. These investigations examined residual stresses, global imperfections, and buckling behaviour.

Research on HSS with yield strengths exceeding 690 MPa was initiated in the 1960s by Nishino et al. [22], who demonstrated that the ratio between the yield strength and the residual stresses, rather than the absolute magnitude of the residual stresses, governs the buckling behaviour. Similar observations were later reported in subsequent studies by Nishino et al. [23].

It was also shown that residual stresses are independent of the yield strength. Consequently, HSS columns were found to exhibit improved buckling performance compared to conventional steel columns, particularly when comparing the numerically obtained buckling reduction factors, χ.

Although residual stresses are recognised as an important parameter influencing the buckling behaviour of steel angle sections, relatively limited research has been specifically devoted to unequal-leg angle sections. Most available investigations concern equal-leg angle sections [24, 25], while studies dedicated to unequal-leg angles remain scarce [2].

In the absence of a widely established residual stress model for unequal-leg angle sections, the residual stress distribution commonly adopted for equal-leg angle sections is also considered in the present study. This assumption is consistent with existing design recommendations and recent numerical investigations, where similar residual stress patterns are employed for both equal-leg and unequal-leg angle sections [2,26].

Residual stresses in hot-rolled angle sections are commonly represented through simplified bilinear distributions defined as a fraction of the yield strength. Although the exact magnitude and distribution of residual stresses remain subjects of discussion in the literature, several experimental investigations on S355 angle sections have reported residual stress amplitudes ranging approximately between $0.2f_y$ and $0.23f_y$ [24, 27].

Experimental measurements performed on higher-strength steel grades, including S420 and S460 sections, have shown that residual stresses do not increase proportionally with the yield strength [25, 28, 29]. Instead, the measured stress magnitudes remain close to those observed in conventional steel grades, resulting in lower relative residual stress levels for high-strength steels.

These observations support the use of residual stress models based on a reference value proportional to $f_y^* = 235$ MPa, such as the distribution adopted by Dai et al. [2], for both conventional and high-strength steel grades.

These studies therefore support the assumption that residual stresses are largely independent of the yield strength. Consequently, high-strength steel members generally exhibit improved structural performance compared to conventional steel grades, due to the lower relative influence of residual stresses on the buckling behaviour.

Furthermore, starting from the Ayrton–Perry formulation on which the buckling curves are based, the imperfection parameter η can be shown to decrease with increasing yield strength, i.e. $\eta \propto 1/f_y$.

This relationship was highlighted by Meng et al. [30] by considering a simply supported column subjected to concentric compression, with an initial geometric imperfection of amplitude $e_0 = L/1000$ and without residual stresses. Under these assumptions, the following expression can be obtained:

$$\eta = \frac{e_0 \cdot A}{W_{el}} = \frac{L}{1000} \frac{A}{W_{el}} = \bar{\lambda} \cdot \pi \sqrt{\frac{E}{A \cdot f_y}} = \left(\frac{\pi}{1000} \sqrt{\frac{E \cdot I}{A}} \right) \cdot \frac{\bar{\lambda}}{f_y} \tag{2.13}$$

Equation (2.13) therefore highlights the reduction of the imperfection parameter η with increasing yield strength under idealised conditions, i.e. in the absence of residual stresses.

However, as discussed previously, experimental investigations have shown that residual stress magnitudes are only weakly dependent on the yield strength. Consequently, the relative influence of both geometric imperfections and residual stresses on the buckling behaviour decreases as the yield strength increases. This suggests that high-strength steel members may exhibit lower imperfection sensitivity and improved buckling performance compared to conventional steel members.

In the current design standards, the same buckling curve is adopted for steel grades up to S460, while a reduction of one buckling curve is applied for higher-strength steel grades (see Figure 2.2).

However, as discussed previously, the imperfection parameter η can theoretically be shown to decrease with increasing yield strength. This suggests that the influence of imperfections on the buckling response becomes less significant for high-strength steel members.

Consequently, the use of a fixed imperfection factor for broad ranges of steel grades may not fully reflect the actual behaviour of high-strength steel members. This observation highlights the potential interest of developing a generalised imperfection factor expressed as a function of the yield strength.

Several researchers have proposed different approaches over the years to explicitly account for the influence of the yield strength f_y in the formulation of the imperfection parameter η. Saufnay et al. [31] identified three general approaches commonly reported in the literature.

1. The first approach consists of introducing a modified imperfection factor, denoted α^*, expressed as:

$$\alpha^* = \alpha \left(\frac{235}{f_y} \right)^n \tag{2.14}$$

   This approach has been the most widely adopted in the literature over the last decades. Its main advantages are: (i) the preservation of the historical buckling curve for S235 steel grades, and (ii) the possibility of using a unified formulation for different steel grades. The exponent n may vary depending on the cross-section type.

2. The second approach consists of modifying the relative slenderness through the factor

$$\epsilon = \sqrt{\frac{235}{f_y}}$$

   This approach was proposed by Jönsson and Stan [32] for hot-rolled sections subjected to major-axis flexural buckling. The use of ϵ implies that the yielding plateau becomes longer as the yield strength increases. The imperfection parameter is then expressed as:

$$\eta = \alpha \cdot (\epsilon \bar{\lambda} - 0.2) \tag{2.15}$$

   However, this approach still requires further validation for minor-axis flexural buckling.

3. The third approach consists of abandoning the existing buckling curves and proposing a fully modified imperfection formulation expressed as a function of ϵ. For hollow sections, Meng et al. [30] proposed modified imperfection formulations together with a reduction of the yielding plateau limit from a relative slenderness of 0.2 to 0.1.

All existing modified imperfection factors reported in the literature are summarised in Table 2.2. It can be observed that unequal-leg angle sections have not yet been specifically investigated within these proposed approaches.

Table 2.2: Existing modified imperfection factors reported in the literature

Cross-section typologie		Imperfection parameter	Imperfection factor	Author, year
Rolled I- or H-sections		$\alpha^*(\bar{\lambda} - 0.2)$	$\alpha^* = \alpha(\frac{235}{f_y})^{0.8}$	Maquoi, 1982 [33]
		$\alpha^*(\bar{\lambda} - 0.2)$	$\alpha^* = (\frac{235}{f_y})^{1.0}$	Johansson, 2005 [34]
		$\alpha^*(\bar{\lambda} \cdot \epsilon - 0.2)$	$\alpha^* = \alpha$	Jönsson et al., 2016 [32]
		$\alpha^*(\bar{\lambda} - 0.2)$	$\alpha^* = \alpha(\frac{235}{f_y}^{0.7}$	Saufnay et al., 2024 [35]
Welded I-sections		$\alpha^*(\bar{\lambda} - 0.2)$	$\alpha^* = \alpha(\frac{235}{f_y})^{0.6}$	Somodi et al., 2017 [36]
		$\alpha^*(\bar{\lambda} - 0.1)$	$\alpha^* = 0.45\left(\frac{235}{f_{y,\text{flange}}}\right)^{0.5}$ for $y-y$ $\alpha^* = 0.55\left(\frac{235}{f_{y,\text{flange}}}\right)^{0.5}$ for $z-z$	Yun et al., 2023 [37]
Hollow section	Hot-finished	$\alpha^*(\bar{\lambda} - 0.1)$	$\alpha^* = 0.24(\frac{235}{f_y})^{0.5}$	Meng et al., 2020 [30]
		$\alpha^*(\bar{\lambda} - 0.2)$	$\alpha^* = \alpha(\frac{235}{f_y})^{0.7}$	Saufnay et al., 2024 [35]
	Cold-formed	$\alpha^*(\bar{\lambda} - 0.2)$	$\alpha^* = \alpha(\frac{235}{f_y})^{0.5}$	Somodi et al., 2018 [36]
		$\alpha^*(\bar{\lambda} \cdot \epsilon - 0.2)$	$\alpha^* = \alpha$	Fang et al., 2018 [38]
		$\alpha^*(\bar{\lambda} - 0.1)$	$\alpha^* = 0.56(\frac{235}{f_y})^{0.5}$	Meng et al., 2020 [30]

Identified Limitations and Research Objectives

The literature review has highlighted that the buckling behaviour of unequal-leg angle sections is governed by complex interactions between torsional and flexural instability modes, which are not fully captured by current design provisions. Existing buckling curves were mainly calibrated on conventional steel grades and symmetric cross-sections, leading to excessive conservatism for low slenderness values and potentially unsafe predictions in the transition region between buckling modes.

The review has also shown that residual stresses appear to be only weakly dependent on the yield strength, while the relative influence of imperfections decreases as the yield strength increases. Consequently, the direct application of current imperfection factors and buckling curves to high-strength steel members may not accurately represent their actual structural behaviour.

Although several modified imperfection formulations have been proposed in the literature for different cross-section typologies, no specific investigations have yet been conducted for unequal-leg angle sections. This highlights the need for improved design approaches capable of accounting for both the interaction between torsional and flexural buckling modes and the influence of high-strength steels on imperfection sensitivity.

The present work therefore aims to investigate the buckling behaviour of unequal-leg angle sections made of high-strength steel and to assess the suitability of existing design approaches, with the objective of proposing improved imperfection formulations and more accurate buckling design recommendations.

Chapter 3

Numerical Model Description and Assumptions

The present work is part of the broader research framework initiated in the doctoral thesis of Loris Saufnay [35] and the master's thesis of Louis Duchêne [39], both focusing on the structural behaviour and design of high-strength steel members. More specifically, the objective of this study is to investigate the buckling behaviour of hot-rolled unequal-leg angle sections and to contribute to the development of improved buckling design formulations for high-strength steels, addressing the limitations identified in Section 2.2.2.

Similarly to these previous studies, the numerical models developed in the present work are implemented using the finite element software FineLG. This software was jointly developed by the University of Liège and the Greisch engineering office and has been extensively used for the numerical investigation of instability phenomena in steel structures.

FineLG has already been validated in numerous previous studies involving geometrically and materially nonlinear analyses of steel members subjected to instability phenomena, which justifies its selection for the present work.

3.1 Scope

This thesis focuses on the buckling behaviour of pin-ended hot-rolled unequal-leg angle section members subjected to axial compression. In order to investigate the influence of the material strength over a broad range of applications, steel grades ranging from conventional mild steels up to high-strength steels are considered, covering yield strengths from S235 to S690.

Within the scope of the present study, only Class 1 to Class 3 cross-sections are considered. Class 4 sections are intentionally excluded in order to avoid local buckling phenomena and the associated reduction of the effective cross-sectional area. This assumption also enables the use of beam element models, avoiding the need for more computationally demanding shell or plate finite element models.

It should be noted that the cross-section classification adopted in this study is based on the rules proposed within the ANGHELY project, which are presented in a later section.

3.2 General Modelling Assumptions

The numerical model used to represent the behaviour of unequal-leg angle members is based on beam finite elements. Following a mesh sensitivity analysis, a discretisation consisting of 10 finite elements along the member length was found to provide sufficient accuracy while maintaining a reasonable computational cost.

The ultimate resistance is determined through geometrically and materially nonlinear analyses with imperfections (GMNIA). The nonlinear analysis is performed using the arc-length method, allowing the post-buckling response and the descending branch after instability to be accurately captured.

The beam elements include seven degrees of freedom per node, namely three translations, three rotations, and one warping degree of freedom. The inclusion of warping is essential since unequal-leg angle sections may exhibit coupled torsional–flexural buckling behaviour. This effect becomes particularly significant when torsional deformations govern the structural response. The beam formulation is based on Vlasov thin-walled beam theory, allowing the coupling between flexure, torsion, and warping to be captured.

The loading configuration consists of a concentric axial compressive load applied through the centroid of the cross-section, i.e. without load eccentricity. The member is assumed to be pin-ended with torsional restraint and free warping at both ends. Lateral translations are prevented at the supports, while axial displacement is allowed at one end. The adopted boundary conditions therefore correspond to pinned supports with restrained torsion and free warping.

3.3 Material Law

An elastic–perfectly plastic material model, as recommended in Eurocode 3 Part 1-14 [4], is adopted for all numerical simulations. The Young's modulus is taken equal to $E = 210$ GPa, while the yield strength is denoted by f_y.

Strain hardening is neglected in the present study. However, a small tangent stiffness equal to $E/10000$ is introduced in the plastic range in order to improve numerical convergence and ensure the stability of the nonlinear solution procedure.

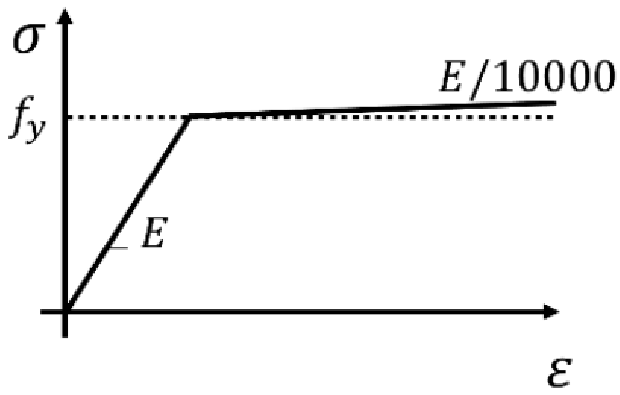

Figure 3.1: linear elastic – perfectly plastic material model with a nominal plateau [4]

3.4 Geometrical and Material Imperfections

Two types of initial geometric imperfections are considered in the present study.

The first imperfection corresponds to a pure minor-axis flexural deformation, denoted by F_v . A semi-sinusoidal imperfection shape is adopted, with a maximum amplitude equal to $L/1000$ at mid-height (see Figure 3.2 (a)). This imperfection is introduced using the first eigenmode obtained from a linear buckling analysis (LBA).

The second imperfection consists of a combined torsional–flexural imperfection shape, denoted by F_vF_uT. In this case, semi-sinusoidal flexural imperfections are introduced simultaneously about both the major and minor axes, each with a maximum amplitude equal to $L/1000$ at mid-height. These flexural imperfections are combined with a torsional imperfection obtained by imposing a rotation along the member length, leading to a maximum twist angle equal to $\arctan(L/1000)$ at mid-height (see Figure 3.2).

The combined shape is obtained through the linear superposition of the individual flexural and torsional components.

The flexural imperfections about the major and minor axes, together with the torsional imperfection, are introduced using positive amplitudes.

The linear buckling analyses used to generate the eigenmodes are performed on geometrically perfect members without material nonlinearities. The flexural eigenmodes obtained from the linear buckling analyses are subsequently normalised and scaled to the prescribed amplitudes before being combined with the torsional imperfection.

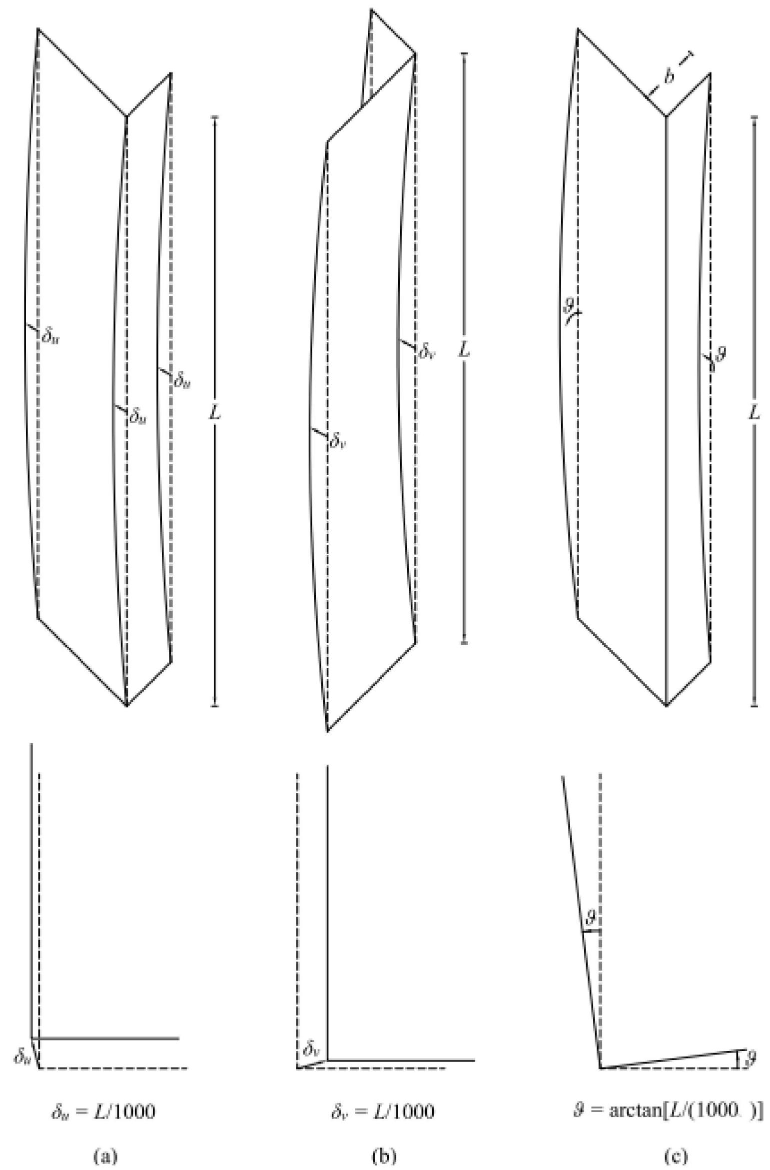

Figure 3.2: Initial geometric imperfection shapes: (a) major-axis flexural, (b) minor-axis flexural and (c) torsional according to [2]

Material imperfections, more specifically residual stresses, are represented using a bilinear residual stress distribution with a peak value equal to $0.3f_y^*$, where $f_y^* = 235$ MPa, leading to a maximum residual stress of approximately 70 MPa (see Figure 3.3). This residual stress pattern is commonly adopted for hot-rolled angle sections and is recommended in several international design recommendations, including EN 1993-1-14:2025 [4].

As discussed in the literature review, experimental investigations have shown that residual stress magnitudes are only weakly dependent on the steel grade. Furthermore, the adopted residual stress distribution has been shown to provide conservative predictions for high-strength steel members. Consequently, the same residual stress model is applied for all considered steel grades, including grades up to S690.

It should also be noted that only limited experimental investigations on residual stress distributions in unequal-leg angle sections are currently available in the literature. Consequently, the residual stress distribution commonly adopted for equal-leg angle sections is also considered for unequal-leg angle sections in the present study. A similar assumption was adopted by Dai et al. [2] in their numerical investigations.

The validation of the residual stress distribution is however beyond the scope of the present work, mainly due to limited experimental data currently available for unequal-leg angle sections.

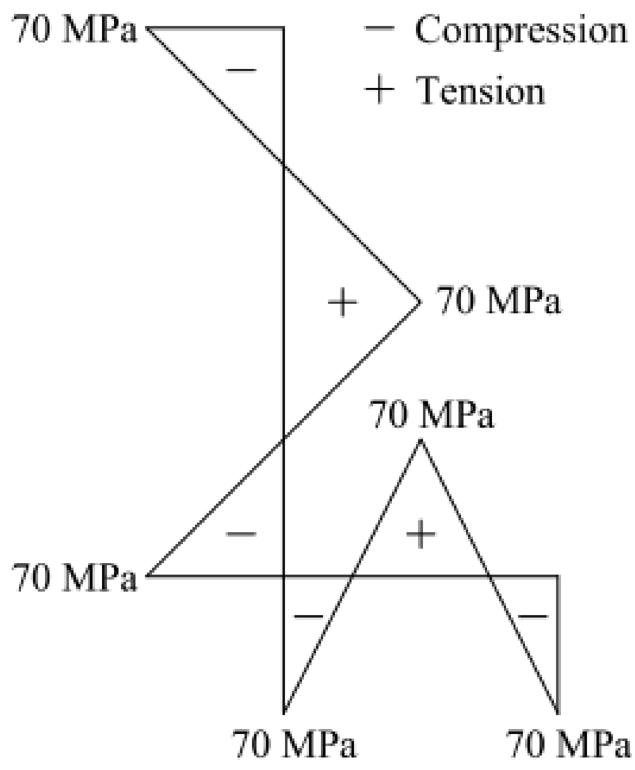

Figure 3.3: Residual stress distribution according to [2]

Chapter 4

Numerical Model Validation

The objective of this chapter is to validate the assumptions and modelling choices adopted for the numerical model presented in the previous chapter. The validation process includes comparisons between numerical predictions and available experimental results, together with several sensitivity analyses aimed at assessing the influence of the main modelling parameters.

Particular attention is devoted to the influence of the mesh density, material modelling assumptions and geometrical imperfections. The relevance of the adopted modelling strategy is evaluated through comparisons of ultimate resistances, buckling responses, and load–displacement curves.

4.1 Description of the Selected Experimental Tests

The experimental results used for the validation of the numerical model are taken from the investigations conducted by Kitipornchai and Lee [5] and Liu et al. [6].

The experimental campaign conducted by Kitipornchai and Lee [5] consisted of six hot-rolled unequal-leg angle section members with different cross-sectional dimensions and member lengths. The specimens were tested under concentric axial compression using pin-ended boundary conditions with restrained torsion. No specific information was provided regarding the warping boundary conditions. However, free warping was assumed in the present study, considering the practical difficulty of fully restraining warping in experimental setups.

The compressive load was applied incrementally, with the magnitude and loading rate adjusted depending on the proximity to failure and the development of buckling deformations. The selected cross-sections were characterised by relatively large width-to-thickness ratios in order to promote torsional–flexural buckling behaviour.

In addition, tensile coupon tests were carried out in order to determine the material properties of the tested specimens, including the yield strength and Young's modulus. An average Young's modulus equal to 2.14×10^5 MPa was reported and is therefore adopted in the corresponding numerical simulations.

The specimen dimensions, member lengths, yield strengths, relative slenderness values, and experimentally obtained ultimate loads are summarised in Table 4.1. The experimental results showed failure modes characterised by coupled torsional–flexural buckling behaviour, which makes this experimental campaign particularly suitable for the validation of the present numerical model.

Section [mm]	Effective length [mm]	f_y [MPa]	$\bar{\lambda}$ [-]	Ultimate load [kN]
64 × 51 × 5	700	295	0.75	141
64 × 51 × 5	900	295	0.97	135
76 × 51 × 5	800	312	0.86	143
76 × 51 × 5	1000	312	1.08	123
102 × 76 × 6.5	1200	296	0.86	277
102 × 76 × 6.5	1500	296	1.07	190

Table 4.1: Geometrical properties, relative slenderness values and experimental ultimate loads of the specimens tested by Kitipornchai and Lee [5]

The experimental campaign conducted by Liu et al. [6] comprised a total of 26 specimens with identical cross-sectional dimensions, namely L76×51×6.4 unequal-leg angle sections. The investigated parameters included both the member length and the load eccentricity.

Within the scope of the present study, only the concentrically loaded specimens are considered. Consequently, five tests are directly relevant for the validation of the numerical model. The selected specimens correspond to two different member slenderness levels, denoted as 12C and 18C. The 12C series was tested three times (12C-a, 12C-b and 12C-c), while the 18C series was tested twice (18C-a and 18C-b). The corresponding geometrical and mechanical properties are summarised in Table 4.2.

Similarly to the experimental campaign conducted by Kitipornchai and Lee [5], the specimens were tested under pin-ended boundary conditions with restrained torsion. No information was provided regarding the warping boundary conditions. Consequently, free warping was again assumed in the present numerical simulations, considering the practical difficulty of fully restraining warping in experimental setups.

During the tests, the compressive load was applied at a constant loading rate equal to 6 kN/min until failure, while both the applied load and the corresponding deformations were recorded at 1 s intervals.

Material coupon tests were also carried out in order to determine the mechanical properties of the specimens. The average yield strength and Young's modulus were reported as 356 MPa and 2.03×10^5 MPa, respectively. These values were therefore adopted in the corresponding numerical simulations.

In contrast with the experimental campaign of Kitipornchai and Lee [5], the initial geometric imperfections of the specimens were also measured. The measured out-of-straightness was characterised by an average amplitude equal to approximately $L/1607$. Furthermore, the measured initial imperfections systematically exhibited a concave deformation towards the centroid of the cross-section, which is consistent with the F_v imperfection shape considered in the present study.

Unlike the previous experimental campaign, all five concentrically loaded specimens failed through a minor-axis flexural buckling mode.

A particular interest of this experimental campaign lies in the availability of experimental P–Δ curves, especially for specimen 12C-c. These results provide valuable information for the validation of the post-buckling response predicted by the numerical model.

Specimen	Section [mm]	Effective length [mm]	f_y [MPa]	$\bar{\lambda}$ [-]	Ultimate load [kN]
12C-a	76×51×6.4	1237	356	1.5	103.6
12C-b	76×51×6.4	1237	356	1.5	98.4
12C-c	76×51×6.4	1237	356	1.5	106.5
18C-a	76×51×6.4	1845	356	2.2	46.8
18C-b	76×51×6.4	1845	356	2.2	50.5

Table 4.2: Geometrical properties, relative slenderness values and experimental ultimate loads of the concentrically loaded specimens tested by Liu et al. [6]

The selected experimental campaigns provide complementary validation data covering both torsional–flexural and pure flexural buckling behaviours, as well as ultimate loads and post-buckling responses. These experimental results are used in the following sections to assess the influence of the modelling assumptions and to validate the numerical model developed in the present study.

4.2 Verification of the Elastic Buckling Behaviour

Before analysing the nonlinear response, the elastic buckling behaviour of the numerical model is verified in order to ensure that the implemented beam formulation correctly reproduces the expected elastic instability behaviour. This comparison is not intended to provide an independent validation of the model, since both the analytical expressions and the numerical beam formulation are based on Vlasov thin-walled beam theory. Rather, it is used as a consistency check to assess whether the adopted numerical formulation, boundary conditions and warping assumptions correctly reproduce the expected elastic torsional–flexural buckling behaviour.

For this verification study, the hot-rolled unequal-leg angle section L100×65×12 is considered. The analyses are performed for steel grade S235 and for member lengths ranging from 100 mm to 3350 mm in order to investigate the evolution of the elastic critical loads over a wide slenderness range.

The selected member lengths cover both short members, for which torsional effects are dominant, and slender members, for which the structural response progressively becomes governed by flexural buckling.

The elastic critical loads obtained numerically from linear buckling analyses are compared with the analytical torsional–flexural critical load $N_{cr,TF}$ introduced previously. The comparison is carried out for two different warping boundary conditions, namely free warping and restrained warping.

The results obtained for free warping conditions are shown in Figure 4.1. The numerical critical loads are in very good agreement with the analytical predictions based on Vlasov theory. This agreement confirms the consistency between the analytical formulation and the numerical beam model when the same warping assumptions are adopted. The figure also shows that, for long members, the torsional–flexural critical load progressively approaches the minor-axis flexural critical load $N_{cr,v}$, indicating that the governing instability mode becomes predominantly flexural as the member slenderness increases.

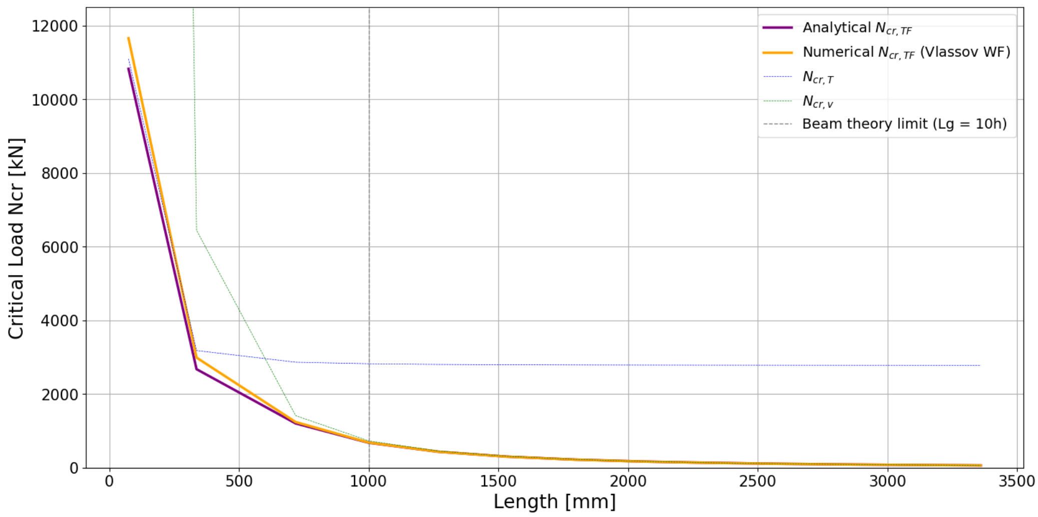

Figure 4.1: Comparison between analytical and numerical elastic critical loads for the L100×65×12 section considering Vlasov theory with free warping conditions

The corresponding analytical-to-numerical ratios are presented in Figure 4.2. For member lengths larger than the beam theory limit $L_g = 10h$, the ratio remains close to unity, confirming that the numerical model accurately reproduces the analytical elastic buckling response in the range where beam theory assumptions are considered valid. Larger discrepancies are observed for shorter members, for which the assumptions of classical beam theory become less representative.

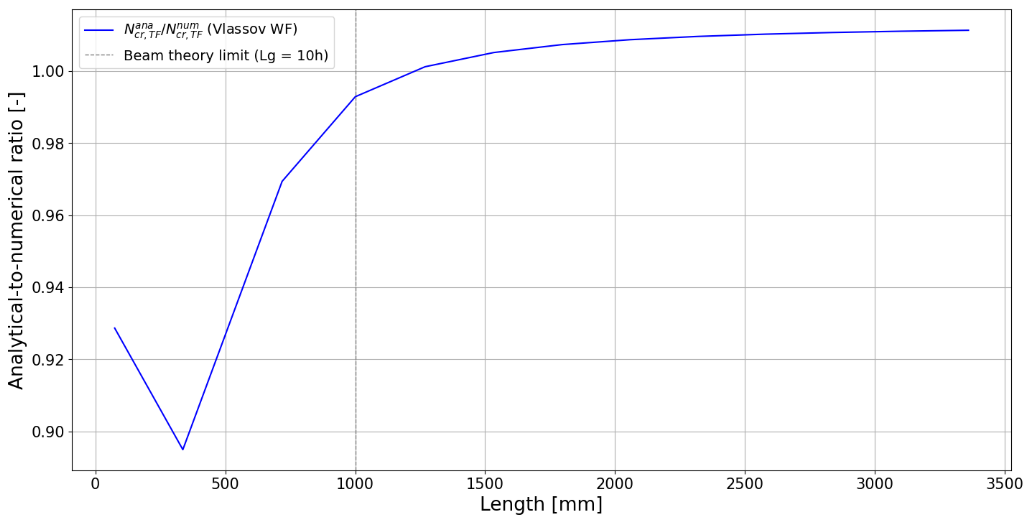

Figure 4.2: Analytical-to-numerical critical load ratio for the L100×65×12 section considering Vlasov theory with free warping conditions

The same comparison is then performed by restraining warping at the member ends. The results are shown in Figure 4.3. A significant influence of the warping boundary conditions is observed, especially for short members. When warping is restrained, the numerical critical load increases markedly for small member lengths due to the additional torsional stiffness provided by the restraint against warping deformation.

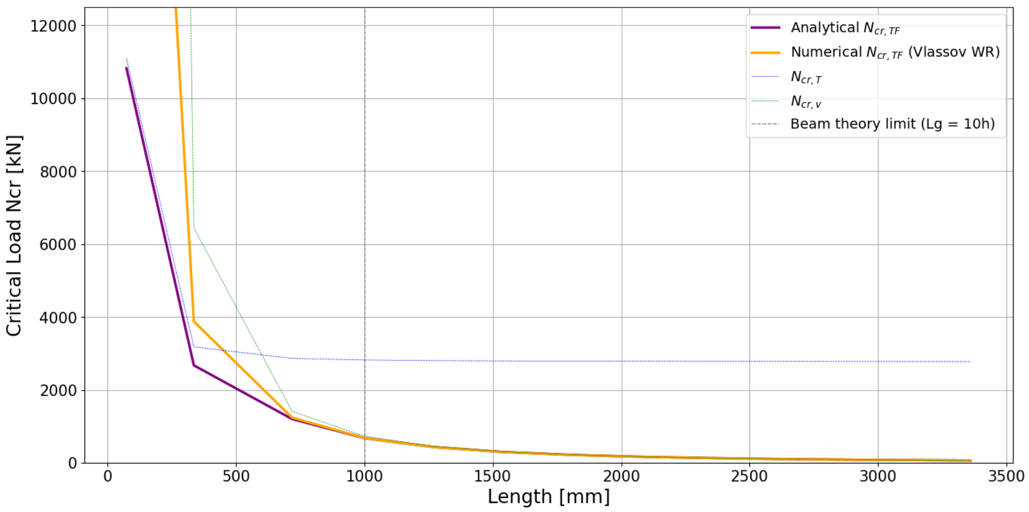

Figure 4.3: Comparison between analytical and numerical elastic critical loads for the L100×65×12 section considering Vlasov theory with restrained warping conditions

This behaviour is also highlighted in Figure 4.4, where large discrepancies are observed for short members. These differences are mainly attributed to the strong influence of warping restraint in the short-length range, where torsional effects are dominant. As the member length increases, the influence of the warping boundary conditions progressively decreases and the numerical results converge towards the analytical predictions. Beyond the beam theory limit $L_g = 10h$, the ratio becomes close to unity, indicating that the numerical and analytical formulations provide consistent results for sufficiently slender members.

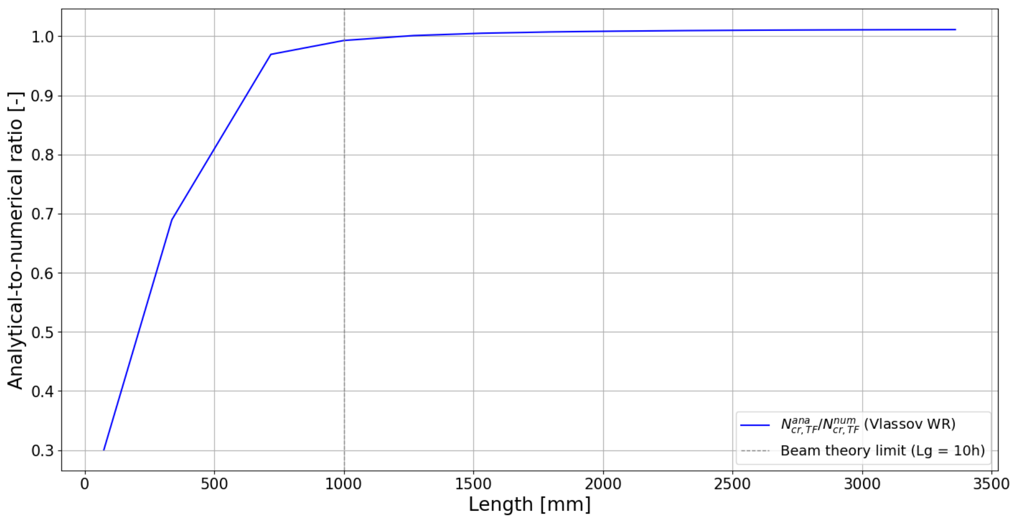

Figure 4.4: Analytical-to-numerical critical load ratio for the L100×65×12 section considering Vlasov theory with restrained warping conditions

These results confirm that the adopted beam finite element formulation is able to reproduce the expected elastic torsional–flexural buckling behaviour when the corresponding warping assumptions are consistently defined. They also highlight the important influence of warping boundary conditions on the elastic critical load, particularly for short members where torsional effects govern the response.

However, this verification should be interpreted with caution. Since both the analytical expressions and the numerical formulation are based on Vlasov beam theory, the comparison mainly represents a theoretical consistency check rather than an independent validation of the numerical model. Nevertheless, it confirms that the implementation of the beam formulation, the adopted boundary conditions and the calculation of the elastic critical loads are coherent with the analytical framework used in the present study.

Furthermore, as discussed previously in Section 2.1.1, the combined torsional–flexural critical load systematically corresponds to the minimum value among the considered elastic critical loads. This indicates that the investigated members are predominantly governed by coupled torsional–flexural instability rather than by pure flexural or pure torsional buckling modes over the considered slenderness range.

It may also be observed that, for short members, the combined torsional–flexural critical load remains close to the pure torsional critical load $N_{cr,T}$, indicating a dominant influence of torsional effects. As the member length increases, the combined critical load progressively converges towards the minor-axis flexural critical load $N_{cr,v}$. A transition zone can therefore be identified between these two regimes, highlighting the gradual evolution from torsion-dominated behaviour to predominantly flexural instability for slender members.

Based on these observations, the numerical model with Vlasov beam elements and free warping boundary conditions is retained for the subsequent nonlinear analyses, consistently with the assumptions adopted for the experimental validation tests.

4.3 Mesh Sensitivity Analysis

Since the numerical model is based on the finite element method, the accuracy of the results depends in particular on the mesh discretisation adopted for the member. It is therefore necessary to determine a mesh density capable of accurately capturing both the structural behaviour and the ultimate resistance.

However, the computational cost should remain reasonable and should not be unnecessarily increased. An appropriate balance between accuracy and computational efficiency must therefore be achieved. Particular attention is given to the influence of the mesh density on both the predicted ultimate resistance and the post-buckling response.

For this purpose, the L100×65×12 unequal-leg angle section was analysed using three different mesh densities consisting of 5, 10 and 20 beam finite elements along the member length. The mesh consisting of 20 elements was considered sufficiently refined to serve as a reference solution for the comparison.

For all analyses, a steel grade S235 was considered together with a member length of approximately 1270 mm, corresponding to a relative slenderness close to $\bar{\lambda} = 1.0$. This slenderness level is generally associated with significant post-buckling effects and is therefore particularly relevant for the present investigation.

The combined geometric imperfection shape $F_v F_u T$ was adopted for this study, since it is expected to be the most sensitive to the mesh density due to the presence of torsional deformations.

The obtained ultimate loads and the relative are summarised in Table 4.3. The relative errors are calculated with respect to the solution obtained using 20 elements.

The corresponding mechanical responses and P–Δ curves are presented in Figure 4.5.

Number of Elements	5	10	20
Ultimate load [kN]	329.61	276.15	276.17
Relative Error [%]	19.35	0.01	-

Table 4.3: Influence of the mesh discretisation on the predicted ultimate load

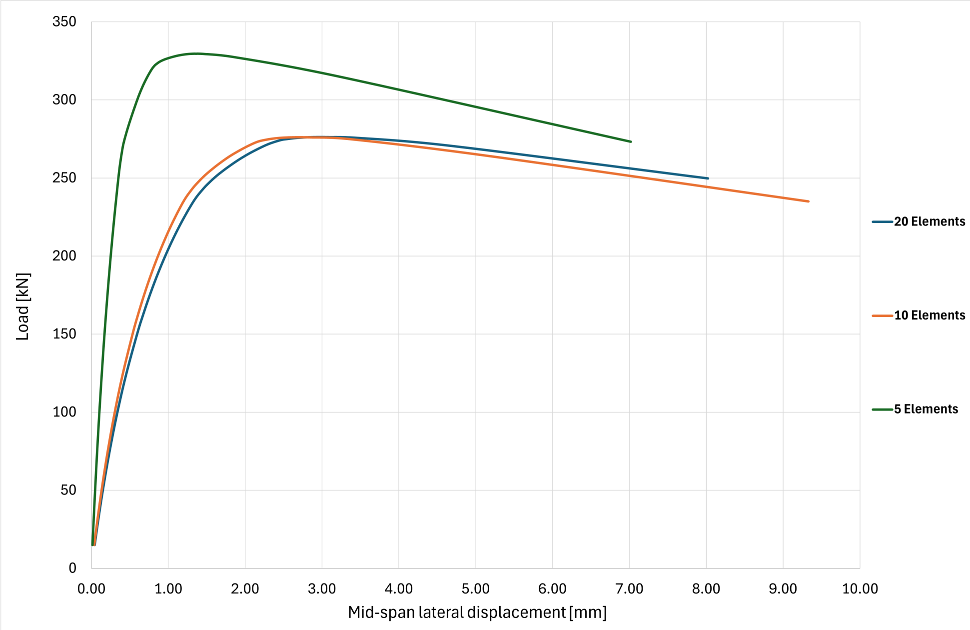

Figure 4.5: Comparison of the numerical P–Δ responses obtained using different mesh discretisations

The results related to the predicted ultimate loads show that a mesh consisting of 5 elements is not sufficient to accurately capture the structural response. In particular, the obtained ultimate resistance is significantly overestimated, leading to unsafe predictions.

In contrast, the mesh consisting of 10 elements provides an ultimate load almost identical to that obtained using 20 elements, with a negligible relative error.

A similar conclusion can be drawn from the comparison of the numerical P–Δ curves. The model using 5 elements does not correctly reproduce either the peak resistance or the post-buckling response. On the contrary, the response obtained using 10 elements is almost identical to that obtained using 20 elements over the entire equilibrium path.

Consequently, a discretisation consisting of 10 beam finite elements is considered sufficient to accurately capture both the ultimate resistance and the post-buckling behaviour, while maintaining a reasonable computational cost.

It should also be noted that a similar discretisation strategy was adopted in the numerical investigations conducted by Dai et al. [2], Saufnay [35], and Duchêne [39].

4.4 Material Law Sensitivity

Another parameter of interest concerns the adopted material constitutive law. According to EN 1993-1-14:2025 [4], hot-rolled steels up to grade S460, as well as steels above S460 satisfying specific carbon content requirements, may be assumed to exhibit a well-defined yield point.

The standard also specifies several material models that may be adopted in materially nonlinear finite element analyses, depending on the required accuracy and strain range:

1. linear elastic–perfectly plastic material model without strain hardening,
2. linear elastic–perfectly plastic material model with a nominal tangent stiffness for numerical stability,
3. linear elastic–linear hardening plastic material model,
4. linear elastic–nonlinear hardening material model based on experimental coupon-test stress–strain curves.

In the present study, no experimental stress–strain curves obtained from coupon tests were available. Consequently, two simplified material models are investigated and compared.

The first model corresponds to a linear elastic–perfectly plastic material law with a nominal tangent stiffness equal to $E/10000$ introduced in the plastic range in order to improve numerical stability (see Figure 3.1).

The second model corresponds to a trilinear elastic–plastic material law including strain hardening, as illustrated in Figure 4.6. The parameters of this model are determined according to the recommendations of EN 1993-1-14:2025 [4].

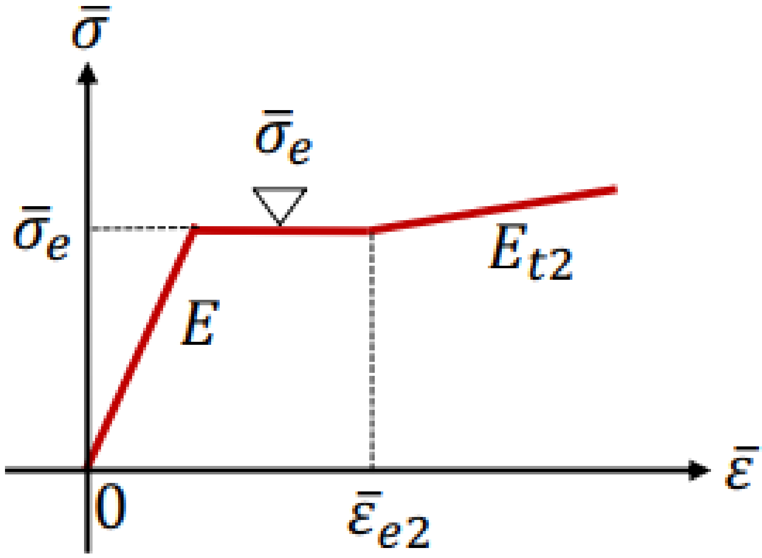

Figure 4.6: Trilinear material model including strain hardening

The adopted parameters are defined according to EN 1993-1-14:2025 [4]. The detailed calculation procedure and the determination of the different parameters are provided in Appendix 7.1.The resulting values are summarised in Table 4.4.

Parameter	**Meaning**	**Value**
$\bar{\sigma}_e$	Yield stress	235 MPa
$\bar{\epsilon}_{e2}$	Strain at beginning of hardening	0.015
E_{t2}	Strain hardening modulus	1616.17 MPa

Table 4.4: Parameters of the adopted trilinear material model according to EN 1993-1-14:2025

The comparison between these two constitutive laws allows the influence of strain hardening on the predicted ultimate resistance and post-buckling response to be evaluated. The obtained results are presented through the numerical P–Δ curves shown in Figure 4.7. The comparison is performed for the same member geometry, boundary conditions and imperfection configuration adopted in the mesh sensitivity analysis.

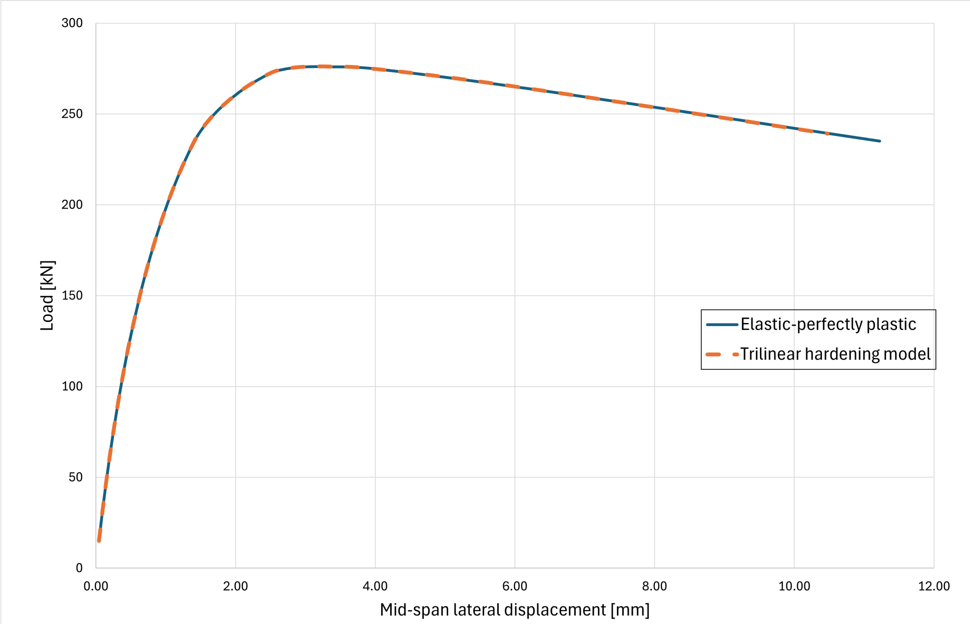

Figure 4.7: Comparison of the numerical P–Δ responses obtained using the elastic–perfectly plastic and trilinear material models

The comparison between the two constitutive laws shows that the influence of strain hardening on both the ultimate resistance and the post-buckling response remains very limited for the considered member. This limited influence can be explained by the fact that, for members with relative slenderness values greater than 0.2, the structural response is primarily governed by global instability rather than by the development of large plastic strains.

Only negligible differences are observed between the two numerical responses, both in terms of ultimate resistance and post-buckling behaviour, indicating that the elastic–perfectly plastic material model is sufficient to accurately capture the structural behaviour within the scope of the present study.

Consequently, the elastic–perfectly plastic material law is retained for the remainder of the numerical investigations, due to its simplicity, robustness and reduced computational cost. Similar conclusions were also reported by Saufnay [35].

4.5 Influence of the geometrical imperfections

Initial geometric imperfections constitute one of the most influential parameters governing the buckling behaviour of steel members. In practice, perfectly straight members do not exist due to manufacturing tolerances, residual deformations induced during fabrication, transport, or assembly processes. Consequently, real structural members always exhibit initial out-of-straightness and geometric deviations from the ideal configuration.

The presence of these imperfections significantly affects the structural response under compression. Indeed, geometric imperfections introduce additional bending moments from the early stages of loading, leading to a reduction of the ultimate resistance and an increase in the sensitivity to instability phenomena. Their influence becomes particularly important for slender members and for cross-sections exhibiting coupled instability modes, such as unequal-leg angle sections subjected to torsional–flexural buckling.

Furthermore, the shape and orientation of the initial imperfections may strongly influence both the governing buckling mode and the post-buckling response. In the case of unequal-leg angle sections, different combinations of flexural and torsional imperfections may lead to significantly different structural responses due to the interaction between minor-axis flexure, major-axis flexure, and torsion.

It is therefore essential to assess the influence of the adopted imperfection shapes on the numerical predictions in order to identify the most representative and mechanically relevant imperfection configurations for the subsequent parametric investigations.

In accordance with the guidance provided in EN 1993-1-14:2025 [4], geometric imperfections considered in nonlinear analyses should be both realistic and representative of the most unfavourable instability mode expected for the structural member. The standard further specifies that, when the governing imperfection shape is not clearly identifiable, several imperfection forms and combinations should be investigated in order to determine the most detrimental realistic configuration.

In the particular case of unequal-leg angle sections, only limited information is currently available in the literature regarding the most representative imperfection configurations. Furthermore, the available experimental investigations exhibit different governing instability modes. The experimental campaign conducted by Kitipornchai and Lee [5] showed coupled torsional–flexural buckling behaviour, whereas the concentrically loaded specimens tested by Liu et al. [6] failed predominantly through minor-axis flexural buckling.

4.5.1 Definition of the investigated imperfection configurations

Consequently, several geometric imperfection configurations are investigated in the present study in order to evaluate their influence on the predicted structural response and to identify the most representative imperfection configuration for the subsequent numerical investigations.

The investigated imperfections are based on the individual flexural and torsional imperfection shapes previously introduced in Section 3.4. The considered imperfections are:

- F_v: minor-axis flexural imperfection,
- F_u: major-axis flexural imperfection,
- T: torsional imperfection.

The flexural imperfections are introduced using semi-sinusoidal deformation shapes with a maximum amplitude equal to $L/1000$ at mid-height, while the torsional imperfection is introduced through a twist angle reaching a maximum value equal to $\arctan(L/1000)$ at mid-height.

Combined imperfections are generated through the linear superposition of the individual imperfection components. Different sign combinations are also investigated in order to account for the possible relative orientations between flexural and torsional deformations.

A positive sign corresponds to the reference orientation adopted for each imperfection component and illustrated in Figure 4.8.

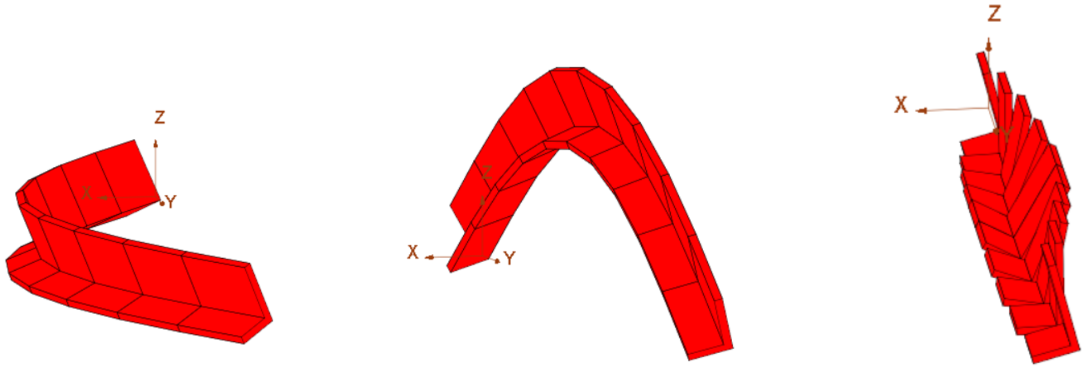

(a) Positive minor-axis flexural imperfection $+F_v$

(b) Positive major-axis flexural imperfection $+F_u$

(c) Positive torsional imperfection $+T$

Figure 4.8: Positive geometric imperfection components considered in the study

For the minor-axis flexural imperfection F_v, a positive sign corresponds to a deformation in which the concave side of the member bends towards the centroid of the cross-section. This imperfection orientation is consistent with the measured initial out-of-straightness reported by Liu et al. [6].

For the major-axis flexural imperfection F_u, a positive sign corresponds to a deformation towards the positive direction of the major principal axis defined by the local coordinate system of the member.

For the torsional imperfection T, a positive sign corresponds to a twist rotation following the positive rotational direction of the local beam coordinate system.

Conversely, a negative sign corresponds to the same imperfection shape applied in the opposite direction.

The investigated imperfection combinations are summarised below:

- F_v,
- $F_v + T$,
- $F_v - T$,
- $+F_v + F_u + T$,
- $+F_v + F_u - T$,
- $-F_v + F_u + T$,
- $+F_v - F_u + T$,
- $+F_v - F_u - T$,
- $-F_v + F_u - T$,
- $-F_v - F_u + T$.

4.5.2 Comparison with Kitipornchai and Lee experimental results

The influence of the different imperfection configurations is evaluated through comparisons between the numerical ultimate loads and the experimental resistances reported by Kitipornchai and Lee [5]. The obtained ratios P_{num}/P_{exp} are summarised in Table 4.5.

Imperfection	64×51×5		76×51×5		102×76×6.5		**Mean**	**COV [%]**
Length [mm]	700	900	800	1000	1200	1500		
Pure flexural and flexural–torsional imperfections								
F_v	0.89	0.78	0.92	0.85	0.83	0.99	0.88	8.3
$F_v + T$	0.90	0.80	0.93	0.86	0.84	1.00	0.89	7.9
$F_v - T$	0.90	0.80	0.94	0.87	0.84	1.00	0.89	8.2
Combined flexural–torsional imperfections								
$+F_v + F_u + T$	0.85	0.74	0.88	0.81	0.78	0.92	0.83	7.9
$+F_v + F_u - T$	0.95	0.90	1.05	0.96	0.95	1.15	**0.995**	**9.0**
$-F_v + F_u + T$	0.88	0.81	0.91	0.85	0.82	1.01	0.88	8.4
$+F_v - F_u + T$	0.95	0.88	1.00	0.93	0.91	1.11	0.96	8.5
$+F_v - F_u - T$	0.86	0.74	0.88	0.81	0.78	0.92	0.83	8.0
$-F_v + F_u - T$	0.82	0.70	0.80	0.74	0.73	0.86	0.77	8.0
$-F_v - F_u + T$	0.82	0.69	0.80	0.73	0.72	0.83	0.77	7.6

Table 4.5: Influence of the investigated geometric imperfection configurations on the numerical-to-experimental resistance ratios

The obtained results clearly show that the predicted resistance is strongly influenced by the adopted imperfection configuration. Significant differences are observed depending not only on the considered imperfection components, but also on their relative signs.

The investigated imperfection configurations lead to average numerical-to-experimental resistance ratios ranging from approximately 0.77 to 1.00.

The isolated minor-axis flexural imperfection F_v already provides satisfactory predictions, with an average numerical-to-experimental resistance ratio of approximately 0.88. Including a torsional component ($F_v \pm T$) modifies this value by less than 2%, indicating that the structural response remains predominantly governed by minor-axis flexural buckling. This behaviour is mechanically consistent, as the torsional imperfection mainly induces a rotation of the cross-section rather than an additional global lateral displacement, thus exerting only a limited influence on the second-order effects associated with flexural instability.

In contrast, the combined $F_v F_u T$ configurations exhibit a significantly larger scatter depending on the adopted sign combination. The average resistance ratios vary from approximately 0.77 for the most conservative configurations up to 0.995 for the $+F_v + F_u - T$ configuration, corresponding to a variation of about 22% between the extreme cases.

A more pronounced influence of the torsional imperfection is however observed when it is combined simultaneously with both major- and minor-axis flexural imperfections ($F_v F_u T$ configurations). In this case, significantly larger variations are obtained depending on the adopted sign combinations.

This behaviour may be explained by the stronger coupling between flexural and torsional deformations when both flexural imperfection components are introduced. The addition of the major-axis flexural imperfection appears to promote a deformation pattern that is more compatible with the torsional–flexural buckling mode observed experimentally for unequal-leg angle sections. Consequently, the torsional imperfection becomes more influential on the global structural response. This increased sensitivity may also be attributed to the inherent monosymmetry of unequal-leg angle sections, for which the centroid and shear centre do not coincide, naturally promoting a stronger coupling between flexure about the principal axes and torsion.

In this configuration, the member no longer deforms predominantly in a single flexural plane. The simultaneous presence of major-axis flexure, minor-axis flexure and torsion promotes a three-dimensional instability mode that is closer to the experimentally observed torsional–flexural buckling behaviour.

A possible additional explanation for this increased sensitivity may also be related to the development of torsional stresses when a fully coupled torsional–flexural instability mode is activated. As discussed by Beyer et al. [40], torsional deformations may generate significant Saint-Venant shear stresses, which contribute to the von Mises stresses and therefore reduce the axial resistance of the member.

Furthermore, the results indicate that the relative orientation of the flexural and torsional imperfections plays a major role in the predicted resistance. Depending on the selected sign combination, the torsional rotation may either amplify or partially counteract the flexural deformations associated with the governing instability mode. This explains the significant differences observed between some imperfection configurations.

It should however be noted that this interpretation remains mainly qualitative and is based on mechanical observations drawn from the present numerical results. To the author's knowledge, only limited studies are currently available in the literature regarding the specific influence of combined imperfection signs on the torsional–flexural buckling behaviour of unequal-leg angle sections.

Among all investigated configurations, the imperfection combination denoted $+F_v + F_u - T$ provides the closest agreement with the experimental results, with an average resistance ratio equal to 0.995 and a coefficient of variation equal to 9.0%. This configuration therefore appears to be the most representative of the experimentally observed behaviour.

It should however be noted that the actual geometric imperfections of the tested specimens were not reported in the experimental campaign conducted by Kitipornchai and Lee [5]. Consequently, the adopted imperfection amplitudes may differ from the real imperfections present in the tested members. In particular, the actual imperfection amplitudes could have been smaller than the adopted value of $L/1000$, which may partly explain the generally conservative character of the numerical predictions.

Conversely, several sign combinations involving negative minor-axis imperfections lead to significantly lower resistance predictions, with average resistance ratios as low as approximately 0.77. These results confirm the high sensitivity of unequal-leg angle sections to the orientation of the initial geometric imperfections.

The obtained observations therefore indicate that not only the imperfection amplitude, but also the relative orientation and interaction between flexural and torsional imperfections, have a major influence on the prediction.

4.5.3 Comparison with Liu et al. experimental results

In order to complement the previous observations, additional comparisons are performed using the experimental results reported by Liu et al. [6].

Three imperfection configurations are retained for this purpose. The isolated minor-axis flexural imperfection F_v is considered in order to remain consistent with the experimentally observed minor-axis flexural buckling behaviour reported by Liu et al. [6]. The combined imperfection configuration $+F_v + F_u + T$ is investigated due to its consistency with the torsional–flexural buckling behaviour observed by Kitipornchai and Lee [5], as well as with the numerical modelling assumptions adopted by Dai et al. [2]. Finally, the imperfection configuration $+F_v + F_u - T$ is also considered since it provided the closest agreement with the experimental results obtained from the experimental campaign of Kitipornchai and Lee [5].

In addition to the standard imperfection amplitude equal to $L/1000$, an additional numerical analysis is also performed using an imperfection amplitude equal to $L/1607$, corresponding to the average geometric imperfection amplitude measured experimentally by Liu et al. [6]. This additional analysis allows the influence of the imperfection amplitude on the predicted structural response to be further assessed.

The numerical and experimental P–Δ responses obtained for specimen 12C-c are compared in Figure 4.9, while the corresponding numerical-to-experimental ultimate load ratios are summarised in Table 4.6.

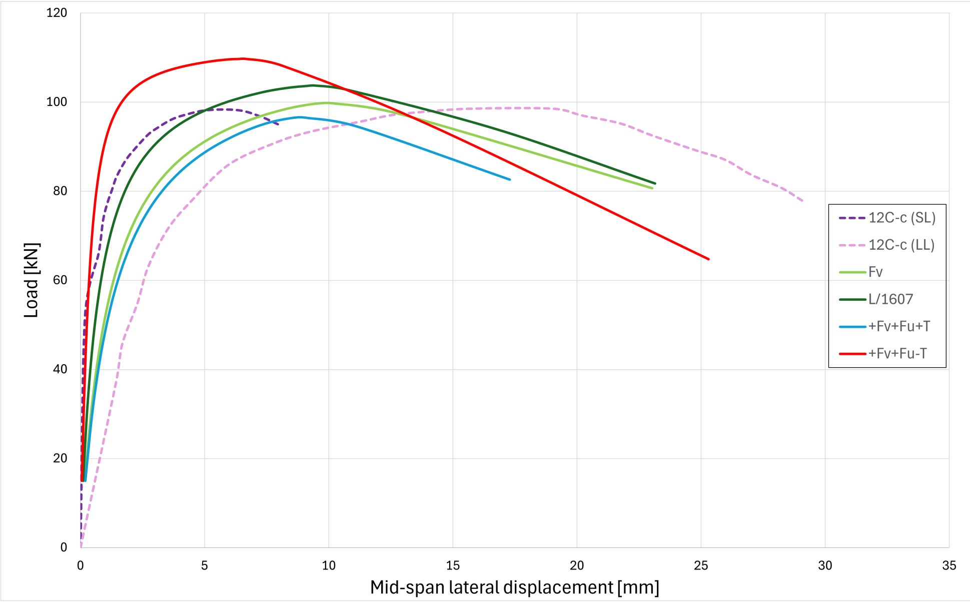

Figure 4.9: Comparison between experimental and numerical P–Δ responses for specimen 12C-c

Imperfection	12C	18C	Mean	COV [%]
F_v	0.97	1.00	0.98	1.9
$+F_v+F_u+T$	0.94	0.98	0.96	3.0
$+F_v+F_u-T$	1.07	1.07	1.07	0.5

Table 4.6: Comparison between numerical and experimental ultimate load ratios P_{num}/P_{exp} obtained for the concentrically loaded specimens tested by Liu et al. [6]

The obtained results show that the isolated minor-axis flexural imperfection F_v provides the most accurate predictions for the specimens tested by Liu et al. [6], with an average numerical-to-experimental resistance ratio equal to 0.98 and a limited coefficient of variation equal to 1.9%.

This observation is consistent with the experimentally observed failure mode, which was predominantly governed by minor-axis flexural buckling. In contrast with the experimental campaign conducted by Kitipornchai and Lee [5], no significant torsional–flexural coupling was reported for the concentrically loaded specimens investigated by Liu et al. [6].

The imperfection configuration $+F_v+F_u+T$ also provides satisfactory predictions, although slightly more conservative results are obtained. Conversely, the imperfection configuration $+F_v+F_u-T$, which previously provided the closest agreement with the experimental results obtained by Kitipornchai and Lee [5], systematically overestimates the resistance of the Liu specimens.

Consequently, although this imperfection configuration appears mechanically realistic for members governed by torsional–flexural buckling, it may lead to non-conservative predictions for members predominantly governed by minor-axis flexural buckling. According to EN 1993-1-14:2025 [4], the adopted geometric imperfections should not only remain realistic, but should also represent sufficiently detrimental configurations for the investigated instability mode. From this point of view, the imperfection configuration $+F_v + F_u - T$ does not appear to be the most appropriate choice for general numerical investigations on unequal-leg angle members.

These observations further confirm that the most representative geometric imperfection configuration strongly depends on the governing instability mode of the member. While coupled flexural–torsional imperfections appear necessary to reproduce the torsional–flexural buckling behaviour observed by Kitipornchai and Lee [5], simpler minor-axis flexural imperfections remain sufficient for members governed primarily by flexural buckling.

The comparison of the complete P–Δ responses shown in Figure 4.9 also highlights the influence of the imperfection amplitude on the predicted structural behaviour. Reducing the imperfection amplitude from $L/1000$ to the experimentally measured average value equal to $L/1607$ increases the predicted stiffness, ultimate resistance and post-buckling deformation capacity.

From a quantitative point of view, the predicted ultimate resistance increases from 99.75 kN for the $L/1000$ imperfection amplitude to 103.71 kN for the experimentally measured imperfection amplitude equal to $L/1607$, corresponding to an increase of approximately 4.0%. This result confirms the strong sensitivity of slender unequal-leg angle members to the adopted imperfection amplitude.

Furthermore, the numerical responses remain globally located between the experimental curves denoted SL and LL, which correspond respectively to the lateral displacements measured at mid-height on the short-leg and long-leg sides of the angle section.

It should be noted that the numerical results correspond to the lateral displacement of the centroid at mid-span, whereas the experimental measurements reported by Liu et al. [6] were obtained at the tips of the angle legs. Consequently, the numerical displacements are expected to lie between the experimental SL and LL responses due to the additional displacements induced by the torsional rotation of the cross-section.

Overall, the obtained results confirm the high sensitivity of unequal-leg angle members to both the shape and amplitude of the adopted geometric imperfections. They also demonstrate that the selection of an appropriate imperfection configuration requires careful consideration of the governing instability mode observed experimentally.

4.5.4 Selection of the retained imperfection configurations

Based on the two considered experimental campaigns, no unique geometric imperfection configuration can be identified as universally representative for unequal-leg angle members. As previously discussed, the most appropriate imperfection shape strongly depends on the governing instability mode, which may correspond either to coupled torsional–flexural buckling or to predominantly minor-axis flexural buckling depending on the considered member geometry and slenderness.

Furthermore, due to the limited number of available experimental investigations and the lack of dedicated studies focusing specifically on the influence of combined geometric imperfection configurations, it remains difficult to draw more general conclusions at this stage.

For the remainder of the present study, two imperfection configurations are therefore retained, namely F_v and $+F_v + F_u + T$. This choice is also consistent with the recommendations of EN 1993-1-14:2025 [4], which specifies that realistic and potentially detrimental imperfection configurations should be considered in nonlinear analyses.

The imperfection configuration $+F_v + F_u - T$ provided satisfactory results for the experimental campaign conducted by Kitipornchai and Lee [5], for which torsional–flexural buckling behaviour was experimentally observed. However, this configuration tends to overestimate the resistance of the specimens tested by Liu et al. [6], which predominantly failed through minor-axis flexural buckling, and may therefore lead to non-conservative predictions when applied to such members.

From a mechanical point of view, the configuration $+F_v + F_u + T$ is expected to be more detrimental than the isolated minor-axis flexural imperfection F_v, due to the simultaneous presence of major-axis flexure and torsion. The major-axis flexural component increases the additional eccentricities and associated second-order effects, while the torsional component may significantly influence the structural response when coupled torsional–flexural instability modes develop.

Nevertheless, the isolated minor-axis flexural imperfection F_v provides consistently safe predictions for both considered experimental campaigns. It is therefore retained in the subsequent analyses to provide a conservative assessment of the structural resistance. The configuration $+F_v + F_u + T$ is included in parallel as a more detrimental case, representing the influence of combined imperfection modes.

These two configurations are thus considered to represent the limiting imperfection scenarios for unequal-leg angle members, respectively governed by pure flexural and by coupled torsional–flexural buckling. Accordingly, the subsequent parametric analyses are performed using both imperfection patterns to ensure a robust evaluation of structural sensitivity to geometrical imperfections.

4.6 Discussion and Conclusion

The validation study presented in this chapter allowed the main modelling assumptions adopted in the numerical model to be assessed and fixed for the subsequent parametric investigations.

The elastic buckling verification confirmed the consistency of the Vlasov beam formulation with the analytical torsional–flexural buckling expressions. The mesh sensitivity analysis showed that 10 beam elements are sufficient to accurately capture both the ultimate resistance and the post-buckling response. The material law sensitivity analysis indicated that strain hardening has only a limited influence on the results. Finally, the investigation of geometric imperfections highlighted the strong sensitivity of unequal-leg angle members to both the shape and orientation of the imposed imperfections.

Based on these observations, the following modelling assumptions are retained for the subsequent parametric study:

- beam finite element formulation based on Vlasov thin-walled beam theory;
- free warping boundary conditions at both member ends;
- mesh discretisation using 10 beam finite elements along the member length;
- elastic–perfectly plastic material law with a nominal tangent stiffness equal to $E/10000$;
- residual stress distribution with a peak value equal to $0.3f_y^*$, with $f_y^* = 235$ MPa;
- two geometric imperfection configurations: F_v and $+F_v + F_u + T$.

The final validation of the retained modelling assumptions is performed by comparing the numerical ultimate resistances with the experimental results reported by Kitipornchai and Lee [5] and Liu et al. [6]. The corresponding numerical-to-experimental resistance ratios are summarised in Table 4.7.

Experimental campaign	**Imperfection**	**Mean**	**COV [%]**	**Comment**
Kitipornchai and Lee [5]	F_v	0.88	8.3	Conservative
Kitipornchai and Lee [5]	$+F_v + F_u + T$	0.83	7.9	More conservative
Liu et al. [6]	F_v	0.98	1.9	Good agreement
Liu et al. [6]	$+F_v + F_u + T$	0.96	3.0	Conservative

Table 4.7: Summary of the numerical-to-experimental resistance ratios obtained using the retained imperfection configurations

Overall, the retained numerical model provides satisfactory and generally conservative predictions of the experimental ultimate resistances, while also capturing the main instability behaviours observed experimentally. The model is therefore considered suitable for the subsequent parametric study devoted to the assessment of existing design rules and the development of improved buckling formulations for high-strength unequal-leg angle section members.

Chapter 5

Parametric Study

Building on the modelling assumptions and validation results established in the previous chapter, this chapter presents a parametric study aimed at analysing the buckling behaviour of hot-rolled unequal-leg angle members over a wide range of geometrical and mechanical parameters. The scope of the study is first defined before comparing the numerical results with EN 1993-1-1 and with existing improved design proposals.

5.1 Scope

In order to perform the parametric study, a sufficiently large and representative set of unequal-leg angle sections was selected. The objective was to ensure a broad coverage of geometrical configurations while maintaining a sufficiently large database for statistically meaningful comparisons with existing design provisions and improved design proposals.

Particular attention was devoted to ensuring that the selected cross-sections cover the main parameters expected to influence the global buckling response.

The parametric study is divided into two complementary parts. The first part focuses on the comparison between the numerical results and the current EN 1993-1-1 buckling design provisions, while the second part aims at assessing and developing improved buckling design proposals for unequal-leg angle sections.

The first selection criterion was the leg ratio h/b, which constitutes one of the most influential geometrical parameters governing the buckling behaviour of unequal-leg angle sections, as highlighted by Dinis et al. [18] and Dai et al. [2]. Consequently, several cross-sections with different h/b ratios were considered in order to investigate their influence on the structural response and buckling resistance.

The investigated h/b ratios range from 1.05 to 2.00, thus covering a broad range of geometrical monosymmetry levels. In total, 17 different cross-sections were selected for the parametric study.

The second selection criterion concerned the cross-section classification. Only cross-sections satisfying at least the Class 3 requirements were retained in order to avoid local buckling effects and to remain consistent with the beam finite element modelling approach adopted in the present study.

Steel grades ranging from S235 to S690 are considered, thus covering both conventional structural steels and high-strength steels and enabling the assessment of potential strength-dependent effects on the global buckling behaviour. As the steel grade increases, the classification criterion becomes progressively more restrictive due to the reduction of the parameter ϵ.

It should be noted that the cross-section classification was not performed directly using the classification limits provided in EN 1993-1-1 (see Figure 2.1). Instead, the following classification criterion was adopted:

$$\frac{c}{t} \leq 14\epsilon = 14\sqrt{\frac{235}{f_y}}$$

This criterion originates from ongoing research work conducted within the framework of the ANGHELY project. Although the related study was still ongoing at the time of writing, the preliminary results obtained have shown encouraging agreement regarding the applicability of this classification criterion for unequal-leg angle sections.

Based on these selection and classification criteria, the numerical database was generated as follows.
In order to generate a complete buckling curve for a given cross-section and steel grade, 13 member slenderness levels are considered, ranging from $\bar{\lambda} = 0.2$ to $\bar{\lambda} = 2.6$, thus covering the transition from stocky to slender members.
The corresponding member lengths are determined from the following expression:

$$\bar{\lambda} = \sqrt{\frac{\beta A f_y}{N_{cr,TF}}}$$

where $N_{cr,TF}$ depends on the member length through the elastic critical loads $N_{cr,T}$, $N_{cr,v}$ and $N_{cr,u}$, according to the formulations presented in Section 2.1.1.
In the present study, the selected cross-sections remain at least Class 3 for the considered steel grade. Consequently, the reduction factor β, corresponding to the ratio between the effective and gross cross-sectional areas, is equal to unity.

For the comparative study against the current EN 1993-1-1 design provisions, steel grade S235 is adopted. All 17 selected unequal-leg angle sections satisfy at least the Class 3 requirements for this steel grade, leading to a total of 221 GMNIA simulations.
As the steel grade increases, the number of cross-sections satisfying the minimum Class 3 requirements progressively decreases. Nevertheless, even for the highest considered steel grades, 7 different cross-sections remain eligible for the parametric investigations. This number is considered sufficient to maintain a representative and statistically meaningful numerical database for the assessment of the buckling behaviour and the development of improved design proposals.

Parameter	**Range**
h/b ratio	1.05–2.00
Steel grades	S235–S690
Reduced slenderness range	0.2–2.6
Number of sections	17
Number of GMNIA simulations	221 (S235)
Imperfection configurations	F_v, $F_v F_u T$
FE model	GMNIA beam model

Table 5.1: Main parameters defining the scope of the parametric study

5.2 Comparison with predictions of EN 1993-1-1

As mentioned previously, the objective of this section is to compare the numerical results obtained from the validated finite element model with the predictions of the current EN 1993-1-1 design rules. The design resistance predictions are determined using the formulation presented in Section 2.1.

As a first step, steel grade S235 is considered in order to assess the accuracy of the current design approach without the additional influence of high-strength steel effects. For S235 unequal-leg angle sections, buckling curve b is adopted according to EN 1993-1-1, corresponding to an imperfection factor equal to $\alpha = 0.34$.

5.2.1 Global comparison with the EN 1993-1-1 buckling curve

The comparison between the numerical reduction factors obtained from the GMNIA simulations and the predictions of EN 1993-1-1 is presented in Figure 5.1. The results are shown separately for the two retained imperfection configurations, namely the combined flexural–torsional imperfection $F_v F_u T$ and the isolated minor-axis flexural imperfection F_v.

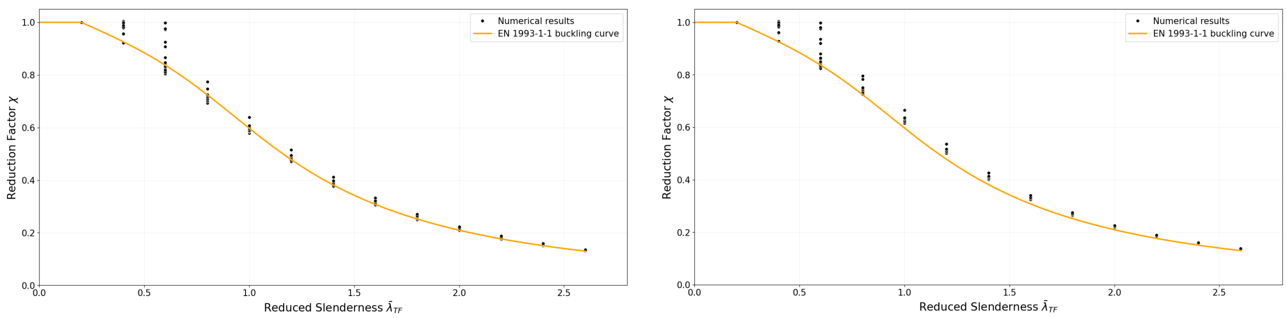

(a) $F_v F_u T$ imperfection configuration (b) F_v imperfection configuration

Figure 5.1: Comparison between the numerical reduction factors and the EN 1993-1-1 buckling curve b for S235 unequal-leg angle members

According to the current EN 1993-1-1 formulation [1], unequal-leg angle members presenting the same reduced slenderness $\bar{\lambda}_{TF}$ should theoretically exhibit the same reduction factor χ.

However, the numerical results reveal a significant dispersion of the reduction factors for identical values of $\bar{\lambda}_{TF}$, particularly in the low and intermediate slenderness range where torsional–flexural effects remain significant.

A clear difference can additionally be observed between the two investigated imperfection configurations. For the isolated flexural imperfection configuration F_v, almost all numerical points remain above the EN 1993-1-1 buckling curve, leading to globally conservative predictions.

Conversely, for the combined flexural–torsional imperfection configuration $F_v F_u T$, several numerical points are located below the EN 1993-1-1 buckling curve, particularly in the intermediate slenderness range. Similar observations were also reported by Dai et al. [2]. These results indicate that the current design formulation may become slightly non-conservative when significant torsional–flexural interactions develop.

This apparent non-conservative character should however be interpreted with caution. Since the EN 1993-1-1 buckling curves were primarily calibrated using flexural imperfection patterns consistent with the F_v configuration, the points falling below the design curve for the $F_v F_u T$ imperfection may partly reflect the increased severity of this imperfection pattern rather than a fundamental inadequacy of the design formulation. Its physical representativeness therefore depends on the actual imperfection shapes governing the behaviour of real members.

For the F_vF_uT configuration, the ratio χ_{num}/χ_{EN} ranges from approximately 0.96 to 1.16 across the full parametric database, highlighting both the non-conservative predictions for specific geometries and the significant conservatism for others.

5.2.2 Influence of the imperfection configuration

In order to better understand the origin of the observed differences between the two imperfection configurations, the underlying instability mechanisms are examined in more detail in the following discussion.

Dai et al. [2] showed that the reduction factors of unequal-leg angle members are strongly influenced by the relative contribution of torsional and flexural instability modes. In particular, the observed scatter is closely related to the ratio $N_{cr,TF}/N_{cr,v}$, which governs the transition between torsion-dominated and predominantly flexural behaviour.

For short and intermediate members, the combined torsional–flexural critical load $N_{cr,TF}$ remains close to the torsional critical load $N_{cr,T}$. In this range, the structural response remains strongly influenced by torsional effects, leading to larger scatter and increased sensitivity to the adopted imperfection configuration.

In the F_vF_uT configuration, the simultaneous presence of minor-axis flexure, major-axis flexure and torsion appears to activate stronger three-dimensional modal interactions than in the isolated F_v configuration. These interactions are believed to trigger the unstable post-buckling behaviour observed for certain members within the transition region.

Conversely, as the member slenderness increases, the combined critical load progressively converges towards the minor-axis flexural critical load $N_{cr,v}$. The structural response therefore gradually becomes governed by classical minor-axis flexural buckling and the numerical reduction factors progressively converge towards the EN 1993-1-1 buckling curve.

It may additionally be observed that, when torsional effects become dominant, several numerical results tend to approach the plate buckling curve provided in EN 1993-1-5 [41]. Such behaviour suggests a more favourable post-buckling response than that associated with classical flexural buckling, which is consistent with the observations reported by Dai et al. [2].

These observations suggest that the reduced slenderness $\bar{\lambda}_{TF}$ alone may not be sufficient to fully characterise the buckling behaviour of unequal-leg angle members. The cross-sectional geometry, the relative importance of torsional effects and the adopted imperfection configuration all appear to significantly influence the resulting reduction factors and post-buckling behaviour.

5.2.3 Influence of low h/b ratios

In order to further investigate the origin of the observed scatter and the non-conservative predictions, the influence of the cross-sectional geometry is examined in more detail through the leg ratio h/b, which constitutes one of the main parameters governing the torsional–flexural behaviour of unequal-leg angle members.

A first comparison is performed for members presenting relatively low h/b ratios, corresponding to cross-sections that are closer to equal-leg angles. The corresponding numerical reduction factors are presented in Figure 5.2 for both investigated imperfection configurations.

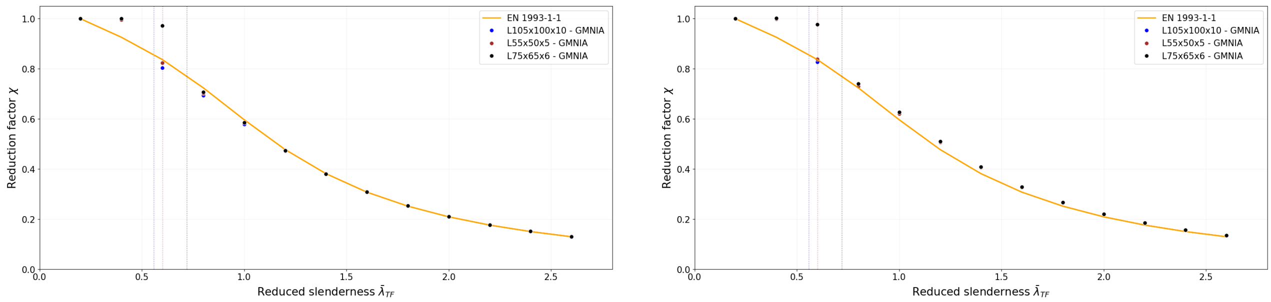

(a) $F_v F_u T$ imperfection configuration (b) F_v imperfection configuration

Figure 5.2: Influence of low h/b ratios on the numerical reduction factors

The influence of the adopted imperfection configuration remains particularly marked for these cross-sections. For the combined imperfection configuration $F_v F_u T$, several numerical points are located below the EN 1993-1-1 buckling curve, confirming the potentially non-conservative character of the current design formulation for members exhibiting strong torsional–flexural interactions.

It may additionally be observed that the non-conservative behaviour becomes progressively more pronounced as the h/b ratio decreases. For a given reduced slenderness, the L105×100×10 section consistently exhibits lower reduction factors than the two other considered sections. This observation suggests that cross-sections closer to equal-leg angles are more sensitive to torsional–flexural interactions and to the associated unstable post-buckling behaviour.

In order to better quantify the accuracy of the EN 1993-1-1 predictions, the ratio between the numerical reduction factors and the design reduction factors predicted by EN 1993-1-1 is additionally presented in Figure 5.3.

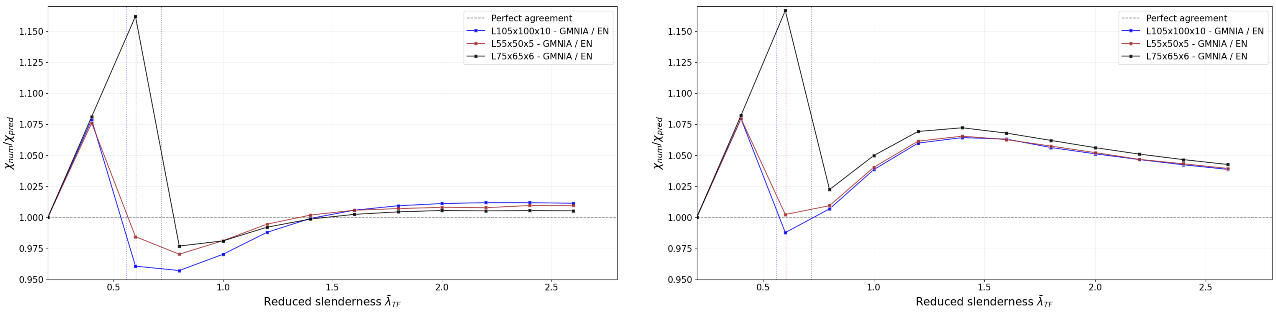

(a) $F_v F_u T$ imperfection configuration (b) F_v imperfection configuration

Figure 5.3: Ratio between numerical reduction factors and EN 1993-1-1 predictions for members presenting low h/b ratios

For the combined imperfection configuration $F_v F_u T$, the ratio χ_{num}/χ_{EN} clearly falls below unity within the transition slenderness range, confirming the non-conservative character of the EN 1993-1-1 predictions for these members.

The most pronounced non-conservative predictions are systematically obtained for the L105×100×10 section, which presents the lowest h/b ratio among the considered cross-sections, with a minimum value of χ_{num}/χ_{EN} reaching approximately 0.96.

For the L55×50×5 and L75×65×6 sections, the minimum ratios remain closer to unity, indicating a less pronounced non-conservative behaviour.

Outside the transition region, the EN 1993-1-1 predictions remain globally conservative, with typical values of χ_{num}/χ_{EN} slightly above unity.

Although limited non-conservative predictions are observed within the transition region, the EN 1993-1-1 formulation remains globally conservative for a large proportion of the investigated members.

In addition to the observed non-conservative predictions, a significant degree of conservatism may also develop for certain members. For the L75×65×6 section, values of χ_{num}/χ_{EN} up to approximately 1.16 are obtained, corresponding to a conservatism of about 16%.

This pronounced conservatism additionally suggests that the current EN 1993-1-1 formulation does not fully capture the favourable post-buckling reserve that may develop for certain unequal-leg angle members subjected to torsional–flexural buckling.

Such behaviour is consistent with the tendency of several numerical results to approach the plate buckling curve from EN 1993-1-5, which is characterised by a more favourable post-critical response than the classical flexural buckling curves of EN 1993-1-1.

The simultaneous presence of both non-conservative and highly conservative predictions further confirms that the current EN 1993-1-1 formulation is unable to consistently reproduce the actual post-buckling behaviour of unequal-leg angle members over the full range of geometrical configurations.

The minimum values of χ_{num}/χ_{EN} occur close to the transition slenderness values $\bar{\lambda}_{lim}$ defined by Dai et al. [2], corresponding to $N_{cr,TF}/N_{cr,v} \geq 0.9$. This strongly supports the interpretation that the non-conservative predictions are associated with modal interactions occurring during the transition from torsion-dominated to predominantly flexural behaviour.

Beyond this transition region, the ratio χ_{num}/χ_{EN} progressively converges towards unity, indicating that the EN 1993-1-1 predictions become increasingly accurate once the structural response becomes governed by classical minor-axis flexural buckling.

In contrast, for the isolated flexural imperfection configuration F_v, the ratio χ_{num}/χ_{EN} remains globally equal to or larger than unity for all considered members. Although a certain scatter remains visible in the transition region, the numerical results remain globally conservative and the non-conservative behaviour observed for the combined imperfection configuration F_vF_uT practically disappears.

5.2.4 Influence of large h/b ratios

A similar comparison is subsequently performed for members presenting larger h/b ratios, corresponding to more geometrically monosymmetric unequal-leg angle sections. The corresponding numerical reduction factors are presented in Figure 5.4 for both investigated imperfection configurations.

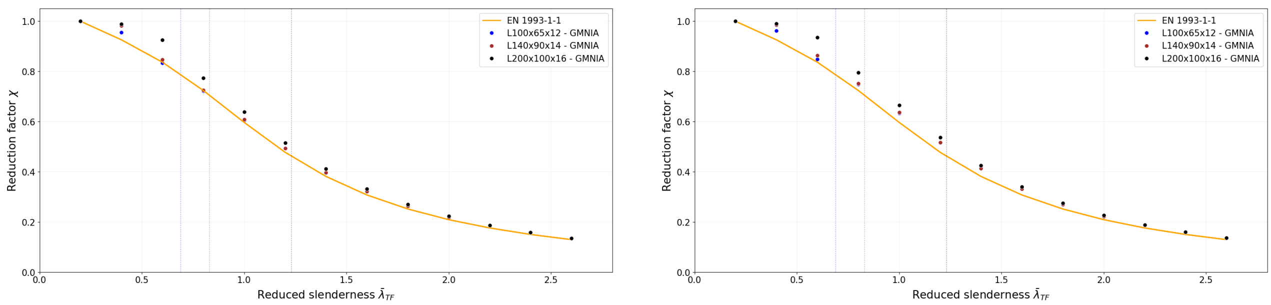

(a) F_vF_uT imperfection configuration (b) F_v imperfection configuration

Figure 5.4: Influence of large h/b ratios on the numerical reduction factors

Compared to members with lower h/b ratios, the results obtained for larger h/b ratios show a smoother transition between instability modes and a reduced sensitivity to the adopted imperfection configuration.

For the combined flexural–torsional imperfection configuration $F_v F_u T$, a certain scatter of the numerical reduction factors can still be observed in the low and intermediate slenderness range. However, the non-conservative behaviour previously observed for low h/b ratios becomes significantly less pronounced and most numerical points remain close to or above the EN 1993-1-1 buckling curve.

For the isolated flexural imperfection configuration F_v, a similar scatter can also be observed within the same slenderness range. Nevertheless, no non-conservative numerical points are obtained and the predictions remain globally slightly more conservative than those associated with the combined imperfection configuration $F_v F_u T$.

These observations are consistent with the mechanical interpretation proposed by Dai et al. [2]. As the h/b ratio increases, the transition between torsion-dominated and flexure-dominated instability modes progressively becomes smoother, resulting in a more stable post-buckling behaviour and reduced modal interaction effects. This trend is further illustrated in Appendix 7.2.1, where the evolution of the initial post-buckling stiffness ratio k_{pb}/k_{in} and the average post-buckling stiffness ratio evaluated over the first 5% of the post-buckling path $k_{pb,5\%}/k_{in}$ is reported for different h/b ratios.

It may additionally be observed that the convergence towards the EN 1993-1-1 buckling curve again occurs around the transition slenderness $\bar{\lambda}_{lim}$ defined by the condition $N_{cr,TF}/N_{cr,v} \geq 0.9$. Beyond this limit, the influence of torsional effects becomes limited and the reduction factors become significantly less sensitive to both the imperfection configuration and the cross-sectional geometry.

5.2.5 General observations and implications

Overall, the comparison between low and high h/b ratios confirms the key role of cross-sectional geometry in the development of torsional–flexural interactions. The most pronounced non-conservative predictions occur for low h/b ratios, where unstable modal interactions remain significant within the transition region.

For both investigated imperfection configurations, this influence is reflected by a significant vertical scatter of the numerical reduction factors, which is not explicitly captured by the current EN 1993-1-1 formulation. However, for the combined imperfection configuration $F_v F_u T$, additional non-conservative predictions are observed. These results further confirm the important influence of torsional–flexural modal interactions, which are not explicitly represented within the current EN 1993-1-1 formulation.

Since the EN 1993-1-1 buckling curves were primarily calibrated on the basis of classical flexural buckling behaviour and conventional flexural imperfection patterns, the current formulation appears unable to fully capture the influence of coupled torsional–flexural imperfection modes and the associated modal interactions observed for unequal-leg angle members.

The present results therefore suggest that improvements to the current design approach may be required. In particular, it was shown that the vertical scatter of the numerical reduction factors is strongly related to the ratio $N_{cr,TF}/N_{cr,v}$, indicating that the relative contribution of torsional and flexural instability modes should be explicitly considered in the formulation of improved reduction factors.

Furthermore, the observed non-conservative behaviour associated with modal interactions was shown to be strongly influenced by the cross-sectional geometry, and more specifically by the h/b ratio. Consequently, an additional parameter accounting for this geometrical influence may also be required in order to accurately reproduce the buckling behaviour of unequal-leg angle members.

These observations therefore establish the mechanical justification for seeking improved design proposals that explicitly account for the torsional–flexural interaction ratio $N_{cr,TF}/N_{cr,v}$ and the cross-sectional geometry of unequal-leg angle members.

5.3 Comparison with existing improved proposals

The limitations of the current EN 1993-1-1 formulation identified in the previous section have also been highlighted by several researchers. In order to overcome these limitations, a number of improved design approaches have been proposed in the literature. Among them, Dai et al. [2] introduced two additional parameters intended to account for the influence of torsional–flexural modal interactions and cross-sectional geometry on the reduction factors of unequal-leg angle members. For clarity purposes, the complete formulation proposed by Dai et al. [2] is reproduced in Appendix 7.3.

In their proposal, two distinct behavioural domains are considered depending on the dominant instability mode. The first corresponds to members for which torsional–flexural buckling remains dominant, while the second corresponds to members governed predominantly by minor-axis flexural buckling. For each domain, an additional correction parameter is introduced in order to improve the prediction of the reduction factors.

The proposed formulation therefore attempts to separately account for: (i) the vertical scatter of the reduction factors observed in the torsional–flexural dominant domain, and (ii) the unstable modal interaction effects developing within the transition region towards predominantly flexural buckling.

Behavioural domain	**Correction**	**Main parameter**	**Objective**
Torsional–flexural dominant	$\chi_{TF} = \chi_F + \Delta_F(\chi_T - \chi_F)$	Δ_F	Capture vertical scatter
Predominantly flexural dominant	Modified Perry formulation	β	Account for modal interaction effects

Table 5.2: Simplified overview of the improved proposal introduced by Dai et al. [2]

5.3.1 Correction of the torsional–flexural dominant domain: parameter Δ_F

The parameter Δ_F is introduced to capture the vertical scatter observed between the upper and lower bounds of the numerical reduction factors for members subjected to torsional–flexural buckling. It represents the relative contribution of torsional and flexural instability effects through the ratio $N_{cr,TF}/N_{cr,v}$ and allows a progressive interpolation between the flexural buckling curve χ_F and the plate-type buckling curve χ_T. Consequently, Δ_F aims to reproduce the gradual transition between torsion-dominated and predominantly flexural behaviour.

The flexural bound χ_F corresponds to a modified flexural buckling curve proposed by Dai et al. [2], while the upper bound χ_T is based on the plate buckling curve from EN 1993-1-5. The latter was shown by Dai et al. [2] to provide a good approximation of the favourable post-buckling response observed for members dominated by torsional effects.

The conceptual role of the parameter Δ_F within the proposed design formulation is illustrated in Figure 5.5. The proposed torsional–flexural reduction factor χ_{TF} is obtained through an interpolation between the lower flexural bound χ_F and the upper torsional bound χ_T, allowing the vertical scatter observed in the numerical results to be represented.

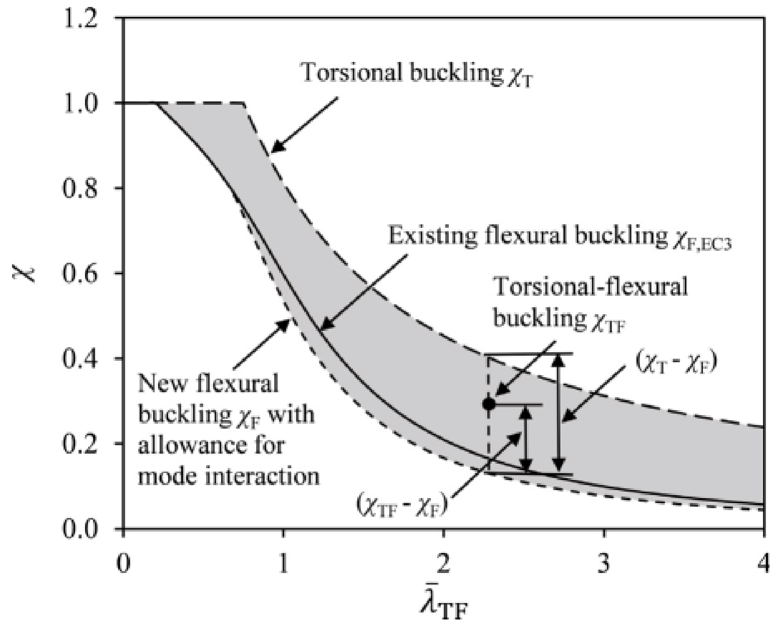

Figure 5.5: Illustration of the role of the parameter Δ_F in the proposed design formulation, adapted from Dai et al. [2]

Based on the numerical observations obtained by Dai et al. [2], the following expression was proposed as a lower-bound approximation of the observed trend:

$$\Delta_F = \left(1 - \frac{N_{cr,TF}}{0.9N_{cr,v}}\right)^2$$

The ability of this approximation to reproduce the behaviour observed in the present numerical study will subsequently be assessed using the results obtained from the validated finite element model.

5.3.2 Correction of the flexural dominant domain: parameter β

The parameter β is introduced in the modified Perry formulation in order to account for the influence of interactive buckling phenomena observed in the transition region between torsional–flexural and minor-axis flexural buckling. This parameter depends both on the interaction ratio $N_{cr,TF}/N_{cr,v}$ and on the cross-sectional geometry through the leg ratio h/b.

Its role is to increase the imperfection sensitivity of members exhibiting strong modal interactions, particularly for low h/b ratios corresponding to sections close to equal-leg angles. This increase in imperfection sensitivity is introduced through a modification of the Perry imperfection parameter η, thereby directly amplifying the reduction effect associated with interactive buckling phenomena:

$$\eta = \alpha \cdot \beta \cdot (\bar{\lambda}_{TF} - 0.2)^{\beta}$$

The parameter β is defined as:

$$\beta = 7.5 \cdot \left(1 - \frac{N_{cr,TF}}{N_{cr,v}}\right) \cdot \left(6 - 5\frac{h}{b}\right) + 1 \qquad \text{with} \qquad 1.0 \leq \beta \leq 1.75$$

Consequently, the value of β increases when the torsional contribution becomes more significant and when the cross-section approaches an equal-leg geometry. The proposed formulation therefore aims to increase the reduction of the buckling resistance within the transition region where strong torsional–flexural modal interactions are expected to develop.

Unlike the parameter Δ_F, which is directly related to the observed transition between torsional and flexural behaviour, the mechanical interpretation of β remains less explicit and appears to rely more strongly on numerical calibration.

It should additionally be noted that the formulation proposed by Dai et al. [2] was calibrated primarily using numerical results obtained for S355 steel members. Consequently, part of the observed improvement may result from compensations between the proposed correction parameters and the increased conservatism associated with the corresponding EN 1993-1-1 buckling curve.

In particular, the absence of pronounced non-conservative predictions in their study does not necessarily imply that the interactive buckling phenomena are fully captured by the parameter β, since part of these effects may already be compensated by the adopted imperfection factor α.

The validity and applicability of the proposed parameters for the present S235 numerical database must therefore also be carefully assessed in the following sections.

5.3.3 Assessment of the parameter Δ_F

As previously discussed, the parameter Δ_F was introduced by Dai et al. [2] in order to reproduce the vertical scatter observed in the reduction factors of unequal-leg angle members subjected to torsional–flexural buckling. The proposed formulation aims to represent the gradual transition between torsion-dominated and predominantly flexural behaviour through the interaction ratio $N_{cr,TF}/N_{cr,v}$.

In order to assess the applicability of this formulation to the present numerical database, the numerical values of Δ_F obtained from the GMNIA simulations are compared with the analytical expression proposed by Dai et al. [2]. The comparison is first performed considering the complete numerical database for both retained imperfection configurations.

For each numerical simulation, the corresponding value of Δ_F is determined by rearranging the interpolation expression:

$$\Delta_F = \frac{\chi_{TF}^{num} - \chi_F}{\chi_T - \chi_F}$$

where χ_{TF}^{num} corresponds to the numerical reduction factor obtained from the GMNIA simulations, while χ_F and χ_T are respectively determined from the analytical flexural and torsional reduction factor expressions proposed by Dai et al. [2].

The resulting numerical values of Δ_F are subsequently compared with the analytical formulation proposed by Dai et al. [2].

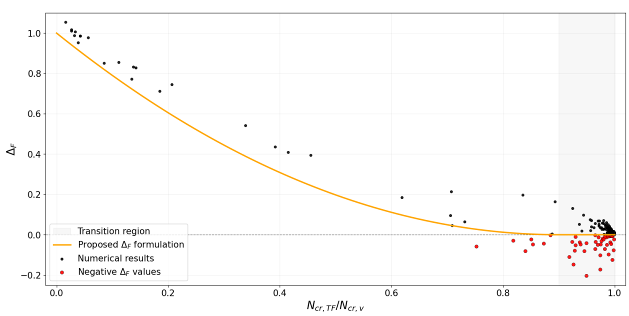

(a) $F_v F_u T$ imperfection configuration

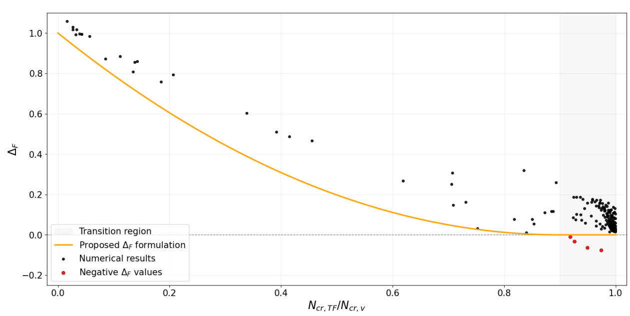

(b) F_v imperfection configuration

Figure 5.6: Comparison between the numerical values of Δ_F and the formulation proposed by Dai et al. [2]

For both imperfection configurations, the proposed formulation correctly reproduces the global evolution of Δ_F with increasing $N_{cr,TF}/N_{cr,v}$. The progressive reduction of the scatter towards the flexural-dominated domain is reasonably captured, especially for low and intermediate values of the interaction ratio. These observations support the mechanical relevance of the interpolation approach introduced through Δ_F.

Nevertheless, several values of Δ_F become negative near $N_{cr,TF}/N_{cr,v} \approx 0.9$, particularly for the F_vF_uT configuration. Since Δ_F represents an interpolation parameter between χ_F and χ_T, such values are not physically meaningful within the proposed framework.

These negative values suggest that the unstable modal interactions developing within the transition region are not fully captured by the proposed analytical formulation. In particular, the simultaneous presence of minor-axis flexure, major-axis flexure and torsion in the F_vF_uT imperfection configuration appears to generate local deviations from the idealised interpolation behaviour assumed by the formulation.

This interpretation is further supported by the results obtained for the isolated flexural imperfection configuration F_v, for which both the number and magnitude of the negative Δ_F values become significantly smaller. This reduction of the discrepancies strongly suggests that the remaining inaccuracies are primarily associated with modal interaction effects rather than with the formulation of Δ_F itself.

In order to further investigate this hypothesis, the validation of the Δ_F formulation is subsequently examined for members presenting large h/b ratios, for which the influence of modal interactions was previously shown to become significantly less pronounced.

Influence of large h/b ratios

The comparison between the numerical values of Δ_F and the proposed analytical formulation is presented in Figure 5.7 for members presenting large h/b ratios.

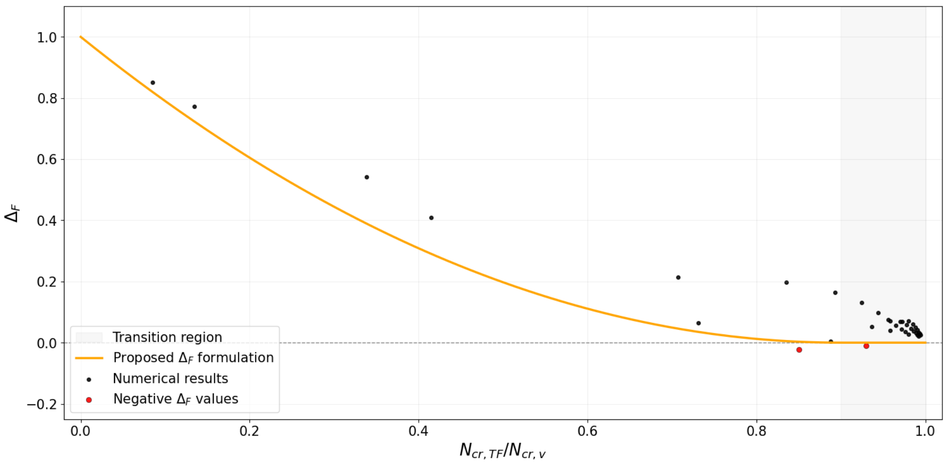

Figure 5.7: Validation of the proposed Δ_F formulation for members presenting large h/b ratios

For members presenting large h/b ratios, the proposed Δ_F formulation provides a significantly improved representation of the observed numerical scatter. Compared to the results obtained for low h/b ratios, only a very limited number of slightly negative Δ_F values remain visible and their magnitude remains small.

These observations strongly suggest that the parameter Δ_F correctly captures the global evolution of the torsional–flexural scatter associated with unequal-leg angle members.

The remaining discrepancies therefore appear to be primarily associated with the unstable modal interactions developing for members presenting low h/b ratios rather than with the formulation of Δ_F itself. This interpretation additionally suggests that the remaining inaccuracies may instead originate from the modified flexural formulation through the parameter β, which directly governs the imperfection sensitivity within the transition region.

Overall, the present results indicate that the mechanical basis of the Δ_F formulation remains physically relevant for S235 steel grades, even though the original proposal was developed using numerical results obtained for S355 steel. In particular, the proposed interaction parameter appears capable of reproducing the global evolution of the reduction factor scatter associated with the gradual transition between torsional–flexural and predominantly flexural behaviour.

5.3.4 Assessment of the effectiveness of the parameter β

This section assesses the effectiveness of the parameter β for capturing modal interaction effects in S235 unequal-leg angle members.

As previously discussed, the parameter β was introduced in order to account for the additional imperfection sensitivity associated with interactive torsional–flexural buckling phenomena occurring within the transition region between torsional–flexural and minor-axis flexural buckling. Since the detailed derivation and calibration procedure of β are not extensively discussed by Dai et al. [2], the present assessment mainly focuses on evaluating the capability of the proposed correction to reduce the non-conservative behaviour observed in the numerical results.

In order to isolate the specific influence of β, the numerical reduction factors are compared directly with the modified flexural buckling curve χ_F proposed by Dai et al., without including the additional interpolation effect associated with the parameter Δ_F. This choice allows the influence of β on the modified Perry formulation to be evaluated independently from the vertical scatter correction introduced through Δ_F.

The assessment is performed for members with low h/b ratios subjected to the $F_v F_u T$ imperfection configuration, since these cases exhibited the strongest modal interactions and the most pronounced non-conservative predictions.

The prediction ratios χ_{num}/χ_{pred} obtained using both the original EN 1993-1-1 formulation and the modified reduction factor χ_F are therefore compared in order to quantify the actual improvement introduced by the parameter β.

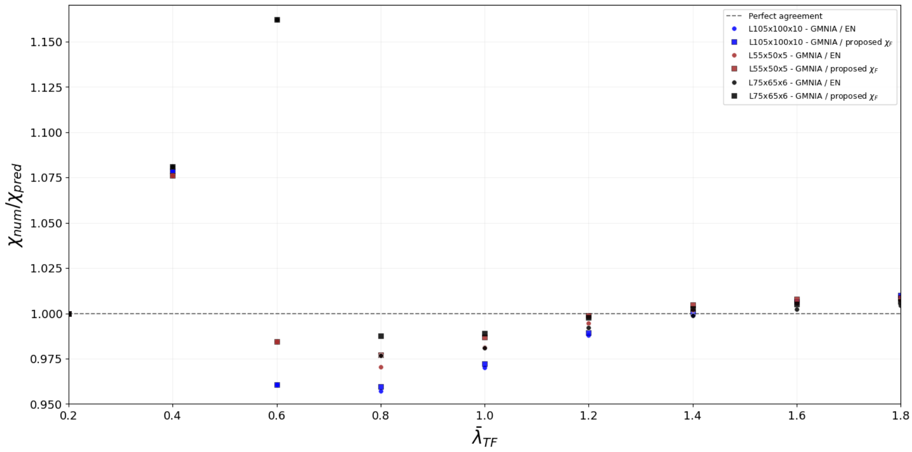

Figure 5.8: Comparison between the prediction ratios obtained using the EN 1993-1-1 formulation and the modified flexural buckling curve χ_F proposed by Dai et al. [2] for low h/b unequal-leg angle members subjected to the $F_v F_u T$ imperfection configuration

The proposed formulation generally leads to a slight improvement of the predictions within the transition region, where modal interactions are expected to be significant. In particular, the modified formulation reduces the magnitude of the most non-conservative predictions and shifts several numerical points closer to the perfect agreement line.

Nevertheless, the improvement remains relatively limited and several numerical points still remain below unity, indicating that the proposed formulation does not fully eliminate the non-conservative behaviour associated with modal interactions.

Although the proposed formulation therefore leads to a certain improvement of the predictions, the remaining non-conservative results suggest that the correction introduced through β remains insufficient for the present S235 numerical database.

The parameters governing the proposed expression for β appear to be mechanically consistent with the observations obtained in the present study. In particular, the dependency on the interaction ratio $N_{cr,TF}/N_{cr,v}$ and on the geometrical ratio h/b is coherent with the strong influence of these parameters on the development of torsional–flexural modal interactions and on the associated post-buckling behaviour.

However, the physical justification of the exact mathematical form of the proposed expression remains difficult to assess, since the detailed development and calibration procedure of the formulation are not explicitly discussed by Dai et al. [2]. The proposed expression therefore appears to rely at least partially on an empirical calibration of the numerical results.

This aspect is particularly important since the formulation was developed using numerical results obtained for S355 steel grade members.

In order to further investigate this effect, an additional comparison between the EN 1993-1-1 predictions and the numerical results obtained for S355 members subjected to the combined imperfection configuration $F_v F_u T$ is presented in Figure 5.9.

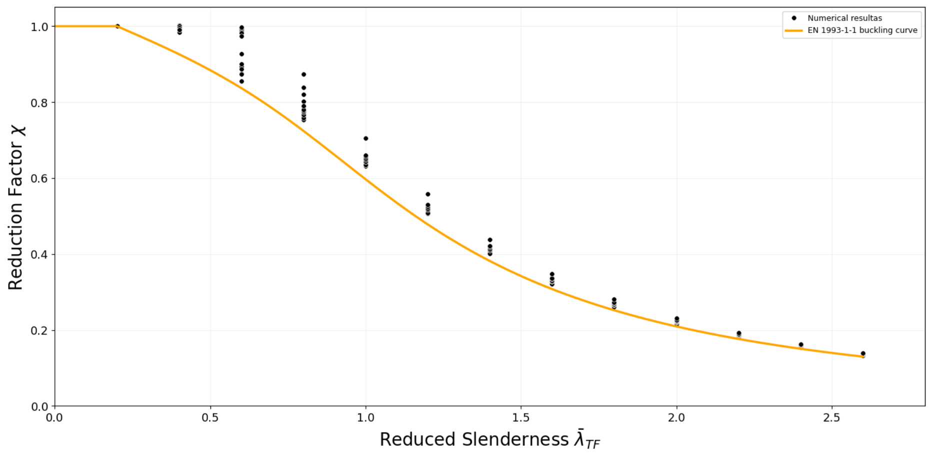

Figure 5.9: Comparison between the numerical reduction factors and the EN 1993-1-1 buckling curve for S355 unequal-leg angle members subjected to the $F_v F_u T$ imperfection configuration

For S355 members, the non-conservative behaviour previously identified for S235 practically disappears, with almost all numerical points located above the EN 1993-1-1 buckling curve.

However, this absence of non-conservative predictions does not imply that torsional–flexural modal interactions no longer occur. A significant vertical scatter of the numerical reduction factors still remains visible within the transition region, indicating that modal interaction effects are still present.

These interaction effects appear to be partially compensated by the additional conservatism introduced through the imperfection factor α adopted for S355 members. As discussed previously in Section 2.2.2, this increased conservatism may compensate part of the resistance reduction induced by modal interactions that are not explicitly accounted for in the current formulation.

This observation is particularly important for the interpretation of the parameter β, since the formulation proposed by Dai et al. [2] was calibrated using S355 numerical results. The relatively limited correction introduced through β may therefore partly reflect the fact that the reference EN 1993-1-1 predictions used during the calibration process were already globally more conservative.

Such behaviour could explain why the proposed correction remains relatively limited when applied to the present S235 numerical results, for which the original EN 1993-1-1 formulation exhibits more pronounced non-conservative predictions.

Overall, the present observations suggest that the parameter β captures part of the mechanical trends associated with torsional– flexural modal interactions, particularly through its dependency on $N_{cr,TF}/N_{cr,v}$ and h/b. However, the relatively limited improvement obtained for the present S235 results indicates that the current formulation does not fully reproduce the destabilising effects associated with modal interactions and remains strongly dependent on the calibration database used during its development.

5.3.5 Assessment of the complete proposed formulation

After assessing Δ_F and β separately, the predictive capability of the complete proposed formulation is evaluated.

Since the final choice of the most representative imperfection configuration remains open, the complete formulation proposed by Dai et al. [2] is assessed for both retained imperfection configurations.

The $F_v F_u T$ configuration represents the most critical case, for which torsional–flexural modal interactions are the most pronounced. As shown in the previous sections, this configuration generated both non-conservative predictions and excessive conservatism when using the EN 1993-1-1 formulation.

Conversely, the F_v configuration allows the behaviour of the proposed formulation to be examined for a case where the EN 1993-1-1 predictions were already globally conservative, although an excessive level of conservatism was still observed.

The corresponding prediction ratios χ_{num}/χ_{pred} are presented in Figure 5.10. The profiles with the lowest h/b ratios were selected since, as previously discussed, they are the most sensitive to torsional–flexural modal interactions and therefore constitute the most relevant cases for assessing the proposed correction.

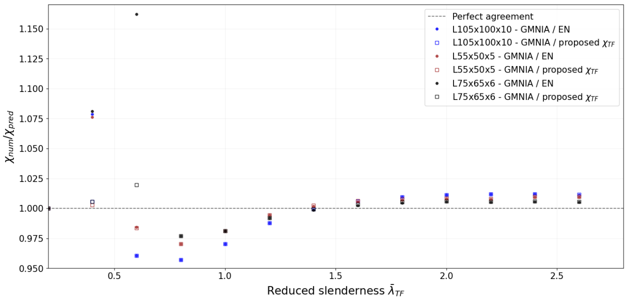

(a) $F_v F_u T$ imperfection configuration

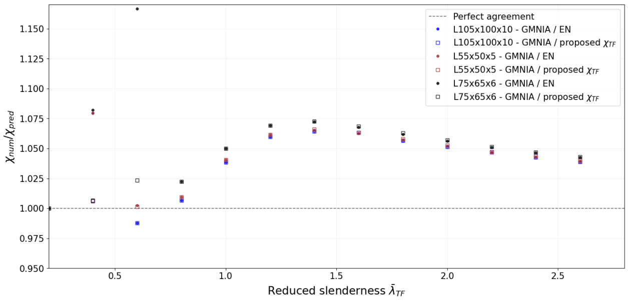

(b) F_v imperfection configuration

Figure 5.10: Prediction ratios χ_{num}/χ_{pred} obtained using EN 1993-1-1 and the complete formulation proposed by Dai et al. [2].

The complete proposed formulation generally leads to a significant improvement of the global predictions compared to the original EN 1993-1-1 formulation.

In particular, the interpolation introduced through the parameter Δ_F considerably reduces the excessive conservatism associated with the EN 1993-1-1 buckling curve and allows the vertical scatter of the numerical reduction factors to be more accurately reproduced.

The most significant improvement is observed within the transition region, where the prediction ratios become substantially closer to the perfect agreement line. For instance, for the L75×65×6 profile subjected to the $F_v F_u T$ imperfection configuration, the prediction ratio decreases from approximately 1.16 using the EN 1993-1-1 formulation to approximately 1.02 using the proposed formulation, corresponding to a reduction of the prediction overestimation of approximately 14%.

However, despite the global improvement introduced by the complete formulation, several non-conservative results still remain visible within the transition region, particularly for the $F_v F_u T$ configuration. These remaining discrepancies indicate that the additional correction introduced through the parameter β remains relatively limited for the present S235 numerical results.

For the F_v imperfection configuration, the influence of modal interactions was previously shown to remain much less pronounced. Consequently, the correction introduced through the parameter β becomes almost negligible. In this case, the proposed formulation mainly reduces the excessive conservatism of the EN 1993-1-1 predictions without introducing any significant additional conservatism, which constitutes a positive aspect of the proposed approach.

This strong dependency on the selected imperfection configuration highlights the important influence of modal interaction development on the effectiveness of the proposed correction.

A statistical comparison of the prediction ratios χ_{num}/χ_{pred} obtained using the EN 1993-1-1 formulation and the complete proposed formulation is additionally presented in Table 5.3.

Profile	Formulation	Mean	Min	Max
L105×100×10	EN	1.001	0.957	1.079
	Proposed	0.996	0.957	1.012
L55×50×5	EN	1.004	0.970	1.076
	Proposed	0.999	0.970	1.010
L75×65×6	EN	1.017	0.977	1.162
	Proposed	1.000	0.977	1.020

Table 5.3: Statistical comparison of the prediction ratios χ_{num}/χ_{pred} obtained using EN 1993-1-1 and the complete proposed formulation for members subjected to the F_vF_uT imperfection configuration.

The statistical results confirm that the proposed formulation mainly reduces the upper prediction ratios. For the L75×65×6 section, the maximum value decreases from 1.162 with EN 1993-1-1 to 1.020 with the proposed formulation. In contrast, the minimum ratios remain almost unchanged for all three profiles. This indicates that the complete formulation is highly effective in reducing excessive conservatism, while the correction of the most critical non-conservative predictions remains limited.

Overall, the proposed formulation provides a substantial improvement of the global prediction quality compared to EN 1993-1-1, although the correction of severe modal interaction effects remains only partial for the present S235 numerical results.

5.3.6 General conclusions on the proposed formulation

Parameter	Positive aspects	Limitations	Applicability
Δ_F	Captures vertical scatter; reduces conservatism	Slight remaining non-conservative predictions	Applicable to S235
β	Accounts for modal interactions; physically relevant variables	Limited correction; empirical calibration based on S355	Mainly relevant for F_vF_uT
Complete formulation	Significant global improvement	Modal interactions not fully corrected	Strong dependence on imperfection configuration

Table 5.4: Summary of the assessment of the improved formulation proposed by Dai et al. [2]

The present assessment showed that the improved formulation proposed by Dai et al. [2] significantly improves the prediction quality compared to the original EN 1993-1-1 formulation for unequal-leg angle members subjected to torsional–flexural buckling.

Among the two introduced parameters, the interpolation parameter Δ_F was shown to provide the main contribution to the improved predictions. In particular, Δ_F efficiently captures the vertical scatter of the numerical reduction factors and considerably reduces the excessive conservatism associated with the EN 1993-1-1 buckling curve within the transition region. The present results further indicate that this interpolation approach remains applicable for S235 members, despite having originally been calibrated using S355 numerical results.

Conversely, the additional correction introduced through the parameter β was shown to remain relatively limited for the present S235 numerical database. Although the dependency of β on the interaction ratio $N_{cr,TF}/N_{cr,v}$ and on the geometrical ratio h/b appears mechanically consistent, the proposed formulation remains strongly dependent on the selected imperfection configuration.

In particular, the correction introduced through β appears mainly relevant for the $F_v F_u T$ imperfection configuration, for which severe torsional–flexural modal interactions develop. For the isolated flexural imperfection configuration F_v, the influence of modal interactions remains much less pronounced and the additional correction introduced through β becomes almost negligible.

Overall, the present results indicate that the interpolation approach introduced through Δ_F provides a promising basis for improving the current EN 1993-1-1 design rules for unequal-leg angle members. However, the remaining non-conservative predictions observed for the $F_v F_u T$ imperfection configuration show that an additional parameter accounting for severe modal interaction effects remains necessary.

The role assigned to β in the formulation proposed by Dai et al. [2] therefore appears mechanically relevant. However, its current calibration, mainly based on S355 numerical results, seems insufficient for the present S235 database. Further investigations are consequently required to refine this correction parameter, particularly through a calibration including S235 members and combined flexural–torsional imperfection patterns.

Chapter 6

Proposal of an improved imperfection factor

The improved formulation proposed in the previous chapter allows the prediction quality to be significantly enhanced by accounting for part of the interaction effects developing between the different instability modes observed in unequal-leg angle members.

Nevertheless, the proposed formulation still relies on the imperfection factor α prescribed by EN 1993-1-1 (see Figure 2.2). As discussed in the state of the art, several previous studies haveshown that the imperfection factors prescribed by EN 1993-1-1 tend to overestimate the imperfection sensitivity of high-strength steel members, resulting in unnecessarily conservative predictions.

These observations suggest that an additional improvement of the proposed formulation may be achieved through a modification of the imperfection factor α, particularly for steel grades higher than the reference grades originally used during the calibration of the EN 1993-1-1 buckling curves.

The objective of the present chapter is therefore to investigate the possibility of introducing a modified imperfection factor α_{mod} adapted to high-strength steel unequal-leg angle members. The analysis first evaluates the conservatism of the proposed formulation for increasing steel grades before determining optimal imperfection factors directly from the numerical database. The resulting evolution of α_{opt} with the steel grade is subsequently compared with modified imperfection factor formulations available in the literature.

In the present study, α_{opt} refers to the optimal numerical values obtained from the calibration procedure, while α_{mod} designates the resulting modified imperfection factor formulation.

In order to isolate the influence of the imperfection factor from the additional effects associated with torsional–flexural modal interactions, only members presenting large h/b ratios are retained for the calibration process. As shown in the previous chapter, these members exhibit a significantly more stable behaviour and a reduced sensitivity to modal interaction effects.

Including members with low h/b ratios would artificially increase the calibrated values of α_{opt}, since the imperfection factor would then partly compensate for the non-conservative effects induced by modal interactions. However, these effects are not intended to be captured through α, but rather through the additional interaction correction introduced by the parameter β or an equivalent formulation.

6.1 Influence of the steel grade on the proposed formulation

Before developing a modified imperfection factor, the applicability of the proposed formulation presented in the previous chapter is first assessed for high-strength steel unequal-leg angle members.

The present investigation is based on three unequal-leg angle sections, namely L100×65×12, L140×90×14 and L200×100×16.

For the section L140×90×14, the classification check gives:

$$\frac{c}{t} = \frac{115}{14} = 8.21$$

compared to the Class 3 limit for S690:

$$14\sqrt{\frac{235}{690}} = 8.17$$

The Class 3 limit is therefore only slightly exceeded. Since the present study mainly focuses on the global buckling behaviour of the members, the influence of local buckling is expected to remain very limited and the section was therefore retained for the investigation of S690 steel grade members.

A similar situation is obtained for the L200×100×16 section, for which:

$$\frac{c}{t} = \frac{169}{16} = 10.56$$

while the corresponding Class 3 limit for S420 becomes:

$$14\sqrt{\frac{235}{420}} = 10.47$$

The exceedance again remains limited and was therefore considered not to significantly affect the global buckling response investigated in the present study.

The comparison between the numerical reduction factors and the predictions obtained using the complete proposed formulation is first presented in Figure 6.1 for the L200×100×16 section and for several steel grades ranging from S235 to S420.

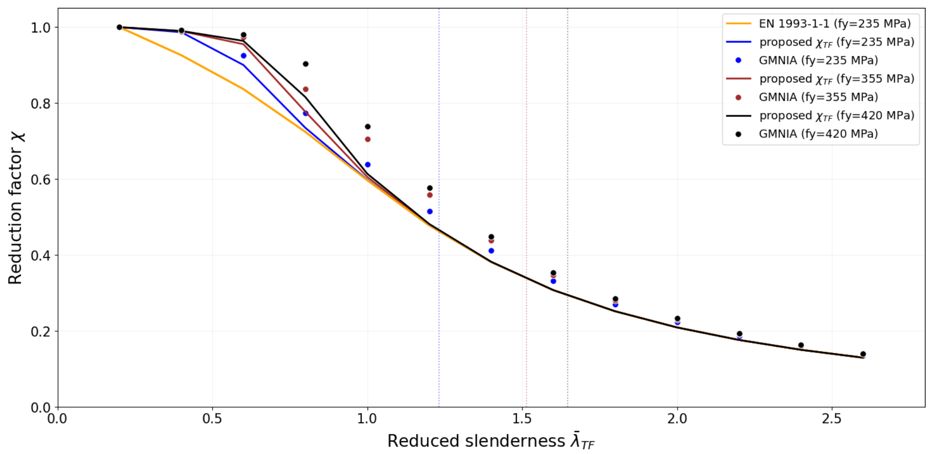

Figure 6.1: Comparison between the numerical reduction factors and the proposed formulation for the L200×100×16 section and different steel grades.

At first sight, the proposed formulation may not be expected to provide a specific improvement for high-strength steel members, since it still relies on the imperfection factor α prescribed by EN 1993-1-1. Nevertheless, the influence of the steel grade is partly introduced indirectly through the parameter Δ_F.

Indeed, for a given reduced slenderness $\bar{\lambda}_{TF}$, an increase in the yield strength requires a shorter member length in order to obtain the corresponding elastic critical load. This modification of the member length affects the relative values of $N_{cr,TF}$ and $N_{cr,v}$ and therefore modifies the interaction ratio $N_{cr,TF}/N_{cr,v}$ used in the definition of Δ_F.

As a result, the proposed formulation appears to partially adapt to the increase in steel grade within the low and intermediate slenderness range, where the interpolation governed by Δ_F remains active. Consequently, the increase in conservatism remains less pronounced than would be expected from the sole use of the unchanged EN 1993-1-1 imperfection factor.

However, as the member slenderness increases and the structural response progressively becomes governed by minor-axis flexural buckling, the influence of Δ_F gradually vanishes. The proposed formulation then progressively converges towards the flexural buckling curve governed by the original imperfection factor α. The beneficial influence of the steel grade is therefore no longer captured, leading to increasingly conservative predictions for high-strength steel members.

In order to better quantify this evolution, the prediction ratios χ_{num}/χ_{pred} obtained using both the EN 1993-1-1 formulation and the complete proposed formulation are presented in Figure 6.2.

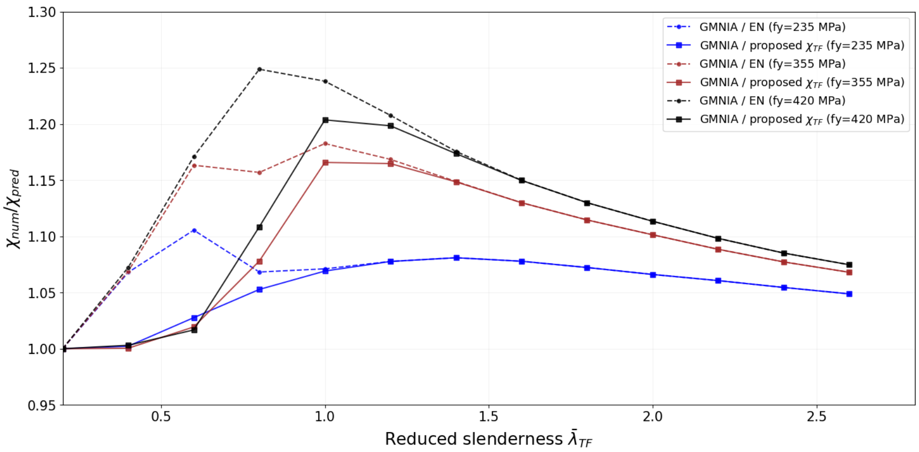

Figure 6.2: Prediction ratios χ_{num}/χ_{pred} obtained using EN 1993-1-1 and the proposed formulation for the L200×100×16 section and different steel grades.

For all considered steel grades, the proposed formulation provides a systematic improvement of the predictions compared to the original EN 1993-1-1 formulation. In particular, the interpolation introduced through Δ_F reduces part of the excessive conservatism observed for unequal-leg angle members subjected to torsional–flexural buckling.

Nevertheless, the predictions become increasingly conservative as the steel grade increases.

For the S420 results, prediction ratios exceeding 1.24 are obtained using the EN 1993-1-1 formulation, while maximum values close to 1.20 still remain visible even when the proposed formulation is adopted. These results indicate that the proposed formulation still significantly underestimates the actual resistance of high-strength steel unequal-leg angle members.

This observation is particularly important since the influence of torsional–flexural modal interactions remains limited for the present high h/b members. The remaining conservatism can therefore mainly be attributed to the imperfection factor α rather than to the interaction correction itself.

These observations therefore confirm the excessive imperfection sensitivity associated with the EN 1993-1-1 imperfection factor for high-strength steel unequal-leg angle members.

A statistical comparison of the prediction ratios obtained for the L200×100×16 section is additionally presented in Table 6.1.

f_y [MPa]	Formulation	Mean	Std. dev.	Min	Max
235	EN	1.071	0.014	1.049	1.106
235	Proposed	1.058	0.022	1.002	1.081
355	EN	1.122	0.040	1.068	1.183
355	Proposed	1.096	0.050	1.000	1.166
420	EN	1.147	0.059	1.072	1.249
420	Proposed	1.113	0.061	1.003	1.204

Table 6.1: Statistical comparison of the prediction ratios χ_{num}/χ_{pred} obtained using EN 1993-1-1 and the proposed formulation for the L200×100×16 section.

The statistical results confirm that the proposed formulation systematically improves the prediction quality compared to the original EN 1993-1-1 formulation. However, the conservatism still progressively increases with the steel grade, even when the contribution of Δ_F is included.

These observations therefore indicate that, although the interpolation introduced through Δ_F partially compensates the increase in conservatism associated with higher steel grades, the imperfection factor α remains excessively conservative for high-strength steel unequal-leg angle members.

The development of a modified imperfection factor α_{mod} therefore appears necessary in order to further improve the prediction quality of the proposed formulation for high-strength steel grades.

6.1.1 Extension to higher steel grades

In order to further investigate the influence of the steel grade on the prediction quality of the proposed formulation, an additional comparison is performed for steel grades ranging from S460 to S690 using the L140×90×14 section.

The corresponding prediction ratios χ_{num}/χ_{pred} obtained using both the original EN 1993-1-1 formulation and the proposed formulation are presented in Figure 6.3.

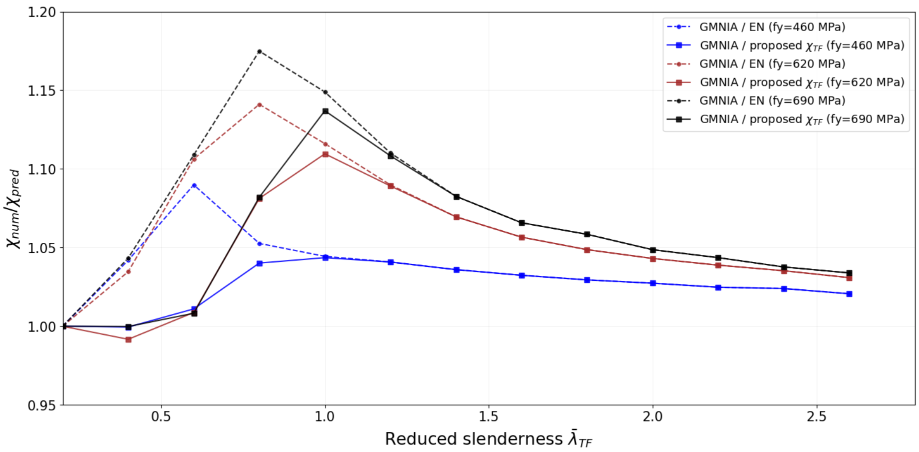

Figure 6.3: Prediction ratios χ_{num}/χ_{pred} obtained using EN 1993-1-1 and the proposed formulation for the L140×90×14 section and steel grades ranging from S460 to S690.

The same trends as those previously observed for S355 and S420 members remain valid for higher steel grades.

Although the proposed formulation still improves the predictions compared to EN 1993-1-1, a marked increase in conservatism is observed for S620 and S690 members, particularly within the flexural-dominant range where the influence of Δ_F progressively vanishes.

This increase in conservatism becomes particularly pronounced for S620 and S690 members, especially within the flexural-dominant range where the influence of Δ_F progressively vanishes and the response becomes mainly governed by the imperfection factor α.

These results further support the need for a modified imperfection factor adapted to high-strength steel unequal-leg angle members.

The present results therefore strongly support the development of a modified imperfection factor formulation specifically adapted to high-strength steel unequal-leg angle members.

6.2 Modified imperfection factor

In order to develop a modified imperfection factor formulation adapted to high-strength steel unequal-leg angle members, the first step consists in determining optimal numerical values of the imperfection factor directly from the GMNIA results.

The objective of this calibration procedure is to identify, for each steel grade, the value of the imperfection factor α leading to the best agreement between the proposed formulation and the numerical buckling resistances while limiting non-conservative predictions.

The calibration is performed separately for each considered steel grade. For a given value of the imperfection factor α, the prediction error is evaluated over the complete investigated slenderness range using the following expression:

$$\delta = \frac{N_{num} - N_{pred}}{N_{num}} \cdot 100$$

where N_{num} corresponds to the numerical ultimate resistance obtained from the GMNIA simulations and N_{pred} corresponds to the buckling resistance predicted by the proposed formulation.

Positive values of δ therefore indicate conservative predictions, while negative values correspond to non-conservative predictions.

The optimal imperfection factor α_{opt} is subsequently determined by minimising the mean absolute prediction error over the complete slenderness range. In addition, a limitation is imposed on the maximum acceptable non-conservative deviation in order to ensure that the resulting formulation remains globally safe.

In the present study, the calibration procedure was performed such that the predicted resistance could not exceed the numerical resistance by more than 2%, corresponding to:

$$\delta \geq -2\%$$

This approach allows an appropriate compromise to be obtained between prediction accuracy and structural safety.

The resulting evolution of α_{opt} with the steel grade is subsequently analysed and compared with modified imperfection factor formulations available in the literature for other structural member types.

The calibrated values of α_{opt} obtained for the investigated profiles and steel grades are summarised in Figure 6.4 for the two retained imperfection configurations.

Section Type		Steel grade								
		S235	S275	S355	S420	S460	S500	S550	S620	S690
L100x65x12	α_{opt}	0.3149	0.2704	0.2092	0.1766	0.1656	0.1557	0.145	0.1316	0.1165
	δ_{mean}	1.73%	1.27%	1.17%	0.00%	0.08%	0.14%	0.19%	0.17%	0.00%
L140x90x14	α_{opt}	0.3083	0.2621	0.2010	0.1774	0.1625	0.1525	0.1394	0.1275	0.1143
	δ_{mean}	1.30%	0.77%	0.03%	0.15%	0.03%	0.12%	0.17%	0.29%	0.43%
L200x100x16	α_{opt}	0.2332	0.1948	0.1671	0.1226					
	δ_{mean}	0.20%	0.17%	0.54%	0.18%					

(a) $F_v F_u T$ imperfection configuration

Section Type		Steel grade								
		S235	S275	S355	S420	S460	S500	S550	S620	S690
L100x65x12	α_{opt}	0.2653	0.2256	0.1733	0.1446	0.1378	0.1304	0.1189	0.1055	0.0946
	δ_{mean}	1.34%	0.88%	0.16%	0.27%	0.05%	0.06%	0.10%	0.19%	0.25%
L140x90x14	α_{opt}	0.2582	0.2169	0.1605	0.1371	0.1283	0.1180	0.1053	0.0932	0.0824
	δ_{mean}	1.17%	0.70%	0.11%	0.18%	0.04%	0.07%	0.20%	0.14%	0.04%
L200x100x16	α_{opt}	0.1967	0.1636	0.1403	0.0960					
	δ_{mean}	0.19%	0.05%	0.05%	0.34%					

(b) F_v imperfection configuration

Figure 6.4: Optimal imperfection factors α_{opt} calibrated from the GMNIA results of the selected unequal-leg angle members with high h/b ratios

For both imperfection configurations, the optimal imperfection factor clearly decreases as the steel grade increases. This trend is consistent with the observations previously reported in the literature for high-strength steel members and confirms that the imperfection sensitivity progressively decreases as the yield strength increases.

The decrease of α_{opt} is particularly pronounced between S235 and S420, after which the evolution becomes progressively smoother for higher steel grades.

A systematic difference can additionally be observed between the two imperfection configurations. The values obtained for the combined imperfection configuration $F_v F_u T$ remain consistently larger than those associated with the isolated flexural imperfection configuration F_v. This behaviour is coherent with the additional destabilising effects induced by torsional–flexural modal interactions for the $F_v F_u T$ configuration.

Nevertheless, despite these differences, both imperfection configurations exhibit a similar global evolution with increasing steel grade, suggesting that the influence of the steel grade on the imperfection sensitivity remains relatively independent of the adopted imperfection configuration.

The relatively small values of the mean prediction error δ_{mean} further indicate that the calibrated values of α_{opt} allow the proposed formulation to reproduce the numerical results with good accuracy over the investigated slenderness range.

Although the global evolution of α_{opt} remains similar for all investigated sections, certain differences can still be observed.

In particular, the sections L100×65×12 and L140×90×14 lead to very similar calibrated values, whereas the more monosymmetric section L200×100×16 generally exhibits lower values of α_{opt}.

These observations suggest that, although modal interaction effects are significantly reduced for members presenting large h/b ratios, the cross-sectional geometry still retains a certain influence on the imperfection sensitivity.

For each steel grade, the reference optimal imperfection factor α_{ref} was selected as the maximum value obtained among the three investigated members presenting large h/b ratios. The resulting reference values are summarised in Table 6.2.

This choice ensures that the resulting modified imperfection factor remains conservative for all investigated cross-sections, while avoiding the excessive sensitivity that would result from selecting the maximum value obtained at individual slenderness levels.

Imperfection	**Steel grade**								
	S235	**S275**	**S355**	**S420**	**S460**	**S500**	**S550**	**S620**	**S690**
$F_v F_u T$	0.3149	0.2704	0.2092	0.1774	0.1656	0.1557	0.1450	0.1316	0.1165
F_v	0.2653	0.2256	0.1733	0.1446	0.1378	0.1304	0.1189	0.1055	0.0946

Table 6.2: Reference optimal imperfection factors α_{ref} retained for the calibration of the modified imperfection factor formulation.

The objective of this comparison is to evaluate whether the evolution observed for unequal-leg angle members remains consistent with the modified imperfection factor trends previously proposed for other structural member types.

The evolution of the reference imperfection factor α_{ref} with the steel grade is subsequently compared with several modified imperfection factor formulations previously proposed in the literature, namely the formulations of Johansson et al. [34], Maquoi et al. [33], Somodi et al. [36] and Saufnay [35].

These formulations generally adopt the following power-law form:

$$\alpha_{mod} = \alpha_0 \left(\frac{235}{f_y} \right)^n$$

where α_0 corresponds to the reference imperfection factor associated with the considered EN 1993-1-1 buckling curve and n is a calibration exponent governing the evolution of the imperfection sensitivity with increasing steel grade.

The comparison between the calibrated values obtained in the present study and the literature formulations is presented in Figure 6.5.

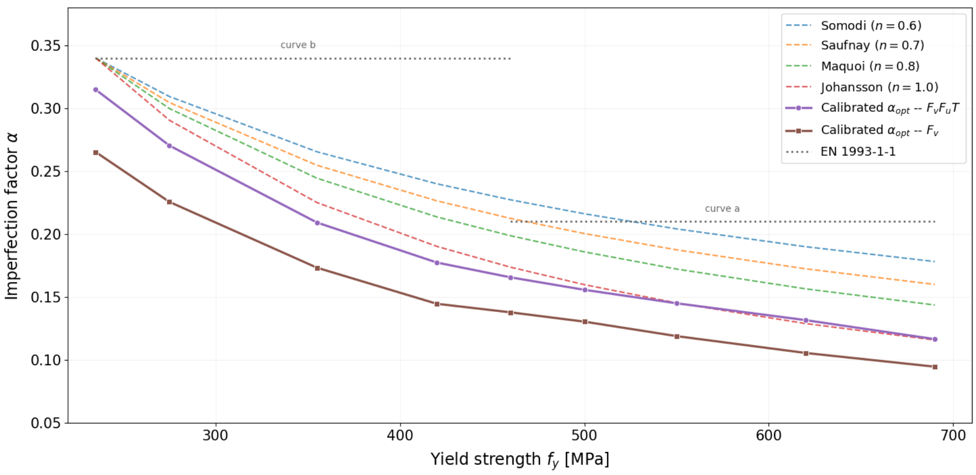

Figure 6.5: Comparison between the calibrated reference imperfection factors α_{ref} and modified imperfection factor formulations proposed in the literature

For both investigated imperfection configurations, the calibrated values clearly confirm the progressive reduction of the imperfection sensitivity with increasing steel grade.

A significant deviation from the constant imperfection factors adopted in EN 1993-1-1 can be observed, particularly for steel grades higher than the reference grades originally used for the calibration of the buckling curves. While the EN 1993-1-1 formulation retains constant values associated with buckling curves b and a, the calibrated values obtained in the present study exhibit a continuous decrease over the complete range of investigated steel grades.

The calibrated values associated with the $F_v F_u T$ imperfection configuration remain systematically higher than those obtained for the isolated flexural imperfection configuration F_v. This behaviour is consistent with the additional destabilising effects induced by torsional–flexural modal interactions.

Nevertheless, both configurations exhibit a similar evolution that is well approximated by a power-law formulation.

Among the investigated literature formulations, the expressions with exponents $n = 0.7$ and $n = 0.8$ provide the closest agreement with the present calibration results. Conversely, the formulation with $n = 1.0$ becomes non-conservative for the $F_v F_u T$ configuration when the reference value $\alpha_0 = 0.34$ corresponding to buckling curve b is adopted.

Although the formulation with $n = 1.0$ provides a closer agreement with part of the F_v results, a design-oriented proposal should not only aim at minimising the distance to the calibrated values. Instead, the selected formulation should provide a relatively uniform safety margin over the complete range of steel grades.

From this perspective, the formulation with $n = 0.7$ appears to provide the most appropriate compromise between accuracy and conservatism. In particular, its evolution remains approximately parallel to the calibrated values obtained for the $F_v F_u T$ configuration while remaining slightly above them over the investigated steel grade range.

The present results therefore demonstrate that the use of a steel-grade-dependent imperfection factor formulation is necessary to accurately reproduce the observed imperfection sensitivity and to maintain a more uniform safety level over the complete range of investigated steel grades.

Consequently, the following modified imperfection factor formulation is proposed:

$$\alpha_{mod} = 0.34 \left(\frac{235}{f_y} \right)^{0.7}$$

6.3 Overall improvement

The previous sections separately investigated the influence of the correction parameters Δ_F, β and α_{mod} introduced to improve the prediction of the buckling resistance of unequal-leg angle members.

The objective of the present section is therefore to evaluate the global performance of the complete proposed formulation obtained by combining these three parameters within the design approach proposed by Dai et al. [2].

In the complete formulation, the conventional EN 1993-1-1 imperfection factor α is replaced by the modified expression:

$$\alpha_{mod} = 0.34 \left(\frac{235}{f_y} \right)^{0.7}$$

The prediction quality of the resulting formulation is assessed through graphical and statistical comparisons of the prediction ratios χ_{num}/χ_{pred} for both imperfection configurations and for members presenting low and high h/b ratios.

The representative sections L75×65×10 and L140×90×14 were selected since they respectively represent low and high h/b members while remaining at least Class 3 up to steel grade S690.

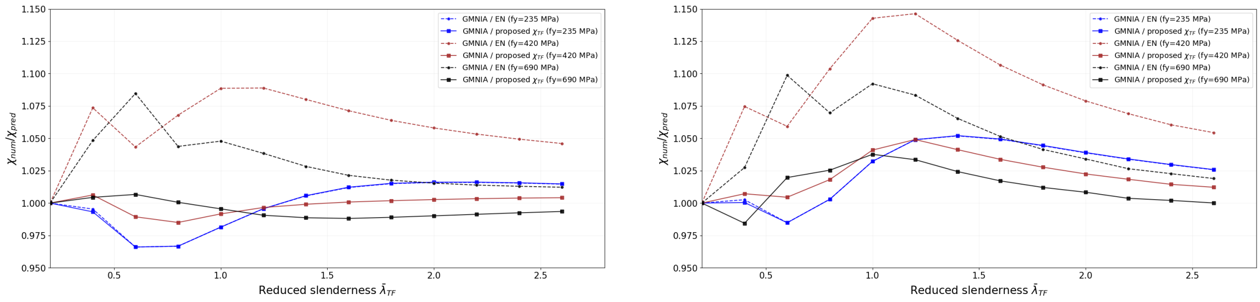

(a) F_vF_uT imperfection configuration (b) F_v imperfection configuration

Figure 6.6: Comparison between the prediction ratios χ_{num}/χ_{pred} obtained using EN 1993-1-1 and the complete proposed formulation for the low h/b section L75×65×10

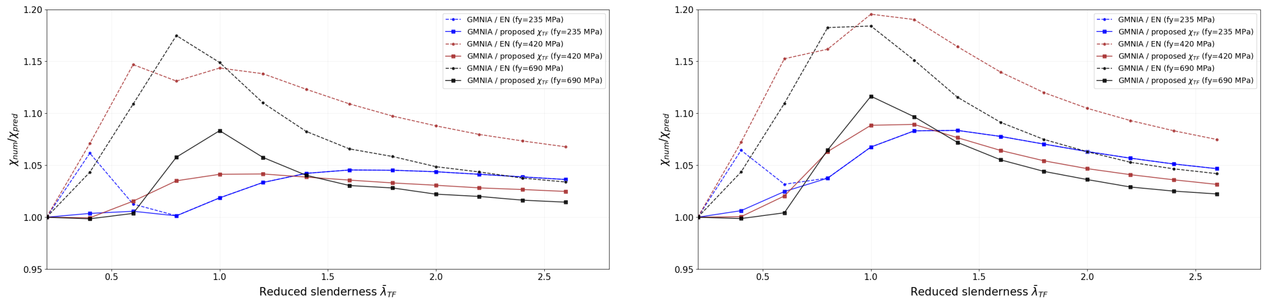

(a) F_vF_uT imperfection configuration (b) F_v imperfection configuration

Figure 6.7: Comparison between the prediction ratios χ_{num}/χ_{pred} obtained using EN 1993-1-1 and the complete proposed formulation for the high h/b section L140×90×14

For both investigated cross-sections and imperfection configurations, the proposed formulation provides significantly better agreement with the numerical results than the original EN 1993-1-1 approach.

A first important observation concerns the influence of the modified imperfection factor α_{mod} for high-strength steel members. For both investigated sections, the excessive conservatism identified for steel grades S420 and S690 is significantly reduced, with prediction ratios remaining much closer to unity over the complete slenderness range.

For the high h/b section L140×90×14, the obtained prediction ratios remain very close to unity for both imperfection configurations. In particular, the excessive conservatism previously observed in the transition region is strongly reduced and the scatter between the different steel grades becomes significantly smaller. These observations confirm that the combination of Δ_F and α_{mod} provides an efficient correction of both the vertical scatter associated with torsional–flexural behaviour and the excessive conservatism induced by the conventional EN 1993-1-1 imperfection factors.

For the low h/b section L75×65×10, the complete formulation also leads to a substantial reduction of the excessive conservatism associated with high-strength steel members. Nevertheless, several non-conservative predictions still remain visible within the transition region, particularly for the F_vF_uT imperfection configuration.

In particular, for steel grade S420, the complete proposed formulation may lead to slightly more non-conservative predictions than the original EN 1993-1-1 formulation. However, these discrepancies should not be directly attributed to the modified imperfection factor α_{mod}, whose role is limited to reproducing the reduced imperfection sensitivity associated with increasing steel grade.

The remaining discrepancies rather indicate that the severe torsional–flexural modal interactions developing for low h/b members are still not fully reproduced by the present interaction correction through β.

These results nevertheless suggest that α_{mod} is not limited to high h/b members, since its physical role remains independent from the modal interaction effects themselves. Its calibration may therefore also be extended to lower h/b members, provided that an appropriate interaction correction is used simultaneously.

However, compared to the original EN 1993-1-1 predictions, the global prediction quality remains significantly improved and the magnitude of the conservatism is substantially reduced for all investigated steel grades.

Overall, the combined use of Δ_F, β and α_{mod} provides a substantially more consistent representation of the buckling behaviour of unequal-leg angle members over a wide range of steel grades and geometrical configurations.

The proposed approach efficiently reduces the excessive conservatism of EN 1993-1-1 for high-strength steel members while maintaining an overall safe prediction level in the presence of strong torsional–flexural interactions.

In addition to the graphical comparisons, statistical indicators were also evaluated in order to quantify the global prediction quality of the complete proposed formulation.

For each investigated configuration, the mean, minimum and maximum values of the prediction ratios χ_{num}/χ_{pred} were calculated over the complete range of investigated slenderness values and representative steel grades.

The statistical results obtained using the complete proposed formulation are compared with those associated with the original EN 1993-1-1 design approach in Tables 6.3 to 6.6.

Table 6.3: Statistical comparison between EN 1993-1-1 and the proposed formulation for the low h/b section L75×65×10 with the F_vF_uT imperfection configuration

f_y	**Formulation**	**Mean**	**Min**	**Max**
S235	EN	1.000	0.966	1.016
	Proposed	1.000	0.966	1.016
S420	EN	1.065	1.043	1.089
	Proposed	0.999	0.985	1.006
S690	EN	1.032	1.012	1.085
	Proposed	0.994	0.988	1.007

Table 6.4: Statistical comparison between EN 1993-1-1 and the proposed formulation for the low h/b section L75×65×10 with the F_v imperfection configuration

f_y	Formulation	Mean	Min	Max
S235	EN	1.029	0.985	1.052
	Proposed	1.029	0.985	1.052
S420	EN	1.093	1.054	1.146
	Proposed	1.024	1.005	1.049
S690	EN	1.053	1.019	1.099
	Proposed	1.014	0.984	1.038

Table 6.5: Statistical comparison between EN 1993-1-1 and the proposed formulation for high h/b sections with the $F_v F_u T$ imperfection configuration

f_y	Formulation	Mean	Min	Max
S235	EN	1.046	0.996	1.106
	Proposed	1.040	0.995	1.081
S420	EN	1.117	1.066	1.249
	Proposed	1.038	1.001	1.107
S690	EN	1.074	1.038	1.144
	Proposed	1.029	0.998	1.083

Table 6.6: Statistical comparison between EN 1993-1-1 and the proposed formulation for high h/b sections with the F_v imperfection configuration

f_y	Formulation	Mean	Min	Max
S235	EN	1.070	1.015	1.122
	Proposed	1.063	1.015	1.122
S420	EN	1.137	1.068	1.278
	Proposed	1.056	1.003	1.143
S690	EN	1.089	1.037	1.184
	Proposed	1.044	0.999	1.116

The statistical results presented in Tables 6.3 to 6.6 globally confirm the observations previously drawn from the graphical comparisons.

For both low and high h/b members, the proposed formulation systematically reduces the excessive conservatism associated with the current EN 1993-1-1 design approach, particularly for high-strength steel grades.

A significant reduction of the mean prediction ratio can notably be observed for S420 and S690 members, for which the proposed formulation generally provides values much closer to unity. At the same time, the scatter of the predictions is also reduced, as illustrated by the lower maximum values obtained with the proposed formulation.

For instance, for the high h/b members subjected to the F_v imperfection configuration, the mean prediction ratio decreases from 1.137 to 1.056 for S420 steel.

For the high h/b members, the proposed formulation provides very consistent predictions over the complete investigated steel grade range, with mean values generally remaining close to $\chi_{num}/\chi_{pred} = 1.0$ while maintaining a limited scatter.

For the low h/b section, the prediction quality is also significantly improved compared to EN 1993-1-1, although some remaining unsafe predictions can still be observed locally due to the stronger modal interaction effects developing in these members.

Overall, the statistical comparisons confirm that the combined use of Δ_F, β and α_{mod} significantly improves the prediction quality and allows a more uniform safety level to be maintained over the complete range of investigated steel grades.

The present results therefore suggest that the excessive conservatism of EN 1993-1-1 for high-strength steel unequal-leg angle members mainly originates from:

- the inability of the conventional formulation to properly reproduce the modal interaction effects developing in unequal-leg angle members,
- and the use of imperfection factors calibrated on conventional steel grades.

The proposed formulation provides a physically consistent framework capable of addressing both effects simultaneously through the combined use of Δ_F, β and α_{mod}.

Although some local non-conservative predictions still remain for members presenting severe torsional–flexural interactions, the present results suggest that interaction corrections based on parameters similar to β provide a promising basis for further improving the prediction consistency of unequal-leg angle members.

6.4 Reliability analysis

The reliability analysis of the flexural buckling design provisions of EN 1993-1-1:2022 and of the proposed modified formulation was carried out according to the procedure specified in EN 1990:2023 [42].

EN 1990 establishes the general principles and requirements for the verification of structural safety and provides a statistical framework for the assessment of design formulations. More specifically, Annex D of EN 1990:2023 provides a procedure for evaluating the reliability of a design rule based on experimental results and/or numerical simulations.

As a first step of the reliability assessment, the predicted buckling resistances R_t are compared with the numerical resistances R_e obtained from the GMNIA simulations. The corresponding comparisons are presented in Figure 6.8 for the current EN 1993-1-1:2022 design approach and in Figure 6.9 for the proposed modified formulation.

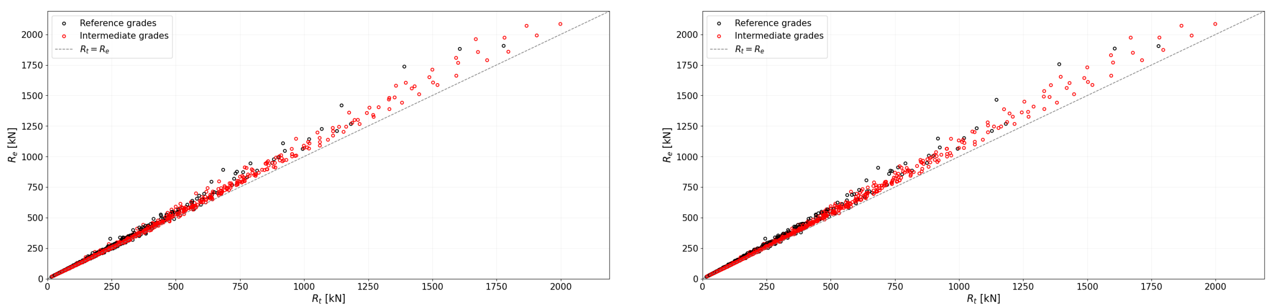

(a) $F_v F_u T$ deformation configuration (b) F_v deformation configuration

Figure 6.8: Comparison between GMNIA numerical buckling resistances and predictions obtained using EN 1993-1-1:2022 for different steel grades

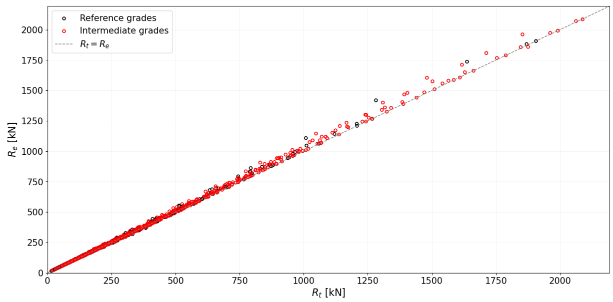

(a) $F_v F_u T$ deformation configuration

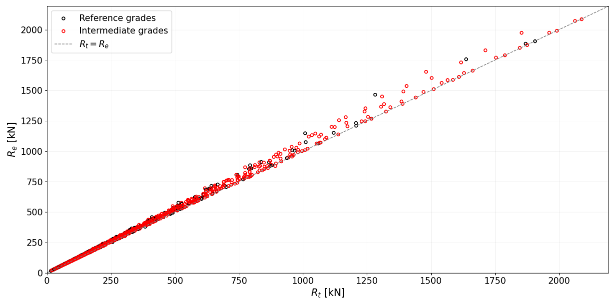

(b) F_v deformation configuration

Figure 6.9: Comparison between GMNIA numerical buckling resistances and predictions obtained using the proposed modified formulation for different steel grades

For the current EN 1993-1-1 formulation, a significant systematic conservatism can be observed, particularly for the intermediate and high-strength steel grades. Most of the numerical results remain clearly above the equality line $R_t = R_e$, indicating that the buckling resistances predicted by EN 1993-1-1 are generally lower than the corresponding numerical resistances.

By contrast, the proposed modified formulation considerably reduces this systematic bias. The numerical results become significantly more centred around the equality line while simultaneously exhibiting a reduced scatter. This behaviour confirms that the proposed formulation provides a more accurate representation of the numerical buckling resistances over the complete range of investigated steel grades.

The improvement is particularly pronounced for the intermediate steel grades, for which the excessive conservatism observed with the current EN 1993-1-1 provisions is substantially reduced.

The procedure detailed in Annex D of EN 1990:2023 [42] was subsequently applied to evaluate the required partial safety factor γ_M^* and thereby assess the adequacy of the proposed design formulation.

To simplify the reliability assessment, the simplified procedure P2 proposed by Tankova et al. [43] was adopted. This procedure has been shown to provide consistently safe-sided results when compared with a strict application of the Annex D methodology.

The statistical evaluation was performed on a database comprising $n = 1188$ GMNIA simulations for each imperfection configuration.

Within this approach, the variability of the basic variables, V_{rt}, is determined from the variability of the yield strength, the cross-sectional area and the Young's modulus according to:

$$V_{rt}^2 = V_{f_y}^2 + V_A^2 + V_E^2$$

Annex E of EN 1990:2023 provides a coefficient of variation of $V_E = 3.0\%$ for the Young's modulus. The coefficient of variation of the cross-sectional area was evaluated from the geometric tolerances reported in Annex E, namely $V_h = 0.9\%$, $V_b = 0.9\%$ and $V_t = 2.5\%$. Following the procedure proposed by Afshan et al. [44], this leads to an estimated value of $V_A \approx 2.8\%$.

For the variability of the yield strength, the most critical value among the investigated steel grades was adopted in order to remain conservative. The maximum value is obtained for S235 and S275 steel grades, resulting in $V_{f_y} = 5.5\%$.

The resulting coefficient of variation of the basic variables is therefore:

$$V_{rt} = 6.86\%$$

The slope of the resistance function b quantifies the average level of conservatism of the considered design formulation, while the coefficient of variation of the errors V_δ characterises the associated model uncertainty. These parameters are subsequently used to evaluate the required partial safety factor γ_{M1}^* according to the procedure described previously.

The comparison allows the influence of the proposed formulation on the prediction accuracy and the resulting safety level to be assessed. Particular attention is given to the evolution of the bias factor and the resulting values of γ^*_{M1} relative to the reference value $\gamma_{M1} = 1.0$ adopted in EN 1993-1-1.

The statistical parameters obtained from the reliability assessment are summarised in Table 6.7.

Table 6.7: Statistical parameters and calibrated partial safety factors obtained from the reliability analysis

Formulation	b	V_δ	γ^*_{M1}
EN (F_vF_uT)	1.0474	4.05%	1.2200
Proposed (F_vF_uT)	1.0133	1.94%	1.2286
EN (F_v)	1.0763	3.97%	1.1855
Proposed (F_v)	1.0415	2.39%	1.2005

The results presented in Table 6.7 confirm the improvements previously observed from the graphical comparisons.

For both imperfection configurations, the proposed formulation significantly reduces the bias factor b, indicating a substantial reduction of the excessive conservatism associated with the current EN 1993-1-1 provisions. A noticeable reduction of the model uncertainty V_δ is also observed, demonstrating a more accurate and more consistent prediction of the numerical buckling resistances. For the F_vF_uT configuration, the coefficient of variation is reduced by more than 50%, decreasing from 4.05% to 1.94%.

Despite these improvements, only limited variations are observed in the calibrated partial safety factor γ^*_{M1}. The slightly larger values of γ^*_{M1} obtained for the proposed formulation should not be interpreted as a reduction in safety. They primarily reflect the reduced conservatism of the proposed model, which is characterised by bias factors closer to unity.

Furthermore, the reliability assessment is also strongly influenced by the variability of the basic variables, for which conservative values were adopted in the present study. In particular, the highest coefficient of variation of the yield strength was retained and the variability of the cross-sectional area was estimated conservatively from the geometric tolerances provided in EN 1990. As a result, the improvements achieved in terms of prediction accuracy and model uncertainty are only partially reflected in the calibrated values of γ^*_{M1}.

The calculated values of γ^*_{M1} for the proposed formulation remain very close to those obtained for the current EN 1993-1-1 provisions. Considering that the current standard adopts a partial safety factor $\gamma_{M1} = 1.0$ for flexural buckling design, the present results suggest that the proposed formulation does not require a higher level of safety than the existing design rules.

Furthermore, Annex D of EN 1990 explicitly recognises that the scatter of the resistance predictions may be reduced through the introduction of additional parameters accounting for physical effects that were previously neglected. The parameters Δ_F, β and α_{mod} introduced in the present study constitute a direct application of this principle, since they explicitly account for modal interaction effects and the influence of steel grade that are not fully represented in the current design provisions.

Consequently, the present results suggest that the adoption of $\gamma_{M1} = 1.0$ together with the proposed formulation may remain appropriate. The proposed formulation therefore appears capable of improving the prediction accuracy while maintaining a reliability level comparable to that of the current design provisions. Nevertheless, a more comprehensive reliability assessment based on experimental evidence would be required before such a recommendation could be formally adopted.

Chapter 7

Conclusions and perspectives

The objective of this work was to investigate the flexural buckling behaviour of hot-rolled unequal-leg angle members over a wide range of steel grades, from S235 to S690, and to assess the suitability of the current EN 1993-1-1 design provisions. Particular attention was devoted to the influence of modal interactions and steel grade on the buckling response, with the aim of developing improved design recommendations for high-strength steel members.

A finite element modelling strategy was first developed and validated against available experimental results. The validation study confirmed the capability of the adopted GMNIA models to reproduce the observed buckling behaviour of unequal-leg angle members. However, the analyses also highlighted the significant influence of the assumed initial imperfection shape on the predicted resistance. Although both the F_v and F_vF_uT imperfection configurations provided satisfactory agreement with the experimental database, the available test results remain insufficient to definitively identify the most representative imperfection pattern for practical design applications.

The subsequent parametric study demonstrated that the current EN 1993-1-1 provisions do not fully capture the complex interaction between torsional–flexural and flexural buckling modes. The influence of these interactions was found to strongly depend on both the adopted imperfection configuration and the cross-sectional geometry.

For the combined imperfection configuration F_vF_uT, significant conservatism was observed for members governed by torsional–flexural buckling, while unsafe predictions developed in the transition region where strong modal interactions occur. For the isolated flexural imperfection configuration F_v, the same general trends were observed, although the unsafe predictions were considerably less pronounced.

Although the general trends observed throughout the study were found to be consistent for both imperfection configurations, the severity of the modal interactions remained strongly dependent on the adopted imperfection shape. The selection of a representative initial imperfection therefore remains an open question and constitutes one of the main sources of uncertainty affecting the numerical predictions.

The analyses further highlighted the importance of the cross-sectional aspect ratio h/b. Members with relatively low h/b ratios exhibited the strongest modal interactions and the largest deviations from the current design predictions, whereas members with larger h/b ratios showed a behaviour more consistent with the assumptions underlying the current EN 1993-1-1 provisions. The cross-sectional aspect ratio h/b was therefore identified as a key parameter governing the development of modal interactions and the resulting buckling behaviour of unequal-leg angle members.

These observations confirm that the current design approach does not fully account for the influence of modal interactions and cross-sectional geometry on the buckling resistance of unequal-leg angle members.

The improved design approach proposed by Dai et al. was then assessed over the complete numerical database. The introduction of the parameter Δ_F was shown to significantly improve the representation of the gradual transition between torsional–flexural and flexural buckling behaviour, particularly for members presenting relatively large h/b ratios.

The interaction parameter β was found to provide a partial correction of the remaining discrepancies associated with modal interactions. However, some unsafe predictions persisted for members exhibiting strong modal interactions, indicating that further developments are still required.

These observations suggest that interaction-based correction parameters provide a promising framework for future improvements of the current design provisions.

Despite these limitations, the combined use of Δ_F and β was shown to provide a more consistent representation of the numerical buckling resistances over a wide range of geometries and slenderness values.

The influence of steel grade was subsequently investigated. The results demonstrated that the conservatism associated with the current EN 1993-1-1 buckling curves increases significantly with increasing yield strength. This behaviour was shown to be primarily related to the use of constant imperfection factors calibrated on conventional steel grades. The numerical results confirmed that the relative influence of initial imperfections decreases as the yield strength increases, leading to a progressive reduction of the imperfection sensitivity of high-strength steel members.

Based on these observations, a modified steel-grade-dependent imperfection factor formulation based on an exponent of n=0.7 was proposed for unequal-leg angle members. The proposed expression follows the same general philosophy as previously published formulations while being specifically calibrated for unequal-leg angle members.

When combined with the modal interaction corrections proposed by Dai et al., the resulting formulation was shown to substantially reduce the excessive conservatism associated with high-strength steel members while maintaining a satisfactory level of safety.

A reliability assessment was finally performed according to the procedure of EN 1990. The statistical evaluation was performed on a database comprising 1188 GMNIA simulations for each imperfection configuration, providing a robust basis for the reliability assessment. The proposed formulation was shown to significantly reduce both the bias factor and the model uncertainty. Furthermore, the resulting values of the calibrated partial safety factor remained very close to those obtained for the current EN 1993-1-1 provisions. These results suggest that the proposed formulation is capable of improving the prediction accuracy without adversely affecting the reliability level associated with the current design rules.

Despite these encouraging results, several aspects deserve further investigation. Firstly, additional experimental studies including detailed measurements of initial geometric imperfections would be valuable to clarify the most representative imperfection shapes for unequal-leg angle members and to further improve the numerical modelling assumptions. Secondly, although the parameter β significantly reduces the unsafe predictions observed for members with low h/b ratios, some discrepancies remain in regions characterised by strong modal interactions. The present results nevertheless indicate that interaction-based correction factors constitute a promising framework for further developments. Finally, the applicability of the proposed formulation to other boundary conditions, cross-sectional classes and loading situations remains to be investigated.

Overall, the present work contributes to a better understanding of the buckling behaviour of unequal-leg angle members by highlighting the mechanical complexities associated with modal interactions and by identifying some limitations of the current EN 1993-1-1 provisions. The results further provide a basis for the future development of more accurate and physically consistent design recommendations for high-strength steel unequal-leg angle members.

7.1 Calculation of the Trilinear Material Model Parameters

$$\bar{\sigma}_e = f_y = 235 \text{ MPa} \qquad f_u = 360 \text{ MPa}$$

$$\bar{\epsilon}_{e2} = \epsilon_{sh} = 0.1\frac{f_y}{f_u} - 0.055 = 0.0103$$

$$\text{with} \qquad 0.015 \leq \epsilon_{sh} \leq 0.03$$

$$\Rightarrow \qquad \epsilon_{sh} = 0.015$$

$$\epsilon_u = 0.6\left(1 - \frac{f_y}{f_u}\right) = 0.2083$$

$$C_2 = \frac{\epsilon_{sh} + 0.4(\epsilon_u - \epsilon_{sh})}{\epsilon_u} = 0.4432$$

$$E_{t2} = E_{sh} = \frac{f_u - f_y}{C_2\epsilon_u - \epsilon_{sh}} = 1616.7 \text{ MPa}$$

7.2 Comparison with predictions of EN 1993-1-1

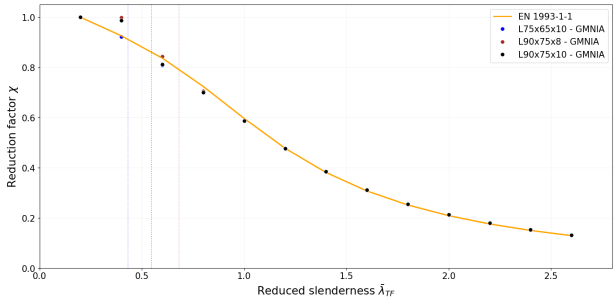

(a) $F_v F_u T$ imperfection configuration

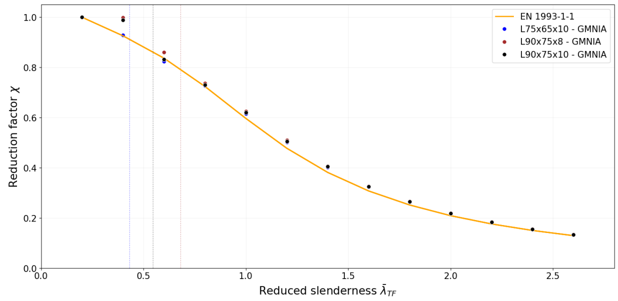

(b) F_v imperfection configuration

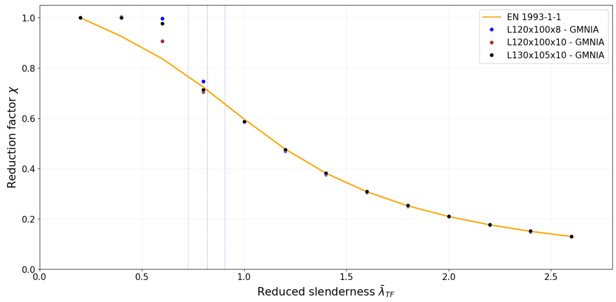

(c) $F_v F_u T$ imperfection configuration

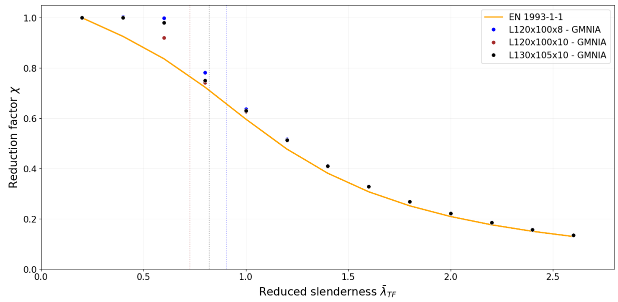

(d) F_v imperfection configuration

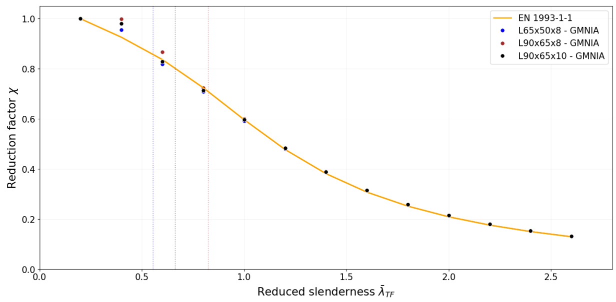

(e) $F_v F_u T$ imperfection configuration

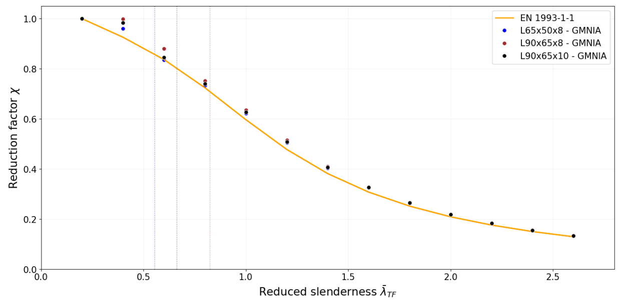

(f) F_v imperfection configuration

Figure 7.1: Comparison between the numerical reduction factors and the EN 1993-1-1 buckling curve b for selected S235 unequal-leg angle members.

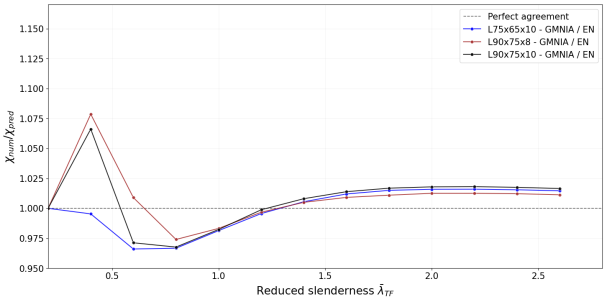

(a) $F_v F_u T$ imperfection configuration

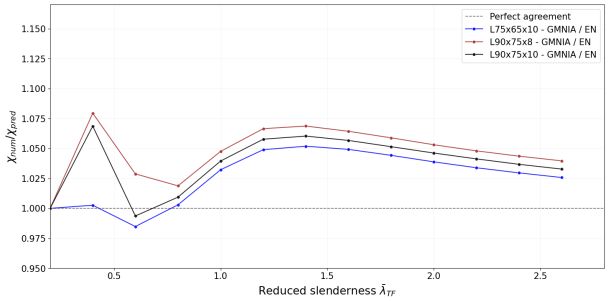

(b) F_v imperfection configuration

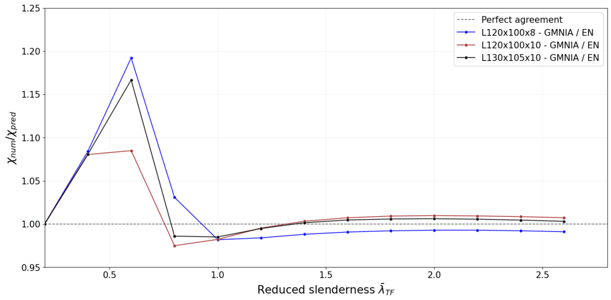

(c) $F_v F_u T$ imperfection configuration

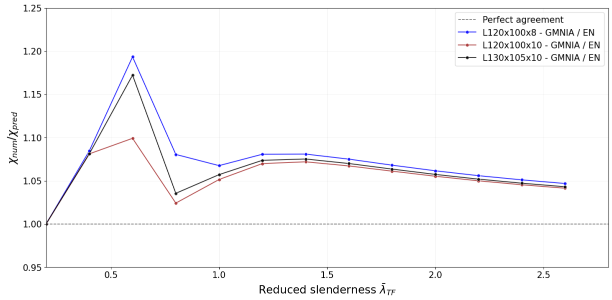

(d) F_v imperfection configuration

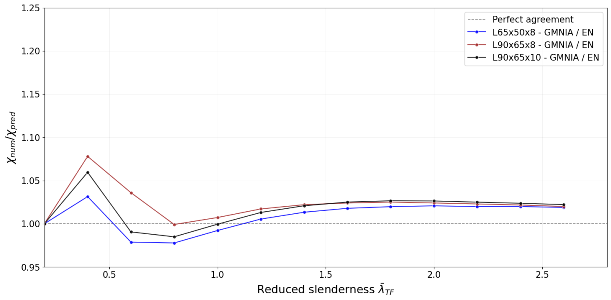

(e) $F_v F_u T$ imperfection configuration

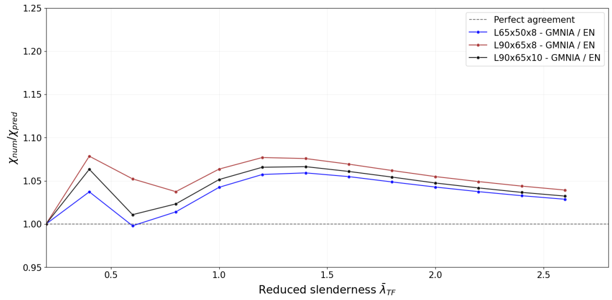

(f) F_v imperfection configuration

Figure 7.2: Ratio between numerical reduction factors and EN 1993-1-1 predictions for selected S235 unequal-leg angle members.

7.2.1 Influence of the cross-sectional aspect ratio on modal interactions

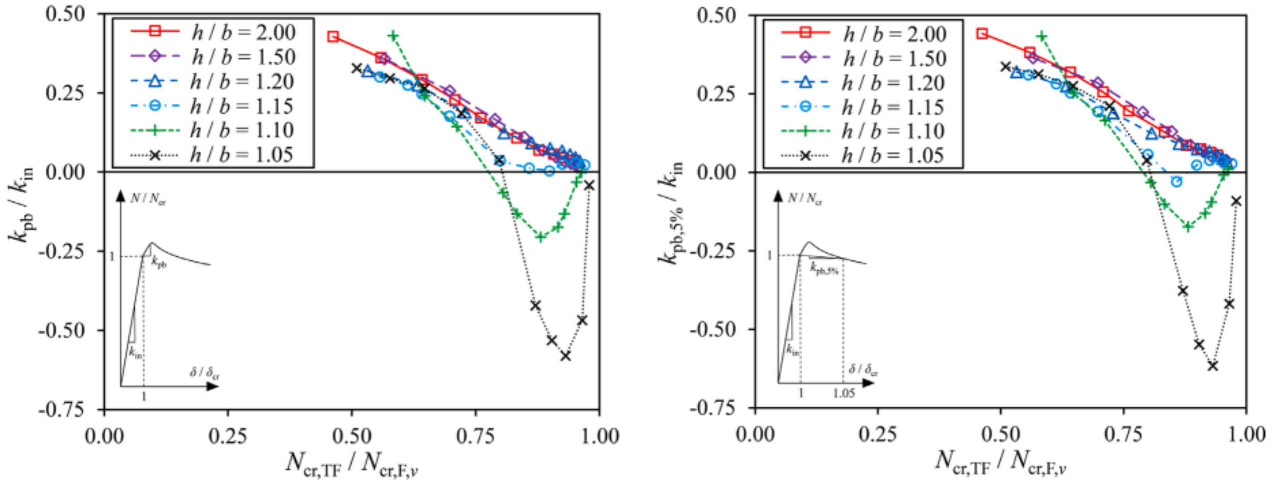

Figure 7.3: Relationship (a) between the ratio of the initial post-buckling axial stiffness to the initial pre-buckling axial stiffness k_{pb}/k_{in}in and the elastic buckling load ratio $N_{cr,TF}/N_{cr,v}$, and (b) between the ratio of the post-buckling axial stiffness at a displacement 5% beyond the elastic critical buckling point ($\delta = 1.05\delta_{cr}$) to the initial axial stiffness $k_{pb,5\%}/k_{in}$ and $N_{cr,TF}/N_{cr,v}$ for fixed-ended unequal-leg angle section columns with various h/b ratios, according to [2].

7.3 Complete formulation proposed by Dai et al.

Table 6

Summary of new design proposals for predicting the ultimate resistance of fixed-ended unequal-leg angle section steel columns.

TF dominant ($N_{cr,TF}/N_{cr,F,v} \leq 0.9$)		F,v dominant ($0.9 < N_{cr,TF}/N_{cr,F,v} < 1.0$)	
Equation	Equation reference	Equation	Equation reference
$N_{b,prop} = \frac{\chi_{TF} A f_y}{\gamma_{M1}}$,	(29)	$N_{b,prop} = \frac{\chi_F A f_y}{\gamma_{M1}}$,	(34)
where:		where:	
$\chi_{TF} = \chi_F + \Delta_F\ (\chi_T - \chi_F)$,	(28)	$\chi_F = \frac{1}{\phi + \sqrt{\phi^2 - \bar{\lambda}_{TF}^2}}$ but $\chi_F \leq 1.0$ and $\chi_F \leq \chi_{F,EC3}$,	(30)
in which:		in which:	
$\Delta_F = \left(1 - \frac{N_{cr,TF}}{0.9 N_{cr,F,v}}\right)^2$,	(26)	$\phi = 0.5\left(1 + \eta + \bar{\lambda}_{TF}^2\right)$,	(31)
$\chi_T = \frac{\bar{\lambda}_{TF} - 0.188}{\bar{\lambda}_{TF}^2}$ but $\chi_T \leq 1.0$,	(27)	$\eta = \alpha\beta\left(\bar{\lambda}_{TF} - \bar{\lambda}_0\right)^\beta$,	(32)
$\bar{\lambda}_{TF} = \sqrt{\frac{A f_y}{N_{cr,TF}}}$,	(22)	in which:	
in which: exact solution of $N_{cr,TF}$ in:	(10),	$\beta = \begin{cases} 7.5\left(1 - \frac{N_{cr,TF}}{N_{cr,F,v}}\right)(6 - 5h/b) + 1 & \text{but } 1.0 \leq \beta \leq 1.75 \quad \text{(hot-rolled)} \\ 4.5\left(1 - \frac{N_{cr,TF}}{N_{cr,F,v}}\right)(6 - 5h/b) + 1 & \text{but } 1.0 \leq \beta \leq 1.45 \quad \text{(cold-formed)} \end{cases}$,	(33)
and approximated solution of $N_{cr,TF}$ in:	(12).	$\alpha = \begin{cases} 0.34 & \text{(hot-rolled)} \\ 0.49 & \text{(cold-formed)} \end{cases}$, and	
Gross cross-sectional area A to be used for Class 1–4 sections.		$\bar{\lambda}_0 = 0.2$.	
		Gross cross-sectional area A to be used for Class 1–3 sections, and effective cross-sectional area A_{eff} to be used for Class 4 sections.	

Figure 7.4: Complete design formulation proposed by Dai et al. [2]

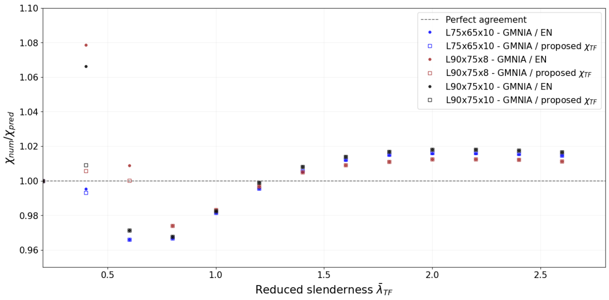

(a) $F_v F_u T$ imperfection configuration

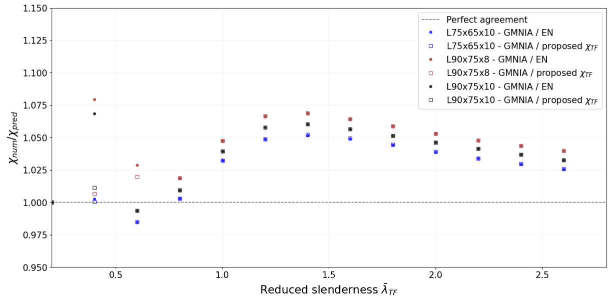

(b) F_v imperfection configuration

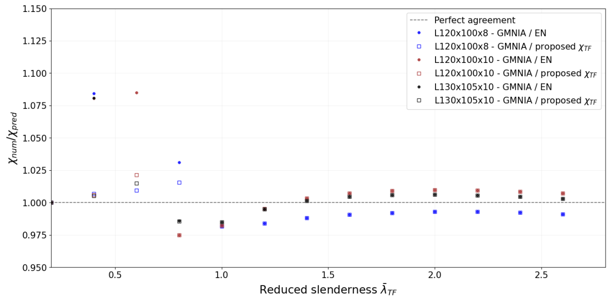

(c) $F_v F_u T$ imperfection configuration

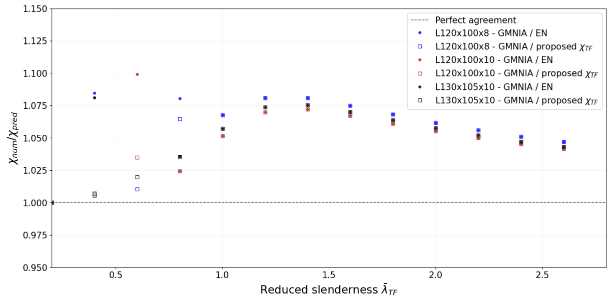

(d) F_v imperfection configuration

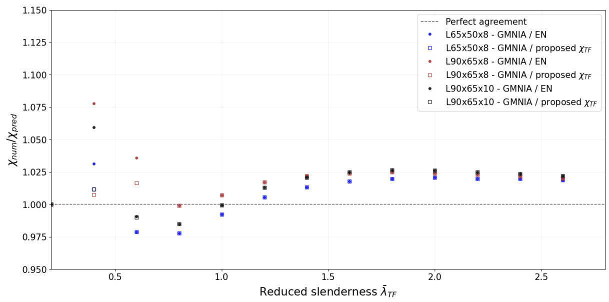

(e) $F_v F_u T$ imperfection configuration

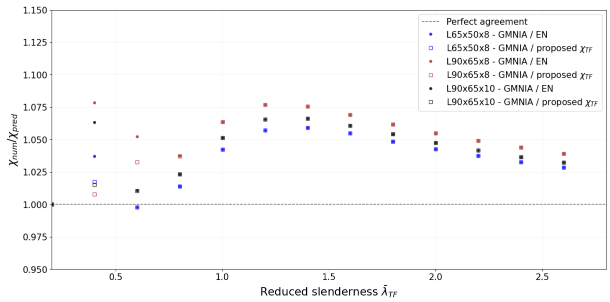

(f) F_v imperfection configuration

Figure 7.5: Prediction ratios χ_{num}/χ_{pred} obtained using EN 1993-1-1 and the complete formulation proposed by Dai et al. [2] for selected S235 unequal-leg angle members.

7.4 Overall improvement

7.4.1 Grade S275 to S420

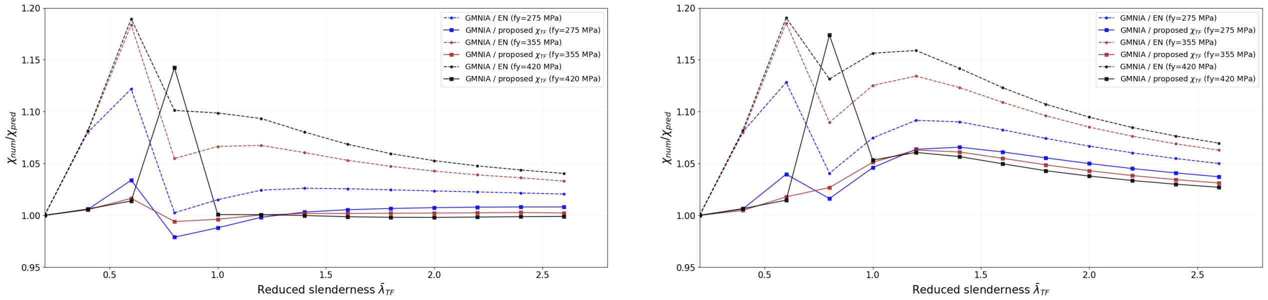

(a) $F_v F_u T$ imperfection configuration (b) F_v imperfection configuration

Figure 7.6: Comparison between the prediction ratios χ_{num}/χ_{pred} obtained using EN 1993-1-1 and the complete proposed formulation for the section L55×50×5

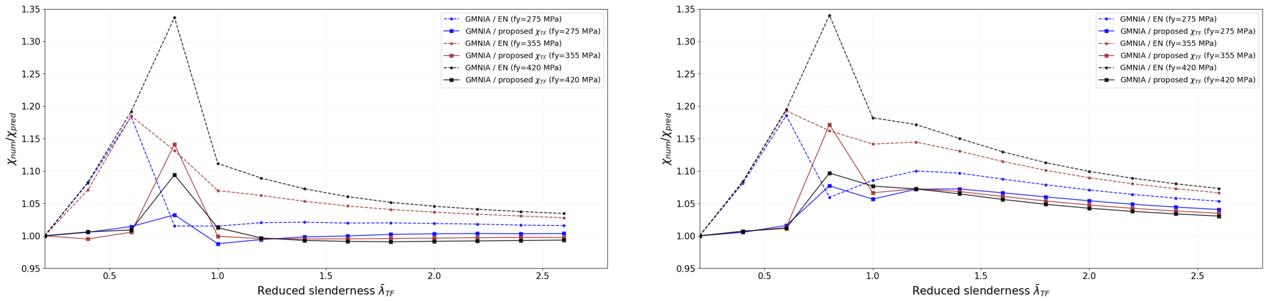

(a) $F_v F_u T$ imperfection configuration (b) F_v imperfection configuration

Figure 7.7: Comparison between the prediction ratios χ_{num}/χ_{pred} obtained using EN 1993-1-1 and the complete proposed formulation for the section L75×65×6

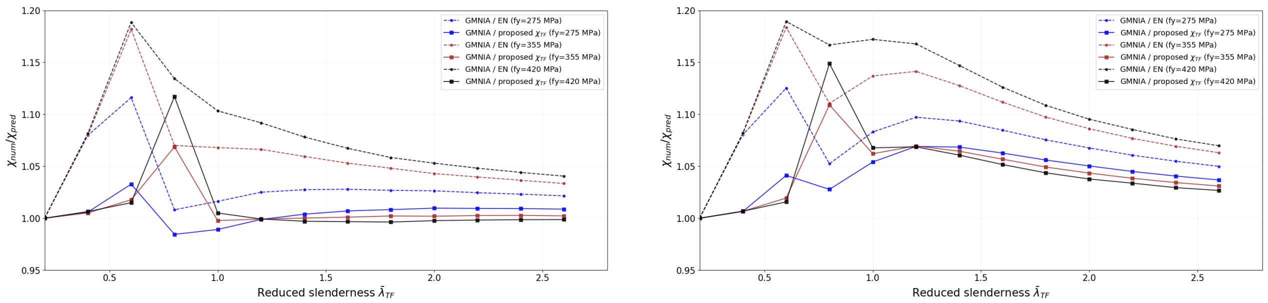

(a) $F_v F_u T$ imperfection configuration (b) F_v imperfection configuration

Figure 7.8: Comparison between the prediction ratios χ_{num}/χ_{pred} obtained using EN 1993-1-1 and the complete proposed formulation for the section L90×75×8

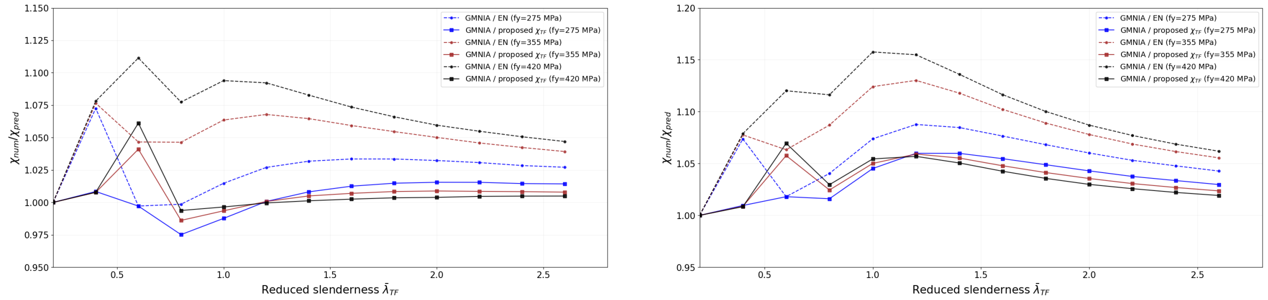

(a) $F_v F_u T$ imperfection configuration

(b) F_v imperfection configuration

Figure 7.9: Comparison between the prediction ratios χ_{num}/χ_{pred} obtained using EN 1993-1-1 and the complete proposed formulation for the section L90×75×10

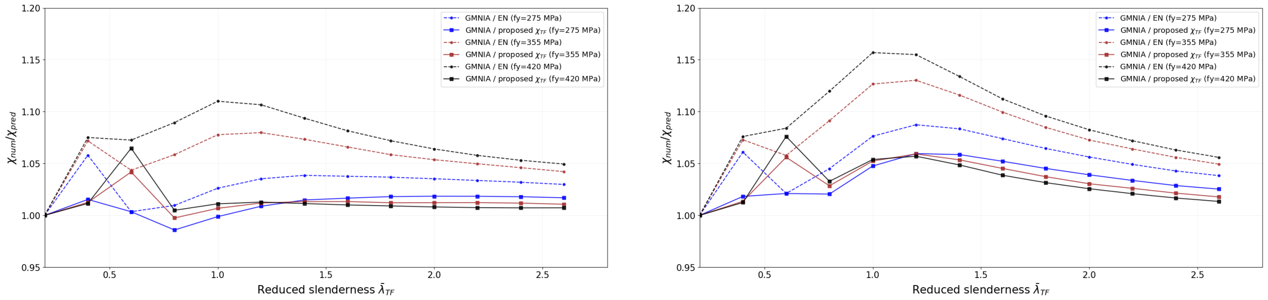

(a) $F_v F_u T$ imperfection configuration

(b) F_v imperfection configuration

Figure 7.10: Comparison between the prediction ratios χ_{num}/χ_{pred} obtained using EN 1993-1-1 and the complete proposed formulation for the section L65×50×8

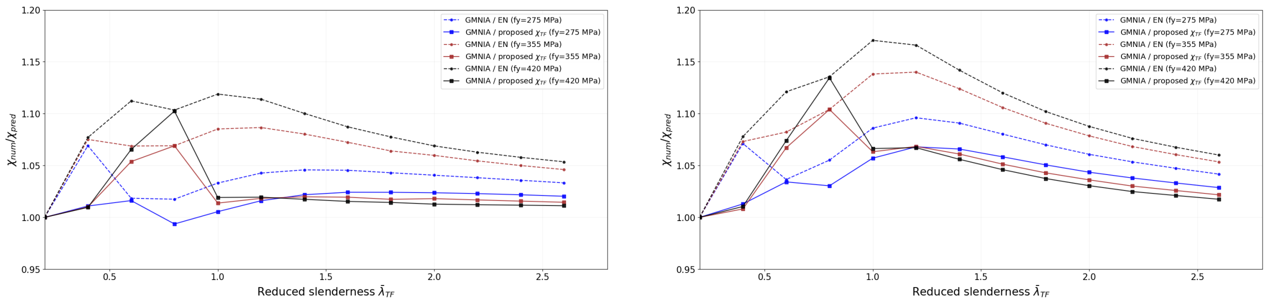

(a) $F_v F_u T$ imperfection configuration

(b) F_v imperfection configuration

Figure 7.11: Comparison between the prediction ratios χ_{num}/χ_{pred} obtained using EN 1993-1-1 and the complete proposed formulation for the section L90x65x10

7.4.2 Grade S460 to S690

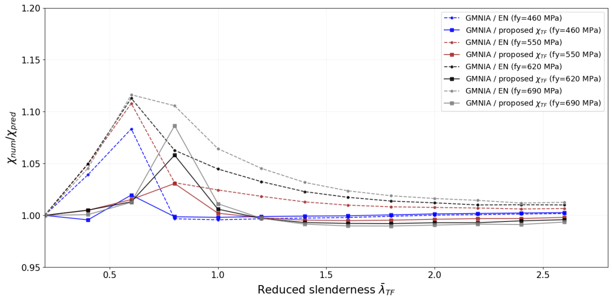

(a) F_vF_uT imperfection configuration

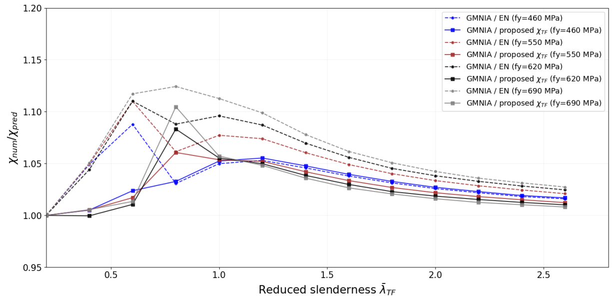

(b) F_v imperfection configuration

Figure 7.12: Comparison between the prediction ratios χ_{num}/χ_{pred} obtained using EN 1993-1-1 and the complete proposed formulation for the section L90x75x10

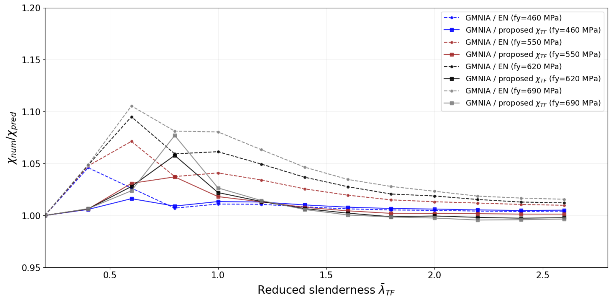

(a) F_vF_uT imperfection configuration

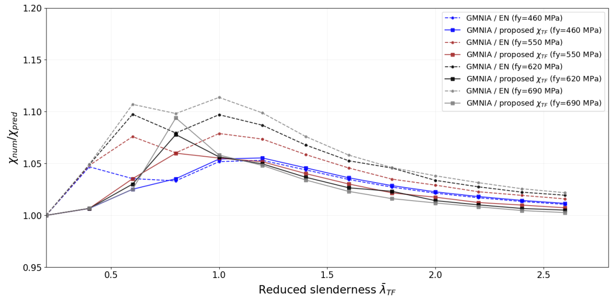

(b) F_v imperfection configuration

Figure 7.13: Comparison between the prediction ratios χ_{num}/χ_{pred} obtained using EN 1993-1-1 and the complete proposed formulation for the section L65x50x8

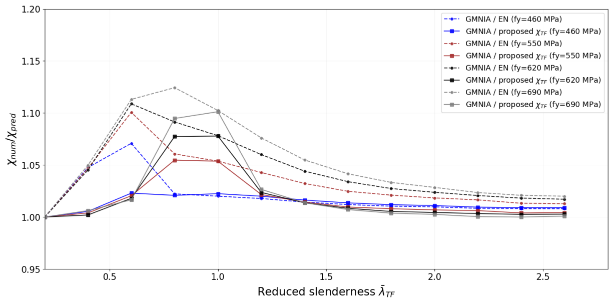

(a) F_vF_uT imperfection configuration

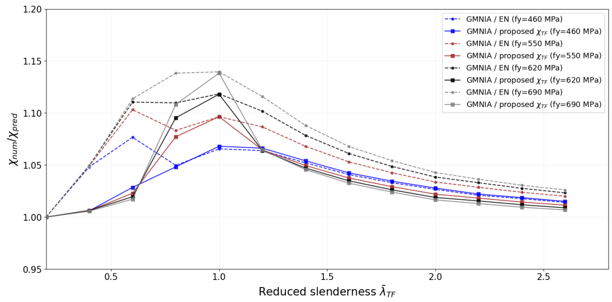

(b) F_v imperfection configuration

Figure 7.14: Comparison between the prediction ratios χ_{num}/χ_{pred} obtained using EN 1993-1-1 and the complete proposed formulation for the section L90x65x10

Bibliography

[1] Eurocode 3: Design of steel structures – part 1-1: General rules and rules for buildings, 2022.

[2] R. Dai, L. Gardner et M. A. Wadee : Behaviour, numerical modelling and design of fixed-ended unequal-leg angle section steel columns. *Journal of Constructional Steel Research*, 235:109828, 2025.

[3] CEN/TC 250/SC 3 : Eurocode 3 - Design of steel structures – Part 1-103: Elastic critical buckling of members. Technical Report CEN/TR 1993-1-103, CEN (European Committee for Standardization), 2025. Secretariat: DIN, Secretary: Kempa, S.

[4] CEN : Eurocode 3 – design of steel structures – part 1-14: Design assisted by finite element analysis, 2025. Belgian implementation: NBN EN 1993-1-14:2025.

[5] S. Kitipornchai et H. W. Lee : Inelastic experiments on angle and tee struts. *Journal of Constructional Steel Research*, 6(3):219–236, 1986.

[6] Yi Liu et Sabine Chantel : Experimental study of steel single unequal-leg angles under eccentric compression. *Journal of Constructional Steel Research*, 67:919–928, 2011.

[7] S. P. Timoshenko et J. M. Gere : *Theory of Elastic Stability*. McGraw-Hill, 2nd édition, 1961.

[8] N. S. Trahair : *Flexural-Torsional Buckling of Structures*. CRC Press, 1993.

[9] V. Z. Vlasov : *Thin-Walled Elastic Beams*. Israel Program for Scientific Translations, 1961.

[10] K. Liao : Compression tests of unequal-leg angles (msc thesis). Mémoire de D.E.A., Ohio State University, Columbus, OH, 1982.

[11] F. H. Wu : Experimental determination of buckling loads for unequal-leg angles with concentric loads (msc thesis). Mémoire de D.E.A., Ohio State University, Columbus, OH, 1982.

[12] Y. Zhang, Y. Wang, Z. Wang, Y. Bu, S. Fan et B. Zheng : Experimental investigation and numerical analysis of pin-ended extruded aluminium alloy unequal angle columns. *Engineering Structures*, 215: 110694, 2020.

[13] Y. Zhang, Y. Bu, Y. Wang, Z. Wang et Y. Ouyang : Study of flexural–torsional buckling behaviour of 6061-t6 aluminium alloy unequal-leg angle columns. *Thin-Walled Structures*, 164:107821, 2021.

[14] M. E. Laracuente, E. J. Sippel et H. B. Blum : Stability considerations of unequal-leg angle stainless steel columns. *In Proceedings of the 2022 SSRC Annual Stability Conference*, pages 1–20, 2022.

[15] M. E. Laracuente, E. J. Sippel et H. B. Blum : Experimental investigation of fixed-ended hot-rolled austenitic stainless-steel unequal-leg angles under compression. *Structures*, 59:105585, 2024.

[16] E. J. Sippel et H. B. Blum : Stability of stainless steel unequal-leg angles with imperfect supports. *In Proceedings of the 2023 SSRC Annual Stability Conference*, pages 1–19, 2023.

[17] Y. Guo, Z. Nie, X. Yao, Y. Liu, C. Chen et K. Zeng : Experimental study and design method of cold-formed thin-walled steel unequal-leg angles under axial compression. *Buildings*, 14(10):3132, 2024.

[18] P. B. Dinis, D. Camotim, K. Belivanis, C. Roskos et T. Helwig : On the buckling, postbuckling and strength behavior of thin-walled unequal-leg angle columns. *In Proceedings of the Annual Stability Conference, Structural Stability Research Council (SSRC)*, Nashville, Tennessee, 2015.

[19] American Iron and Steel Institute (AISI), Washington, D.C., USA. *North American Specification for the Design of Cold-Formed Steel Structural Members (AISI S100-16)*, 2016.

[20] American Institute of Steel Construction (AISC), Chicago, IL, USA. *Specification for Structural Stainless Steel Buildings*, 2021.

[21] Eurocode 9: Design of aluminium structures – part 1-1: General structural rules, 2007.

[22] F. Nishino, Y. Ueda et L. Tall : Experimental investigation of the buckling of plates with residual stresses. Rapport technique, Lehigh University, 1966. Lehigh Preserve Institutional Repository.

[23] Fumio Nishino et Lambert Tall : Experimental investigation of the strength of t-1 steel columns. Rapport technique 290.9, Fritz Engineering Laboratory, Department of Civil Engineering, Lehigh University, Bethlehem, Pennsylvania, USA, 1970.

[24] P. Može, D. Beg et A. Štern : Residual stress distribution of large steel equal leg angles. *Journal of Constructional Steel Research*, 2014.

[25] H. Ban, G. Shi, Y. Shi et Y. Wang : Residual stress tests of high-strength steel equal angles. *Journal of Constructional Steel Research*, 2012.

[26] ECCS : European recommendations for steel construction, 1976.

[27] J. V. Bhilawe et L. M. Gupta : Experimental investigation of steel equal angle subjected to compression. *Engineering Structures and Technologies*, 7(2):55–66, 2015.

[28] G. Shi, Z. Zhang, L. Zhou et Y. Gao : Experimental study and modeling of residual stresses of q420 large-section angles. *Journal of Constructional Steel Research*, 167:105958, 2020.

[29] M.-Z. et al. Bezas : Buckling resistance of star-battened angle members made of high-strength steel. *Structures*, 58:105274, 2023.

[30] X. Meng et L. Gardner : Behavior and design of normal- and high-strength steel shs and rhs columns. *Journal of Structural Engineering*, 146(11):04020227, 2020.

[31] Loris Saufnay, Jean-Pierre Jaspart et Jean-François Demonceau : Improvement of the prediction of the flexural buckling resistance of hot-rolled mild and high-strength steel members. *Engineering Structures*, 315:118460, 2024.

[32] Jeppe Jönsson et Tudor-Cristian Stan : European column buckling curves and finite element modelling including high strength steels. *Journal of Constructional Steel Research*, 2017.

[33] R. Maquoi : Some improvements to the buckling design of centrally loaded columns. *In Proceedings of the Structural Stability Research Council Annual Meeting*, 1982.

[34] B. Johansson : Buckling resistance of structures of high strength steel. *In Use and Application of High-Performance Steels for Steel Structures*, chapitre 5.3, pages 120–128. International Association for Bridge and Structural Engineering (IABSE), 2005.

[35] Loris Saufnay : *High-Strength Steels and Innovative Design Approaches for Sustainable Steel Structures*. Phd thesis, University of Liège, 2024.

[36] B. Somodi et B. Kövesdi : Flexural buckling resistance of cold-formed hss hollow section members. *Journal of Constructional Steel Research*, 128:179–192, 2017.

[37] X. Yun, Y. Zhu, X. Meng et L. Gardner : Welded steel i-section columns: Residual stresses, testing, simulation and design. *Engineering Structures*, 282:115631, 2023.

[38] H. Fang, T.-M. Chan et B. Young : Structural performance of cold-formed high strength steel tubular columns. *Engineering Structures*, 177:473–488, 2018.

[39] Louis Duchene : Establishment of a modified imperfection factor for cold-formed hollow sections. Master thesis, Faculté des Sciences appliquées, Université de Liège, Liège, Belgium, 2025. Promoters: Jean-François Demonceau and Loris Saufnay.

[40] A. Beyer, A. Bureau, J.-P. Jaspart, J.-F. Demonceau et M.-Z. Bezas : Torsional, flexural and torsional-flexural buckling of angle section members – an analytical approach. *In Modern Trends in Research on Steel, Aluminium and Composite Structures*, pages 400–406. Routledge, 2021.

[41] European Committee for Standardisation (CEN) : *Eurocode 3: Design of Steel Structures – Part 1-5: Plated Structural Elements*. European Committee for Standardisation, Brussels, Belgium, 2006.

[42] Eurocode – basis of structural and geotechnical design, 2023.

[43] Trayana Tankova, Luís Simões da Silva, Liliana Marques, Carlos Rebelo et Andreas Taras : Towards a standardized procedure for the safety assessment of stability design rules. *Journal of Constructional Steel Research*, 103:290–302, décembre 2014.

[44] S. Afshan, P. Francis, N. R. Baddoo et L. Gardner : Reliability analysis of structural stainless steel design provisions. *Journal of Constructional Steel Research*, 114:293–304, 2015.